JOINT TRANSPORTATION
RESEARCH PROGRAM
INDIANA DEPARTMENT OF TRANSPORTATION
AND PURDUE UNIVERSITY

Structural Evaluation of Full-Depth Flexible Pavement Using APT

Tommy E. Nantung, Jusang Lee,
John E. Haddock, M. Reza Pouranian, Dario Batioja Alvarez,
Jongmyung Jeon, Boonam Shin, Peter J. Becker

SPR-4212 • Report Number: FHWA/IN/JTRP-2021/17 • DOI: 10.5703/1288284317319

RECOMMENDED CITATION

Nantung, T. E., Lee, J., Haddock, J. E., Pouranian, M. R., Alvarez, D. B., Jeon, J., Shin, B., & Becker, P. J. (2021). *Structural evaluation of full-depth flexible pavement using APT* (Joint Transportation Research Program Publication No. FHWA/IN/JTRP-2021/17). West Lafayette, IN: Purdue University. https://doi.org/10.5703/1288284317319

AUTHORS

Tommy E. Nantung, PhD, PE
Section Manager
Office of Research and Development
Indiana Department of Transportation
(765) 463-1521
tnantung@indot.in.gov
Corresponding Author

Jusang Lee, PhD, PE
Asphalt Pavement Research Engineer
Office of Research and Development
Indiana Department of Transportation

John E. Haddock, PhD, PE
Professor of Civil Engineering
Director of the Indiana Local Technical Assistance Program
Lyles School of Civil Engineering
Purdue University

M. Reza Pouranian, Post Doctoral Research Assistant
Dario Batioja Alvarez, Post Doctoral Research Assistant
Jongmyung Jeon, Research Associate
Lyles School of Civil Engineering
Purdue University

Boonam Shin
Pavement Structure Research Engineer
Office of Research and Development
Indiana Department of Transportation

Peter J. Becker
Pavement Structure Research Engineer
Office of Research and Development
Indiana Department of Transportation

JOINT TRANSPORTATION RESEARCH PROGRAM

The Joint Transportation Research Program serves as a vehicle for INDOT collaboration with higher education institutions and industry in Indiana to facilitate innovation that results in continuous improvement in the planning, design, construction, operation, management and economic efficiency of the Indiana transportation infrastructure. https://engineering.purdue.edu/JTRP/index_html

Published reports of the Joint Transportation Research Program are available at http://docs.lib.purdue.edu/jtrp/.

NOTICE

TECHNICAL REPORT DOCUMENTATION PAGE

1. Report No. FHWA/IN/JTRP-2021/17	2. Government Accession No.	3. Recipient's Catalog No.
4. Title and Subtitle Structural Evaluation of Full-Depth Flexible Pavement Using APT		**5. Report Date** March 2021 **6. Performing Organization Code**
7. Author(s) Tommy E. Nantung, Jusang Lee, John E. Haddock, M. Reza Pouranian, Dario Batioja Alvarez, Jongmyung Jeon, Boonam Shin, and Peter Becker		**8. Performing Organization Report No.** FHWA/IN/JTRP-2021/17
9. Performing Organization Name and Address Joint Transportation Research Program Hall for Discovery and Learning Research (DLR), Suite 204 207 S. Martin Jischke Drive West Lafayette, IN 47907		**10. Work Unit No.** **11. Contract or Grant No.** SPR-4212
12. Sponsoring Agency Name and Address Indiana Department of Transportation (SPR) State Office Building 100 North Senate Avenue Indianapolis, IN 46204		**13. Type of Report and Period Covered** Final Report **14. Sponsoring Agency Code**

15. Supplementary Notes

Conducted in cooperation with the U.S. Department of Transportation, Federal Highway Administration.

16. Abstract

The fundamentals of rutting behavior for thin full-depth flexible pavements (i.e., asphalt thickness less than 12 inches) are investigated in this study. The scope incorporates an experimental study using full-scale Accelerated Pavement Tests (APTs) to monitor the evolution of each pavement structural layer's transverse profiles. The findings were then employed to verify the local rutting model coefficients used in the current pavement design method, the *Mechanistic-Empirical Pavement Design Guide* (MEPDG). Four APT sections were constructed using two thin typical pavement structures (seven- and ten-inches thick) and two types of surface course material (dense-graded and SMA). A mid-depth rut monitoring and automated laser profile systems were designed to reconstruct the transverse profiles at each pavement layer interface throughout the process of accelerated pavement deterioration that is produced during the APT. The contributions of each pavement structural layer to rutting and the evolution of layer deformation were derived.

This study found that the permanent deformation within full-depth asphalt concrete significantly depends upon the pavement thickness. However, once the pavement reaches sufficient thickness (more than 12.5 inches), increasing the thickness does not significantly affect the permanent deformation. Additionally, for thin full-depth asphalt pavements with a dense-graded Hot Mix Asphalt (HMA) surface course, most pavement rutting is caused by the deformation of the asphalt concrete, with about half the rutting amount observed within the top four inches of the pavement layers. However, for thin full-depth asphalt pavements with an SMA surface course, most pavement rutting comes from the closet sublayer to the surface, i.e., the intermediate layer. The accuracy of the MEPDG's prediction models for thin full-depth asphalt pavement was evaluated using some statistical parameters, including bias, the sum of squared error, and the standard error of estimates between the predicted and actual measurements. Based on the statistical analysis (at the 95% confidence level), no significant difference was found between the version 2.3-predicted and measured rutting of total asphalt concrete layer and subgrade for thick and thin pavements.

17. Key Words	18. Distribution Statement
MEPDG, rutting performance model, accelerated pavement testing, rutting distribution	No restrictions. This document is available through the National Technical Information Service, Springfield, VA 22161.

19. Security Classif. (of this report)	20. Security Classif. (of this page)	21. No. of Pages	22. Price
Unclassified	Unclassified	86 including appendices	

EXECUTIVE SUMMARY

Introduction

Many state agencies around the country have recorded various forms of pavement surface distresses. Among these distresses, permanent deformation, also known as rutting, is one of the most severe types of flexible pavement distress. The fundamentals of rutting behavior for thin full-depth flexible pavements (i.e., asphalt thickness thinner than 12 inches) are investigated in this study. The scope incorporates an experimental study using full-scale accelerated pavement tests (APTs) to monitor the evolution of each pavement's structural layer's transverse profiles. The findings were then employed to verify the local rutting model coefficients used in the current pavement design method, the *Mechanistic-Empirical Pavement Design Guide* (MEPDG).

Methodology

Four APT sections were constructed using two thin, typical pavement structures (7- and 10-inch thicknesses) and two types of surface course material (dense-graded and SMA). A mid-depth rut monitoring and an automated laser profile system were designed to reconstruct the transverse profiles at each pavement layer interface throughout the process of accelerated pavement deterioration that is produced during the APT. The contributions of each pavement structural layer to rutting and the evolution of layer deformation were derived. This study found that the permanent deformation within full-depth asphalt concrete significantly depends upon the pavement thickness. However, once the pavement reaches sufficient thickness (more than 12.5 inches), increasing the thickness does not significantly affect the permanent deformation. Additionally, for thin full-depth asphalt pavements with a dense-graded Hot Mix Asphalt (HMA) surface course, most pavement rutting is caused by the deformation of the asphalt concrete, with about half of the rutting amount observed within the top 4 inches of the pavement layers and only around 10% of the rutting observed in the subgrade. However, for thin full-depth asphalt pavements with an SMA surface course, most pavement rutting comes from the closet sublayer to the surface, i.e., the intermediate layer.

Findings

In SPR-3307, local MEPDG (version 2.3) rutting prediction coefficients were developed using a database that contains both APT thick full-depth pavement sections and field roadway segments. A particular procedure was followed to verify the accuracy of that MEPDG model on thin full-depth asphalt pavements. This procedure provides the most faithful simulations of the APT conditions using virtual weather station generation, particular traffic configuration, and falling weight deflectometer evaluation. The accuracy of the MEPDG's prediction models for thin full-depth asphalt pavement was evaluated using some statistical parameters, including bias, the sum of squared error, and the standard error of estimates between the predicted and actual measurements. Based on the statistical analysis (at the 95% confidence level), no significant difference was found between the version 2.3-predicted and measured rutting of total asphalt concrete layer and subgrade for thick and thin pavements. A new version of MEPDG (i.e., Pavement ME Design version 2.6), is available, and INDOT has a plan for the implementation. However, the current local model is not applicable to version 2.6, and a recalibration for the rutting model in version 2.6 is needed. The ongoing study, SPR-4447: *MEPDG Implementation*, performs local calibrations for the version 2.6 implementation. The rutting distributions in terms of pavement layers found in this study will be provided to SPR-4447 for the recalibration process. The INDOT Pavement Design Office will implement the study findings in the pavement design process.

CONTENTS

LIST OF TABLES

LIST OF FIGURES

1. INTRODUCTION AND BACKGROUND

1.1 Background

Pavement engineers have been producing long-lasting asphalt pavements since the 1960s. To ensure that asphalt concrete pavement, also known as flexible pavement, performs well in the field, the pavement must be designed properly in terms of structure and material. Since the first transcontinental highway, the Lincoln Highway, was built across the United States at the beginning of the 20th century, pavement design has always been challenging. Pavement design engineers are inevitably faced with a great variety and uncertainty of design factors, such as the environment, construction materials, and traffic load, which fluctuate greatly due to climate, technology, economic growth, and population changes. The experiences indicate that properly designed, well-constructed pavements can perform for extended periods. Many of these pavements in the past were the products of full-depth flexible pavement, and it has been shown to provide adequate strength over the extended service life. Full-depth pavements are constructed by placing asphalt layers directly on top of subgrade soil and typically consists of three structural layers.

- Hot mix asphalt (HMA) base layer, the bottom layer designed to resist bottom-up fatigue cracking.
- The intermediate layer, the middle layer designed to carry most of the traffic load.
- The surface layer, the top layer designed to resist surface-initiated distresses such as top-down cracking and rutting.

The Indiana Department of Transportation (INDOT) had been typically designed a full-depth asphalt pavement with five asphalt layers until 2019, including a surface layer, an intermediate layer, an upper base layer, an open-graded (OG) drainage layer, and a lower base layer. Such pavement structure was the primary pavement type considered in the INDOT *Mechanistic-Empirical Pavement Design Guide* (MEPDG) implementation effort.

The MEPDG was first developed in the early 2000s as part of the National Cooperative Highway Research Program (NCHRP) Project 1-37A to replace the 1993 American Association of State Highway and Transportation Officials (AASHTO) design approach. In 2005, INDOT began to explore the MEPDG as a pavement design tool. INDOT has been implementing MEPDG since January 1, 2009, with the INDOT MEPDG input database developed by the Office of Research and Development and the Office of Pavement Engineering. The inputs include traffic, climate, materials, performance calibration factors, and policies (e.g., all MEPDG inputs and their performance criteria and related reliability levels).

When the MEPDG was first developed, it was globally calibrated using the Long-Term Pavement Performance (LTPP) database. However, the global calibration factors almost certainly do not adequately reflect local conditions, such as climate, materials, pavement structure, and construction practice. For instance, Indiana is geographically located in a wet-freeze soil-climate and limestone aggregate resource zone. The MEPDG used a total of 94 asphalt LTPP sections for the global calibration. However, the wet-freeze limestone zone has only three LTPP asphalt sections. Besides, Indiana has no LTPP full-depth asphalt section.

Without taking the local factors into account, the prediction performance of the MEPDG will be compromised. For example, the globally calibrated MEDPG rutting models tend to overestimate the degree of rutting for Indiana pavements. This is especially true for the subgrade rutting prediction. A recently completed INDOT research project has successfully calibrated the MEPDG rutting transfer functions for thick full-depth flexible pavement, i.e., the pavement thickness greater than 12 inches. With the calibration, the MEPDG prediction performance has been significantly improved (i.e., the prediction errors have been reduced by 73%). INDOT has been implementing the new rutting calibration factors since 2017. However, the calibrated models' applicability to the pavements thinner than 12 inches has never been verified.

To understand the effect of the pavement thickness on the rutting behavior, two mechanical simulations were performed. First, the subgrade vertical strain level was analyzed using multilayer linear elastic analysis program WESLEA v3.0 as shown in Figure 1.1. The vertical strain at the top of the subgrade is a major factor dominating the subgrade rutting. It was observed that the strain level exponentially decreases with increasing the pavement thickness, and the rate of decrease is more significant for thinner pavements. For illustration, the strain on top of subgrade for a 4-inch thick pavement is 1980 micro-strain. If the pavement was thickened to 12 inches, the strain decreases significantly by 1421 micro-strain. However, further increasing the pavement thickness by 8 inches only reduces the strain by 249 micro-strains. Similar observations were made by Uge and van de Loo (1974) that the increase of permanent deformation was minimal with increased pavement thickness once the pavement is sufficiently thick.

Secondly, the accelerated pavement testing (APT) with a 9,000 lbs. loaded half standard axle was simulated using a two-dimensional finite element analysis, as plotted in Figure 1.2. At a depth of 4 inches, the stress level is 60% higher with two concentration areas underneath the loaded wheels, and the influential stress zone (i.e., the stress contour "bulb") is narrower than that at a depth of 12 inches. According to the mechanical simulation results, it can be expected that the pavement thickness has a great impact on the rutting behavior of the full depth flexible pavement. The MEPDG rutting models that were calibrated for thick pavements conditions might not be applicable for thinner pavements. Therefore, a calibration for the thin pavements is required for a more accurate prediction.

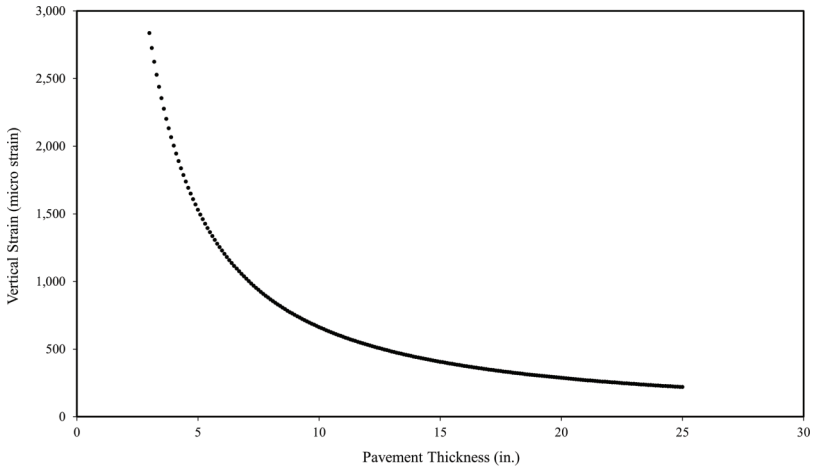

Figure 1.1 Effect of pavement thickness on the strain at the top of the subgrade.

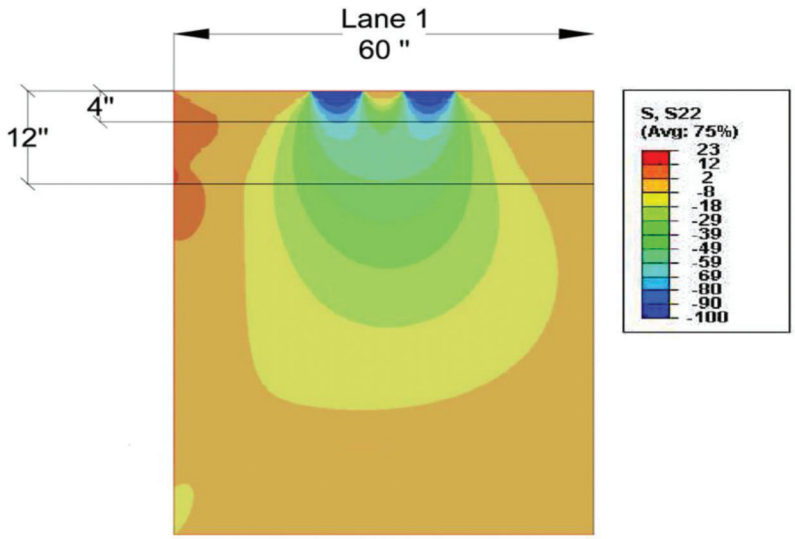

Figure 1.2 Vertical stress distribution in a 12-inch, full-depth flexible pavement.

1.2 MEPDG Local Calibration

The MEPDG calibration process's overall goal is to adjust pavement performance transfer functions systematically. The MEPDG can predict pavement performance without bias and determine the standard error associated with the transfer functions. Two statistical measures are used to evaluate the goodness-of-fit between the predicted and observed values: bias and precision. The efforts undertaken by several states' DOTs in calibrating the MEPDG are summarized in the following paragraphs.

The Arizona DOT conducted local calibration for MEPDG v. 1.0 in 2010. Three flexible pavement transfer functions for fatigue cracking, rutting, and roughness were calibrated. According to the Arizona calibration results, the global model could not predict fatigue cracking and rutting in asphalt concrete layers and over predicted rutting in the subgrade (Souliman et al., 2010).

The Arkansas State Highway and Transportation Department calibrated MEPDG v. 1.1 using both LTPP program sections and Arkansas State Highway and Transportation Department Pavement Management System (PMS) sections. Alligator cracking and rutting transfer functions were considered in this study. Concerns were reported regarding the data quality during the calibration process. The different definitions of "transverse cracking" between the MEPDG and LTPP programs were believed to be critical to the data collection process (Hall et al., 2011).

The North Carolina DOT conducted its MEPDG local calibration (i.e., MEPDG v. 1.1) in 2011 using both LTPP and non-LTPP program pavement sections. All of the LTPP program sections were used for calibration, and the non-LTPP program sections were used for validation. Material-specific HMA rutting plastic deformation factors were developed for 12 commonly used North Carolina HMA mixtures based on triaxial repeated load permanent deformation tests.

Two approaches, i.e., a generalized reduced gradient (GRG) method and a genetic algorithm method, were used as the optimization techniques. Several conclusions were drawn in this study: (1) the MEPDG tends to over predict rutting, especially in the subgrade; (2) local calibration reduces bias and standard error, but the improvement is not enough, and so, the null hypothesis that no difference exists between the predicted and measured values cannot be accepted at the 95% confidence level; and (3) forensic investigation is recommended for future studies to quantify the contribution of each layer to total rutting (Kim et al., 2011).

The Nevada DOT started MEPDG implementation in 2005. It recently has conducted local calibration of the fatigue cracking and rutting models in the Pavement ME v. 2.0 (i.e., the current version of the MEPDG) using Nevada's local PMS database. A materials database consisting of field-produced mixtures, mostly polymer-modified binder mixtures, was built, and material properties such as the dynamic modulus and binder properties were tested. Recalibration was recommended to increase the accuracy of the predictions because the calibration method used test sections with only around 10 years of service life (Nabhan, 2015).

The Oregon DOT (ODOT) calibrated Darwin ME v. 1.1 (one version of the MEPDG) in 2013. The research focused on rehabilitating existing pavement structures, which is most pavement work conducted by the ODOT. Rutting, alligator cracking, longitudinal cracking, and thermal cracking models were calibrated. The ODOT found that (1) the MEPDG over predicted total rutting and that most of the predicted rutting occurred in the subgrade; (2) all of the calibrated models provided less bias and standard error than the global models; and (3) large variations remained between the predicted and observed values, especially for longitudinal and transverse cracking (Williams & Shaidur, 2013).

The Iowa DOT calibrated MEPDG v. 1.1 using jointed plain concrete pavement (JPCP) sections, HMA pavement sections, and HMA over JPCP sections. Required inputs were collected from the Iowa DOT PMS database. JPCP faulting, transverse cracking, roughness, rutting, and fatigue cracking models were calibrated. For flexible pavements, acceptable bias and standard errors were found for the global fatigue cracking model; however, the global rutting model over predicted the subgrade rutting while underestimating the asphalt concrete layer rutting (Ceylan et al., 2013).

The Indiana DOT developed a guideline to calibrate the MEPDG prediction models using a database that contains both APT sections and field roadway segments and accounts for the rutting in individual pavement layers (Nantung et al., 2018). The APT sections supplement the field roadways used in the calibration process to overcome issues such as small sample size and low distress levels of field roadways. The results of model validation using Jack-knife resampling techniques confirmed that the calibrated models provided accurate and statistically sound pavement performance predictions.

1.3 Accelerated Pavement Testing Techniques

1.3.1 Benefits and Impacts

APT techniques provide an opportunity to investigate pavement behavior in cost- and time-efficient ways whereby the amount of damage that might take more than 10 or even 20 years to occur in the field can be achieved in a matter of months. Metcalf (1996) summarized a list of 35 full-scale APT facilities around the world. During the past several decades, there has been an increased interest in APTs. APT facilities and methods, such as circular tracks, linear tracks, and mobile loading machines, have been developed worldwide.

APTs have been used extensively in areas such as the following.

- The development and validation of pavement analysis and design models
- Research into pavement mechanics and damage mechanisms
- Identification of deficiencies in current practices
- Development of performance-based specifications or tests for asphalt concrete pavements
- Investigations into correlations between laboratory experiments and real long-term pavement performance
- The efficiency and impacts of implementing innovative materials, designs, specifications, construction standards, vehicle technology, rehabilitation techniques, etc.
- Evaluation of load damage equivalency and the remaining life of pavements
- Improved vehicle–pavement interaction, including advanced load and contact stress models

1.3.2 Evaluation of Permanent Deformation of Flexible Pavement

Many research studies have been conducted to analyze rutting behavior using APT facilities. Sivasubramaniam and Haddock (2006) evaluated Superpave designed mixtures using the National Center of Asphalt Technology (NCAT) test track and full-scale APT and PUR Wheel laboratory wheel trackers. Saeed et al. (2010) compared the rutting performance of an SMA mixture and dense-graded airfield HMA mixture under an F-15E aircraft load cart. They found the SMA mixture to have much better rutting resistance than the HMA mixture. Villiers et al. (2005) evaluated pavement layers' contribution to total rut depth using a falling weight deflectometer (FWD) test and transverse profiles. They also validated their findings with a forensic trench study. Gibson et al. (2010) studied the rutting susceptibility of mixtures compacted with a Superpave Gyratory Compactor (SGC) and field compaction rollers. They found that the SGC-compacted mixtures exhibited a higher rate of rutting development in the early loading stage, whereas the rate decreased when the loading was continued.

Several mechanistic or mechanistic-empirical models have been developed using the APT method. Monismith et al. (2006) and Li et al. (2011) developed a

relationship between rutting and mixture shear properties obtained from triaxial compressive strength and repeated load permanent deformation tests. Park et al. (2004) developed an elasto–viscoplastic model based on Perzyna's viscoplastic theory and the Druker–Prager yield function to predict rutting in APTs. Onyango and Romanoschi (2010) evaluated three mechanical models: The Druker–Prager, elasto-viscoplastic, and creep models for rutting prediction. Immanuel and Timm (2007) developed two mechanistic-empirical models using NCAT test track data; one model is based on the vertical strain on top of a granular layer. The other is based on the maximum shear strain in the HMA layer. Both models exhibited reasonable accuracy. Xu and Mohammad (2008) developed a mechanistic-empirical model that used power law and vertical strain and conducted their tests at the Louisiana Accelerated Load Facility (ALF).

1.3.3 MEPDG Analysis

Azari et al. (2008) validated the MEPDG rutting models using both Level 1 and Level 3 inputs with Federal Highway Administration Accelerated Loading Facility (FHWA ALF) data. They found that both Level 1 and Level 3 simulations over predicted the rutting. Gibson et al. (2011) analyzed FHWA ALF tests using the MEPDG. They used special axle configuration features in the MEPDG to customize their super-single tire assembly. They employed a surrogate of the MEPDG to bypass various MEPDG features, such as the inherent climate model and global aging system, which challenged the ability to simulate ALF testing conditions.

Hong and Chen (2008) calibrated the MEPDG rutting model using data obtained from eight sections tested at the Cold Regions Research and Engineering Laboratory (CRREL). These researchers simulated APT traffic by constructing a particular vehicle with only one tandem axle in the MEPDG. The spacing between the two axles was set above 100 inches so that one repetition in the MEPDG equals two passes in the APT. Hong and Chen (2008) conducted the optimization process by considering the entire history of rutting development instead of only the final rut depth measured at the end of the pavement service life.

1.4 Scope of Study

This research was initiated to investigate rutting behavior fundamentals for thin full-depth flexible pavements (7–10 inches). The scope incorporates an experimental study using full-scale APT techniques to monitor the evolution of each pavement structural layer interface's transverse profiles. The findings are then employed to improve the rutting model embedded in the current pavement design method, the MEPDG.

2. RESEARCH APPROACH

2.1 Research Objectives

The objectives of this research effort are the following.

- To investigate the rutting behavior of thin full-depth flexible pavements.
- To verify the prediction performance of the previously calibrated MEPDG rutting models for thin pavements.

2.2 Testing Plan

An APT experiment was designed in this study to address the issues discussed in Chapter 1 and accomplish the research objectives. Four APT sections were constructed using two typical thin pavement structures and two types of surface course material. A mid-depth rut monitoring and automated laser profile system were designed to reconstruct the transverse profiles at each pavement layer interface throughout the accelerated pavement deterioration produced during the APT. Thus, each pavement structural layer's contributions to rutting and layer deformation evolution could be derived.

APT techniques were employed to improve current mechanistic-empirical pavement design methods and assist in MEPDG local calibration. The APT sections served to supplement the field roadways used in the calibration process. All the qualified roadway segments had been in service for less than 10 years and exhibited "fair" pavement conditions. On the other hand, the APT sections showed distress levels close to the failure design criterion met by accelerated load applications. Also, the use of the APT sections can reduce the required number of field roadway segments, as the APT sections led to lower standard errors of the estimates due to well-controlled test conditions and measurement procedures.

Once the database was formed, the measured rut depths were distributed into the asphalt concrete layers and subgrade. The unbound layer rutting model was calibrated externally, and then the asphalt concrete layer rutting model was calibrated using a mixed method. Then, a procedure was developed to provide the most faithful simulations of the APT conditions that include climate, traffic, and aging conditions using virtual weather station generation, a particular traffic configuration, and FWD evaluation.

3. FULL SCALE ACCELERATED PAVEMENT TESTING

3.1 Introduction

The Indiana Department of Transportation's Accelerated Pavement Testing (APT) Facility is located at the INDOT's Research and Development site in West Lafayette. The APT site consists of a pit 20 ft (6.10 m) in width and length and 6 ft (1.83 m) deep.

The APT loading is performed by a heavy vehicle prototype consisting of a set of wheels with full-scale tires mounted to a large steel frame carriage, as shown in Figure 3.1. The loading applied is operated using a set of pneumatic cylinders that provide steady loading during the APT trafficking. For this study, the loading applied was set to 20,000 lb. (9.07 ton) using a conventional dual tire set-up with a tire pressure of 100 psi (0.69 MPa). The continued APT loading allows mimicking many years of in-service pavement loading in just a few months.

The INDOT APT heavy vehicle also includes an automated laser system mounted behind the wheel assembly. The laser system can be used to measured longitudinal and transversal pavement profiles over time. The facility is equipped with a radiant heating system and ground heating lamps, as shown in Figure 3.1, to maintain elevated air and pavement temperatures. The APT loading machine can apply both unidirectional and bi-directional trafficking. Only unidirectional movement was used during this study. The APT control room is equipped with two computers and a control panel. One computer is used for APT control and programming, and the other is used for data acquisition.

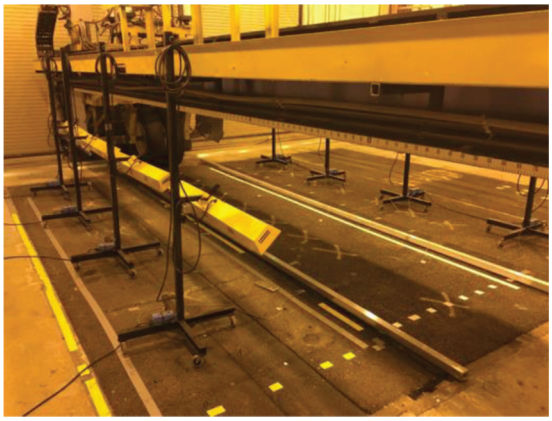

Figure 3.1 APT loading machine trafficking a pavement section.

3.2 Pavement Structure

Four different thin, flexible full-depth pavement sections were designed and constructed following conventional INDOT full-depth flexible pavement specifications. As shown in Figure 3.2, Lanes 1 and 2 have an overall asphalt thickness of 10 inches. Both lanes are identical except that Lane 1 has a 1.5-inch dense-graded Hot Mix Asphalt (HMA) surface layer, and Lane 2 has a 1.5-inch Stone Matrix Asphalt surface layer. Both lanes have a 2.5-inch intermediate asphalt course and a 6-inch asphalt base course. Lane 3 and Lane 4 have an overall pavement thickness of 7 inches and identical except for the surface course, as shown in Figure 3.2. While Lane 3 has an SMA surface course, Lane 4 has a dense-graded HMA course. Both lanes present a 2.5-inch intermediate layer with a 3-inch asphalt base course. The asphalt layers were constructed on top of a layer of lime-treated A-6 soil subgrade over untreated A-6 subgrade. In the APT project, SMA also was included as a surface course material. Both surface mixes are Superpave 4-designed with a 9.5-mm nominal maximum aggregate size.

3.3 Paving Materials

The paving materials used in this APT study were designed to replicate a previous APT study (Nantung

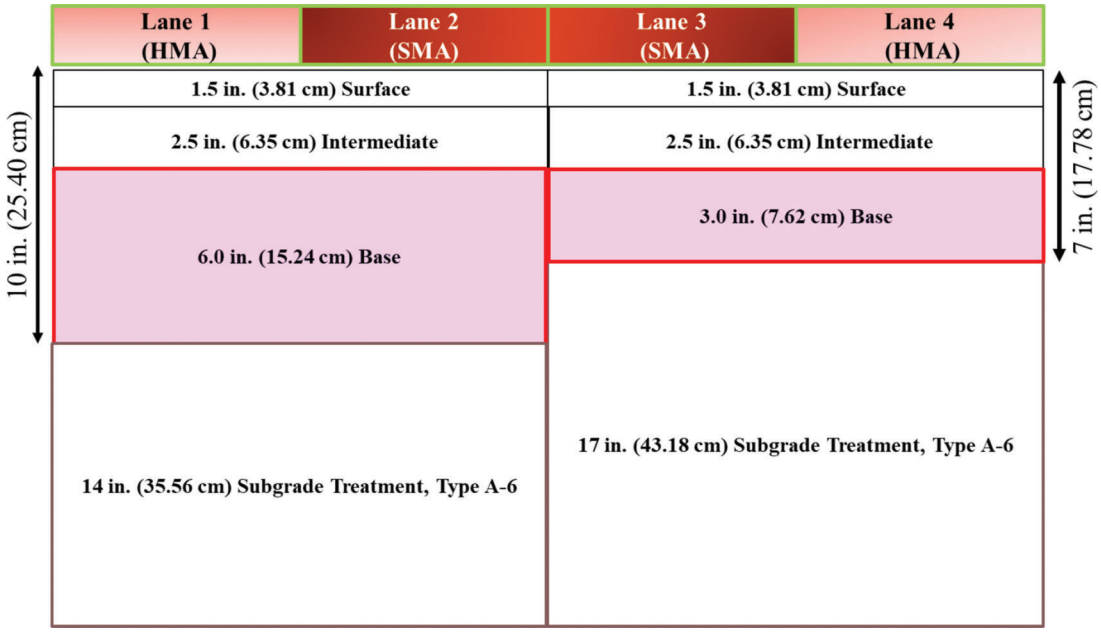

Figure 3.2 Test section structures.

et al., 2018). Information about asphalt mixes, aggregate size, and PG are presented in Table 3.1. For example, both surface mixes (HMA and SMA) have a performance grade of 70-22 and NMAS 9.5, a conventional mix PG used for surface courses in Indiana. The intermediate and base mixes have similar characteristics except for the binder, the performance grades are 64-22 and 76-22 PG, respectively. Aggregate gradation charts along with corresponding control points as specified by INDOT are presented in Table 3.2. It should be noted that intermediate and base courses consist of the same aggregate gradation. Figures 3.3, 3.4, and 3.5 also provide a schematic of the mixes' gradations curves.

3.3.1 Lime Stabilized Subgrade

A-6 silt-clay, a typical subgrade soil in Indiana, was used as subgrade material in this study. Lime was used to treat the upper A-6 soil layers to improve their workability and load-bearing capacity. The maximum dry unit weight and optimum moisture content information, and other properties are shown in Table 3.3.

3.4 Test Lanes Construction

3.4.1 Construction of Subgrade Soil

The different phases of the subgrade construction are depicted in Figure 3.6. The APT pit was filled with A-6 subgrade soil from a nearby soil pit located in Lafayette, Indiana. The subgrade soils were placed in the test pit up to 24 inches below the surface in six lifts (approximately 50 inches from the bottom of the test pit. During placement, the lift thickness was limited to 8 inches. The exposed surface was thoroughly compacted with a hydraulic hand-operated sheep foot roller compactor after each lift's placement, as shown in Figure 3.6(b). Lime-stabilization of the A-6 subgrade soils followed the placement of the untreated subgrade. The subgrade soil stabilization was conducted following INDOT specifications. As shown in Figure 3.6(d–e), the original A-6 soil was first spread inside the pit, and then 5% lime was applied and mixed using a soil mixer. Once the soil was thoroughly blended with the lime, it was compacted in lifts, and water was added between lifts to activate the lime and allow it to develop to its maximum strength. Soil compaction was performed using the roller compactor and a jumping jack tamper. The lime-treated subgrade was cured for several days after construction to allow strength to develop. Figure 3.6(f) shows the finished subgrade surface.

The subgrade was monitored for several days until it could develop enough strength to continue with paving operations. The evaluation was conducted using a dynamic cone penetrator (DCP) and lightweight deflectometer (LWD).

DCP is a hand-operated in situ testing device used to assess the strength and stiffness of unbound pavement materials. DCP testing under ASTM D6951 involves dropping a 17.6 lb (8 kg) weight from 22.6 inches (0.575 m) onto a steel rod tipped with a cone-shaped tip and then measuring the resulting penetration (i.e.,

TABLE 3.1
Mixtures design summary

Layer	Nominal Maximum Aggregate Size (NMAS)	Binder Performance Grade (PG)
Surface	9.5-mm	70-22
Intermediate	19.0-mm	70-22
Base	19.0-mm	64-22

TABLE 3.2
Aggregate gradations for pavement layers

	Surface Dense Graded HMA		Surface SMA		Intermediate/Base	
Sieve Size	% Passing	Spec	% Passing	Spec	% Passing	Spec
37.5 mm (1 1/2")	100		100		100	
25.0 mm (1")	100	100	100	100	100	100
19.0 mm (3/4")	100	90–100	100	90–100	93.8	90–100
12.5 mm (1/2")	100	<90	100	<90	74.7	<90
9.5 mm (3/8")	94.9		87.2		61.3	
4.75 mm (No. 4)	64		35.2		39.8	
2.36 mm (No. 8)	37.3	23–49	21.3	23–49	27.1	23–49
1.18 mm (No. 16)	23.3		16.3		17.4	
0.6 mm (No. 30)	15.3		13.4		11.7	
0.3 mm (No. 50)	9.5		11.8		7.7	
0.15 mm (No. 100)	6.6		10.7		5.6	
0.075 mm (No. 200)	5.4	2–10	8.2	2–10	4.6	2–10

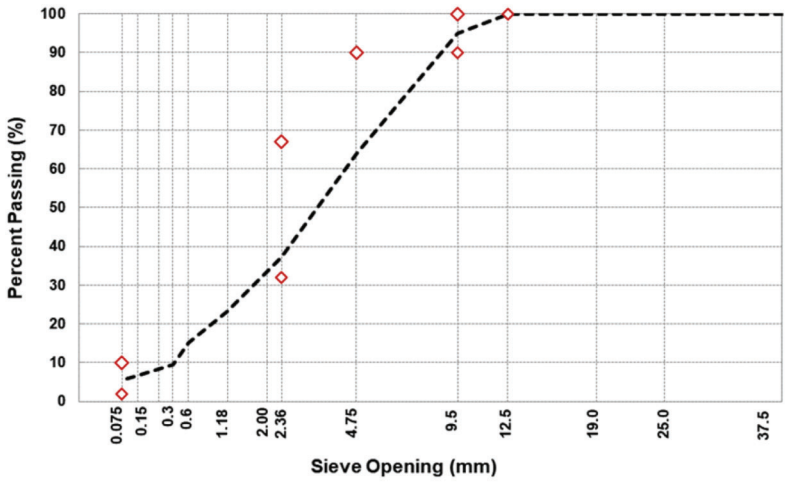

Figure 3.3 Aggregate gradation for the surface dense-graded HMA mix.

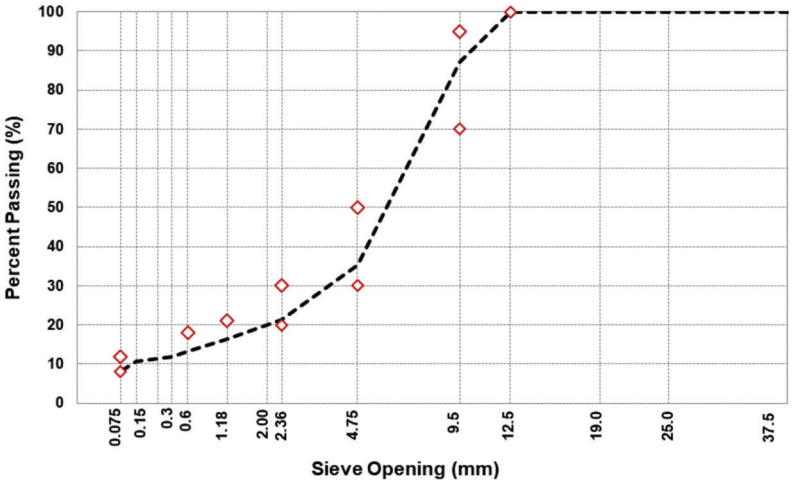

Figure 3.4 Aggregate gradation for SMA surface mix.

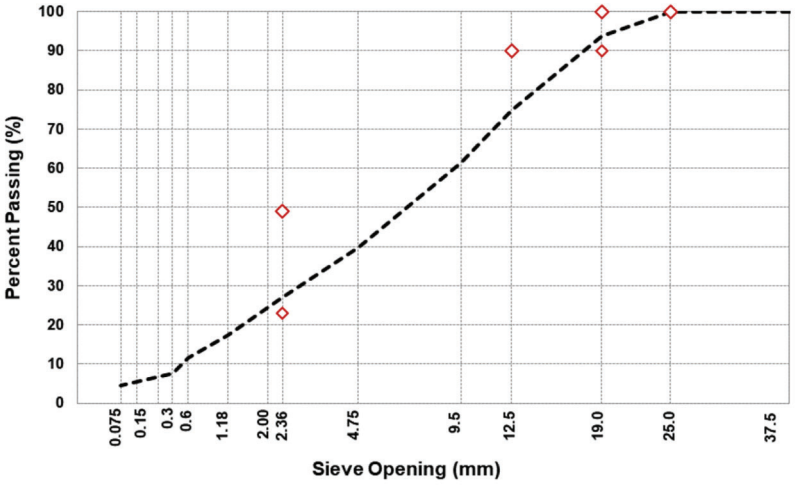

Figure 3.5 Aggregate gradation for intermediate/base mix.

TABLE 3.3
Subgrade and lime soil modification design parameters

Subgrade Soil Information	
Property	**Value**
Maximum Dry Unit Weight	102 pcf
Optimum Moisture Content	18.6%
Borrow Pit Moisture Content	17%
Treated Soil Information	
Subgrade Treatment Layer Thickness	17 inches
Number of Lifts per Layer	3 lifts
Compacted Lift Thickness	5.67 inch/lift
Design Lime Content	5.0%
Lime Apparent Specific Gravity	2.60
Lime Slurry Content and Distribution Rate	
Unit Volume per Lift per ft^2	0.472 ft^3/lift
Lime and Soil Weight per Lift per ft^2	48.17 lb/ft^2/lift
Lime Weight per Lift per ft^2	2.29 lb/ft^2/lift

penetration index) (ASTM D6951, 2015). DCP penetration depths in this study generally extended to about 30 inches below the then-existing ground surface. California bearing ratio (CBR) values were correlated from DCP measurements using Equation 3.1.

$$CBR = \frac{292}{PI^{1.12}} \qquad \text{(Eq. 3.1)}$$

where,

CBR = California bearing ratio (%); and
PI = penetration index (mm/blow).

DCP tests were conducted on top of lime-modified subgrade layers shortly following placement (up to 1 week) to (1) establish subgrade engineering properties and (2) observe the development of subgrade strength/stiffness with increasing time (i.e., lime curing). Sections

(a) Soil placement into test pit
(b) Subgrade soil compaction
(c) Scarification and compaction of stabilized soil
(d) Lime addition during subgrade stabilization
(e) Mixing operations during subgrade stabilization
(f) Subgrade finished surface

Figure 3.6 Subgrade construction phases.

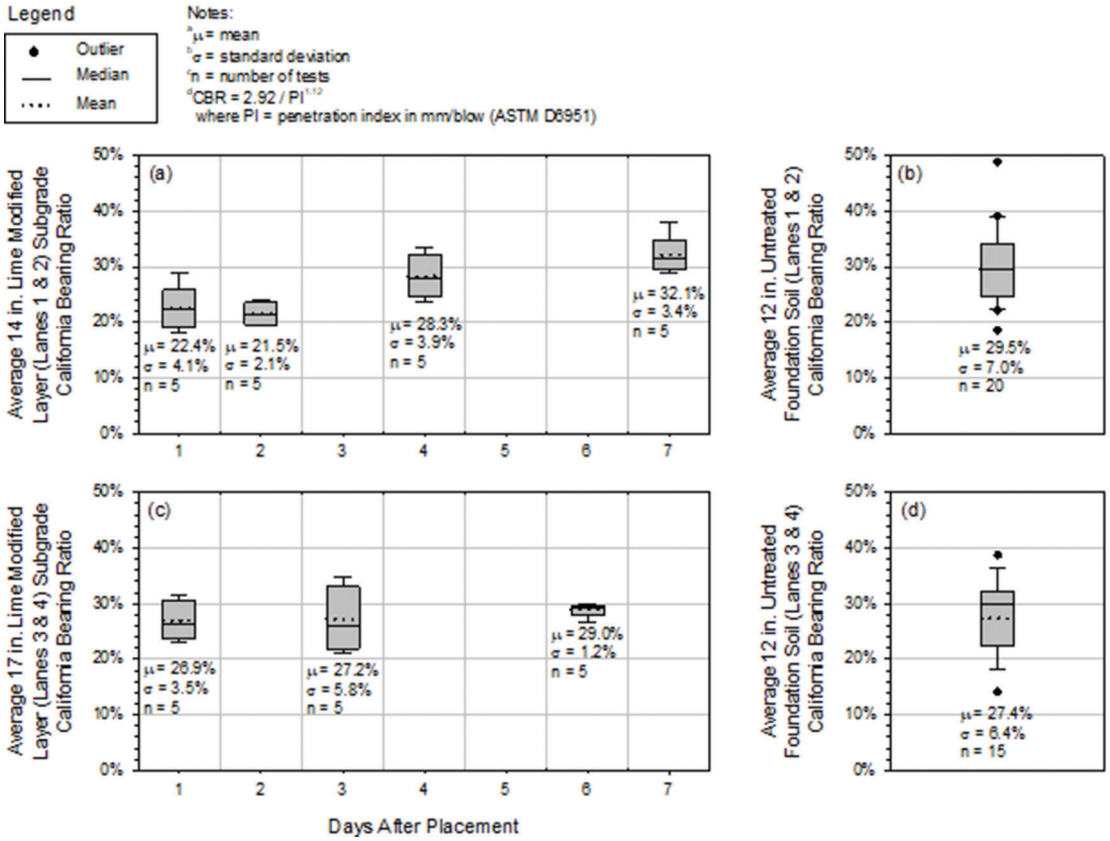

Figure 3.7 Summary of layer CBR values for (a) 14-inch-thick lime-modified subgrade sections, (b) untreated foundation soil underlying 14-inch-thick lime-modified subgrade sections, (c) 17 inch-thick-modified subgrade sections, and (d) untreated foundation soil underlaying 17-inch-thick lime modified subgrade sections.

with 14-inch-thick lime-modified subgrade (10-inch dense-graded and SMA pavements) were tested 1 day, 2 days, 4 days, and 7 days after placement. Sections with 17-inch-thick lime-modified subgrade (7-inch dense-graded and SMA pavements) were tested 1 day, 3 days, and 6 days after placement. Appendix A provides DCP profiles (i.e., CBR with depth) for each of the DCP tests. Figure 3.7 summarizes the DCP test results for 14-inch-thick lime-modified subgrade sections (Lanes 1 and 2) and 17-inch-thick lime modified subgrade sections (7-inch pavements).

DCP-based CBR values for lime-modified subgrade tend to increase with increasing time, demonstrating that strength/stiffness of lime-treated soils increases as lime modifiers cure. At 7 days, DCP-based CBR for the 14-inch-thick lime-modified subgrade averaged 32.1%, with a standard deviation of 3.4%. DCP-based CBR values for the untreated foundation soil underlying the 14-inch-thick lime-modified subgrade averaged 29.5%, with a standard deviation of 7.0%. At 6 days, DCP-based CBR for the 17-inch-thick lime-modified subgrade averaged 29.0%, with a standard deviation of 1.2%. DCP-based CBR values for the untreated foundation soil underlying the 17-inch-thick lime-modified subgrade averaged 27.4%, with a standard deviation of 6.4%.

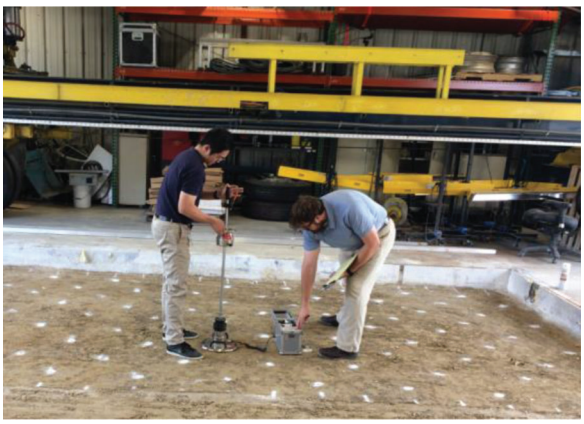

Figure 3.8 Light weight deflectometer testing.

The LWD test was used to measure the *materials' in situ modulus values* following ASTM E 2583, *Standard Test Method for Measuring Deflections with a Light Weight Deflectometer (LWD)*. As part of this project, the LWD tests were performed at the lime-stabilized subgrade surface before the instrumentation installation, as shown in Figure 3.8. Figure 3.9 provides the subgrade strength evaluation results (deflections) from

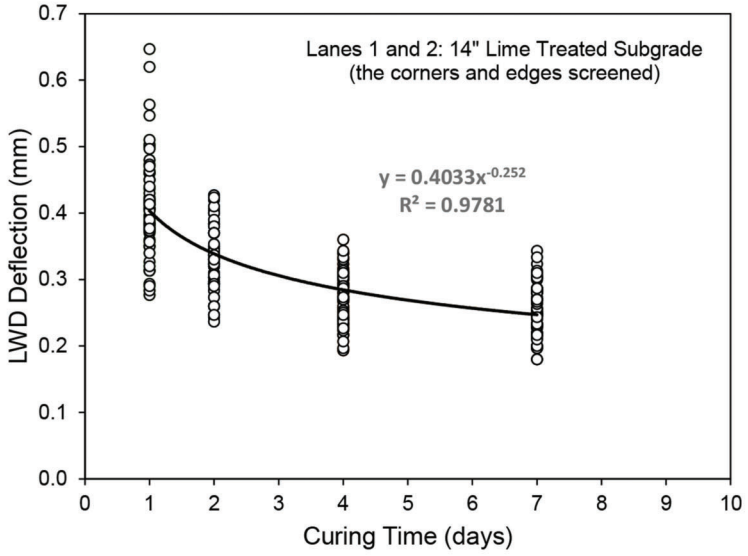

(a)

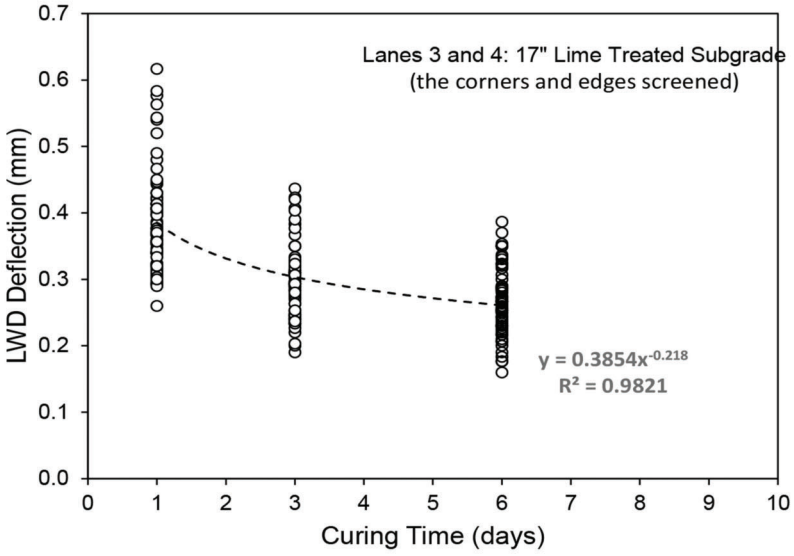

(b)

Figure 3.9 Deflection variations with curing time for (a) 17-inch subgrade and (b) 14-inch subgrade.

LWD tests. It illustrates an apparent reduction in the magnitude of deflections when comparing 4-day vs. 7-day deflections. Also, a clear decreasing trend in average deflection with increasing time can be observed in Figure 3.9. Locations and test results of lightweight deflectometer tests on subgrade soil are shown in Figure 3.10.

3.4.2 Construction of HMA Layers

The construction of the asphalt layers was completed after installing the subgrade instrumentation, covered in the following section (see Section 3.5). It should be noted that the instrumentation was set on top of the subgrade, and the APT lanes were covered with asphalt mix manually before asphalt paving operations to prevent sensor damage. Figure 3.11 describes the different construction stages of the HMA layers. The asphalt base layer in all APT lanes was paved manually because a full-size paver could not operate inside the APT facility (see Figure 3.11(a, b)). During the paving operations, the HMA material was transferred to the pit using a shuttle buggy to prevent mixture segregation. Next, the base layers were compacted using a roller

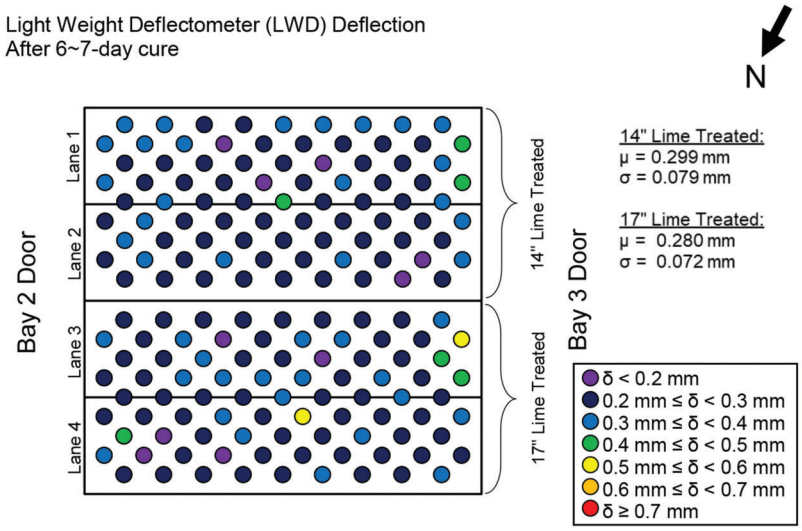

Figure 3.10 Locations and test results of lightweight deflectometer tests on subgrade soil.

compacter shown in Figure 3.11(c). A manual vibratory plate was also used during the compaction operations, especially on the pit's edges, where the full-size compactor could not reach. After the base layers were compacted, the intermediate and surface layers were paved using a full-size paver and a 10-ton roller compactor. During these paving operations, the mat density was monitored using a pavement quality indicator (PQI). The PQI measures the density of asphalt pavement as estimated from the material's dielectric constant. A tack coat was applied between each of the asphalt concrete layers to ensure full bonding. A sampling of all different HMA materials was conducted for materials laboratory characterization.

It should be mentioned that the HMA surface layers (Lane 1 and Lane 4) were removed (milled off) using a grinder and repaved by the contractor due to problems during the production of the material at the plant. The HMA materials were found significantly off from the specified INDOT JMF and were replaced by proper materials. Figure 3.12 summarizes the steps during these operations. During the milling and repaving of the defective surface layers, all pavement sensors were monitored by connecting all sensors to the data acquisition system (see Figure 3.13) to verify their responsiveness during grinding, paving, and compacting activities. After the repaving was completed, adequate sensor performance was confirmed.

During the paving operations, the target density of the HMA materials was set to 93%, as specified by INDOT. Table 3.4 summarizes the number of compactor passes and the asphalt mat's density obtained from the PQI. The 93% density goal was generally achieved for intermediate and surface layers, as shown in Table 3.4. However, the base courses' in-place density was below the established threshold due to the inability to use a full-size compactor and paver for the asphalt base construction.

3.5 Instrumentation

As mentioned before, an extensive instrumentation plan, including pressure cells, strain gauges, thermocouples, and moisture sensors, was installed to measure and monitor the pavement's responses. A nondestructive testing (NDT) program, including Ground Penetrating Radar (GPR) evaluations and FWD testing, was used to evaluate the pavement's layer thickness and *in situ* modulus, respectively. Surface profile measurements were also used to determine pavement surface rutting and individual layer rutting during trafficking.

3.5.1 Pavement Sensor Types and Locations

All sensors were installed on top of the stabilized subgrade and along the APT wheel path. Figure 3.14 shows a schematic of the sensor's instrumentation. Each lane had three horizontal strain gauges positioned to monitor both longitudinal and transverse directional strains. The lanes had two vertical strain gauges, except Lane 2 that had only one vertical gauge. Vertical gauges were installed to measure vertical strains on top of the subgrade, usually associated with rutting behavior in the subgrade layer. Construction Technology Laboratory (CTL) manufactured the horizontal and vertical strain gauges and are shown in Figure 3.15(a, b) respectively. Each lane had one Geokon model 3500 earth pressure cells, as shown in Figure 3.15(c). Pressure cells were used to measure the vertical pressure on top of the subgrade. Pressure cells consist of two round steel plates with a diameter of 9 inches (22.86 cm). The gap between the two plates is filled with de-aired oil, and hence, the earth pressure is measured through the fluid pressure.

Thermocouples were also included in the instrumentation plan at each layer's interface (subgrade/asphalt base, asphalt base/asphalt intermediate, asphalt inter-

(a) Asphalt base construction (material transfer)

(b) Manual spreading of asphalt base material

(c) Compaction

(d) Tack coat application

(e) Surface course paving operations (Lane 1)

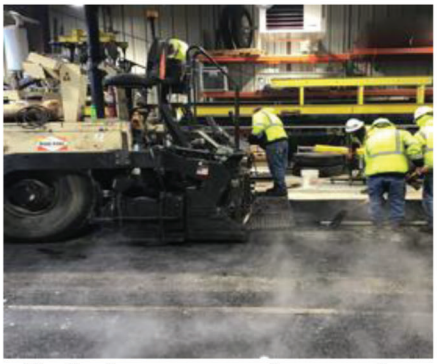

(f) Surface course paving operations (Lane 4)

Figure 3.11 HMA layer paving operations.

mediate/asphalt surface) in all the test lanes to monitor the temperature profile across the pavement. Four moisture gauges were installed on top of the subgrade to monitor the relative humidity at that location, as shown in Figure 3.15(d). The moisture gauges were 5tm soil moisture and temperature sensors manufactured by Decagon Devices, Inc. These moisture gauges measure the volumetric water content with high accuracy and with an operational temperature from -40°C to 60°C (-40°F to 140°F). Figure 3.16 shows the entire set of sensors after installation. It should be noted horizontal strain gauges were secured on the subgrade surface using an asphalt binder. The performance of the sensors was checked before and after installation. Strain gauges and pressure cells were connected to a data acquisition system and reviewed to determine their stability, responsiveness in the neutral condition, and external tension or compression stimulus. Calibration of the strain gauges and pressure sensors was performed individually following manufacturer specifications. Before paving the asphalt layers, loose asphalt mixture material was used to cover the sensors and then hand-compacted to protect the sensors from the construction process. Table 3.5 summarizes information on the gauges and pressure cells installed in the test sections.

Figure 3.12 Removal and repaving of HMA surface layers (Lanes 1 and 4).

Figure 3.13 Monitoring of pavement sensors during repaving operations.

The computer used for data acquisition is networked to two Vishay Micro-Measurement System 6000 scanners, as shown in Figure 3.17. Each scanner has 20 input channels, with the highest sampling rate of 10 kHz. By installing four thermocouple cards (model 6020), 20 strain gauge cards (model 6010), and 5 high-level cards (model 6030), 4 thermocouples, 18 strain gauges, and 5 load cells can be monitored at the same time.

3.5.2 Pavement Surface Profile Measurement Using Laser Profiler

An automated laser profile system was used to scan the pavement surface during loading. The pavement total rutting and individual layer rutting measurements

TABLE 3.4
Number of passes and asphalt mat densities

Asphalt Layer	Property	10-inch Dense-Graded	10-inch SMA	7-inch SMA	7-inch Dense-Graded
Surface	No. Passes	5	3	3	6
	Density (%)	92.3	92.0	93.0	93.6
Intermediate	No. Passes	2	3	4	3
	Density (%)	93.0	93.2	92.5	93.0
Base	No. Passes	4	4	4	3
	Density (%)	88.2	89.3	88.1	88.5

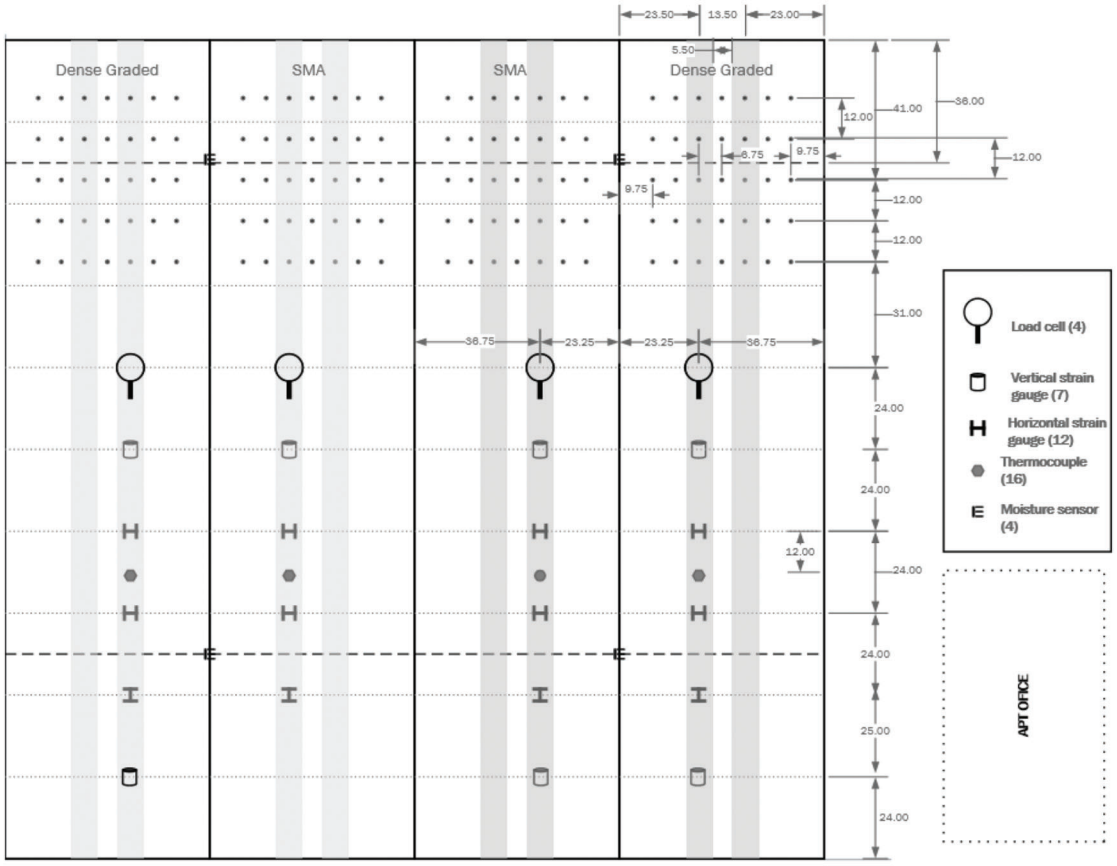

Figure 3.14 Instrumentation plan.

were obtained based on the measured profile. In this laser profiler system, a motor moves the laser gauge horizontally (north to south), and the wheel moves the system longitudinally (east to west). Once the transverse profile is requested, the wheel first moves the system to the desired longitudinal location, and then the motor drives the laser gauge to scan the requested transverse profile. Once the longitudinal profile is asked, the motor first moves the laser gauge to the desired transverse location, and then the wheel drives the laser gauge to scan the requested longitudinal profile. Through programming, the transverse and longitudinal profiles of a test lane can be measured at any desired location and at any time.

For this study, the system consisted of a Parker MPJ Series Motor and an Accurange AR700 laser distance gauge, shown in Figure 3.18(a, b), respectively. These devices were mounted beside the wheel assembly; the laser gauge was about 10 inches (25.4 cm) above the pavement surface, which was also approximately at the center of the laser gauge span, which was 6 inches (15.24 cm) as shown in Figure 3.19. The profile scan resolution was 0.16 mm (0.00630 inches)/data point with an accuracy of 0.15 mm (0.00590 inches).

Because most rutting occurs at the primary stage, the profile measurements were taken more frequently at the beginning of the load application. Table 3.6 provides the detailed profile measurement plan. Thirty-four sets

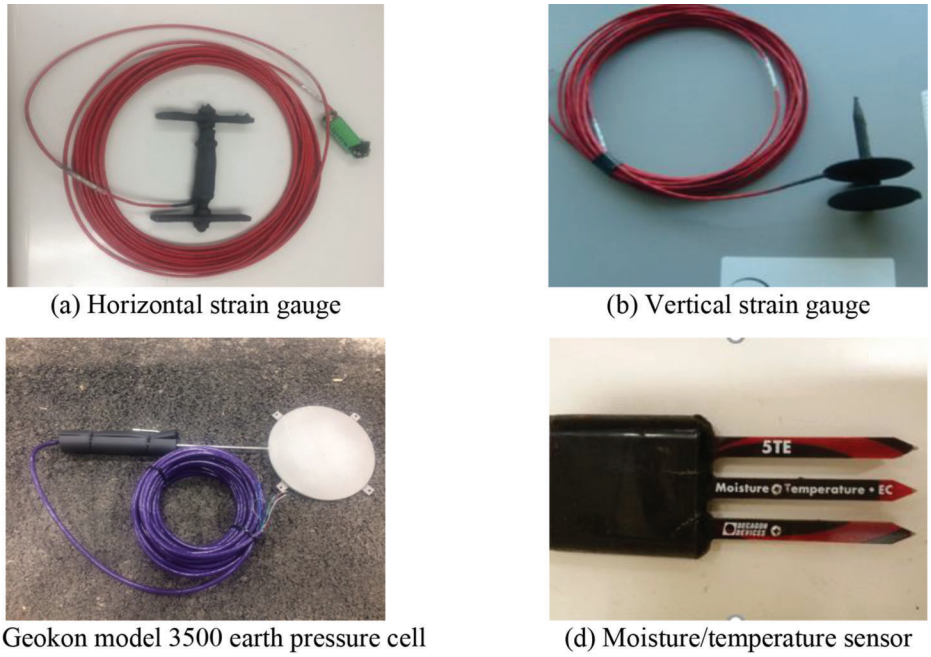

(a) Horizontal strain gauge (b) Vertical strain gauge

(c) Geokon model 3500 earth pressure cell (d) Moisture/temperature sensor

Figure 3.15 Sensor types.

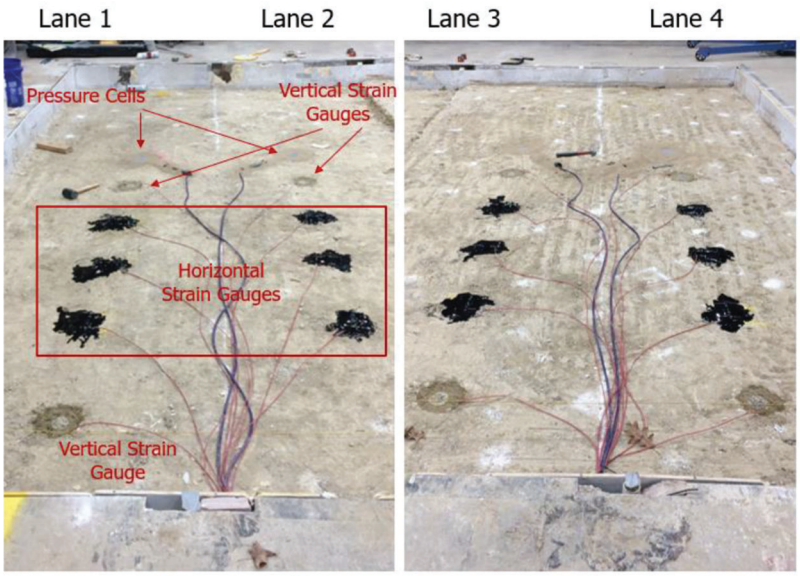

Figure 3.16 Installed APT instrumentation.

of profiles were taken for each test lane during 50,000 load applications. Each set contained five transverse profiles (P1-P5) located at the intact portion of the test lane and within the constant speed zone, as shown in Figure 3.20, and seven longitudinal profiles for the mid-depth rut measurements.

3.5.3 Monitoring Layer Deformation

A series of monitoring holes were drilled into the pavement surface to monitor the rutting within each layer. At least seven points (one point between the two tires, one point in the middle of each tire, one point on the outside of each tire, and one point further outside each tire) were required to reconstruct the layer's transverse profile interface under dual tire loading. Five sets of monitoring holes were drilled, one for each layer interface. By measuring the change in elevation at the bottom of the monitoring holes, each interface's profile could be calculated at the seven points transversely across the test lanes. These profiles could be used to determine the rutting that occurs in each layer.

It is essential to choose the correct spacing for monitoring holes to capture an interface profile. Ideally, each point should be positioned at either the highest point of upheaving or the lowest depression point, but these

TABLE 3.5
Gauge nomenclature

Lane	Sensor Type	Sensor Notation
Lane 1 (10 inches of dense-graded)	Vertical Strain Gauge	L1 S2
	Horizontal Strain Gauge	L1 S4
	Horizontal Strain Gauge	L1 S6
	Horizontal Strain Gauge	L1 S8
	Vertical Strain Gauge	L1 S10
	Pressure Cell	L1 S12
Lane 2 (10 inches of SMA)	Horizontal Strain Gauge	L2 S4
	Horizontal Strain Gauge	L2 S6
	Horizontal Strain Gauge	L2 S8
	Vertical Strain Gauge	L2 S10
	Pressure Cell	L2 S12
Lane 3 (7 inches of SMA)	Vertical Strain Gauge	L3 S2
	Horizontal Strain Gauge	L3 S4
	Horizontal Strain Gauge	L3 S6
	Horizontal Strain Gauge	L3 S8
	Vertical Strain Gauge	L3 S10
	Pressure Cell	L3 S12
Lane 4 (7 inches of dense-graded)	Vertical Strain Gauge	L4 S2
	Horizontal Strain Gauge	L4 S4
	Horizontal Strain Gauge	L4 S6
	Horizontal Strain Gauge	L4 S8
	Vertical Strain Gauge	L4 S10
	Pressure Cell	L4 S12

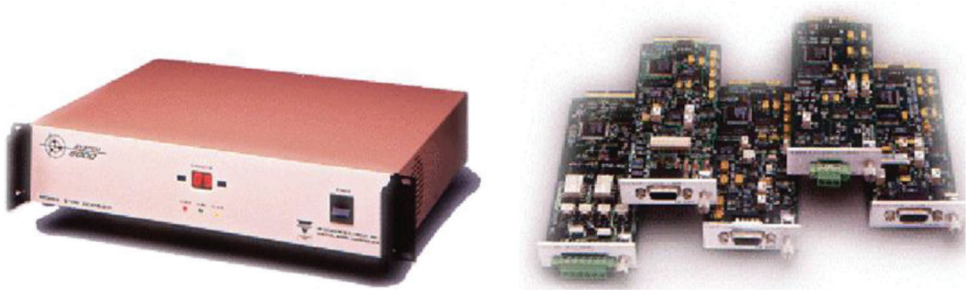

Figure 3.17 Vishay Micro-Measurements System 6000.

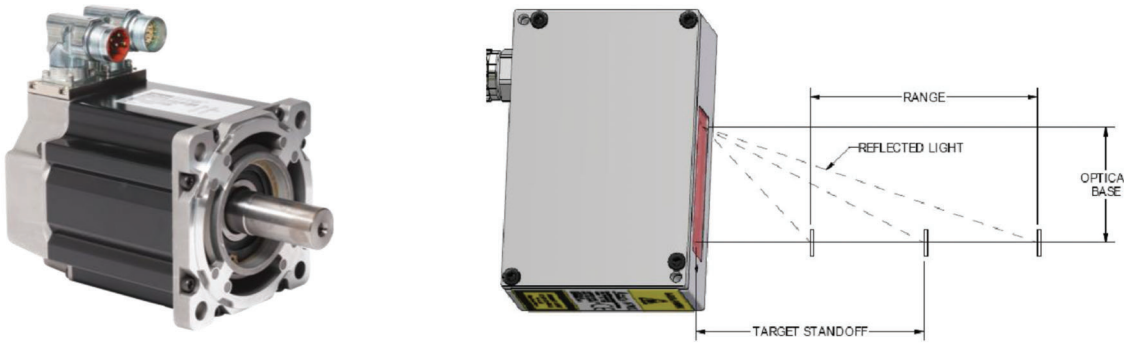

(a) Parker MPJ Series Motors (b) Accurange AR700 laser distance gauge

Figure 3.18 Laser profile system components.

locations are difficult to determine *a priori*. For this study, as the best estimate based on a similar previous project, monitoring hole spacing of 6.75 inches (17.15 cm) was deemed appropriate. Five sets of holes were drilled in all lanes. Figure 3.21 provides a longitudinal cross-section view of the monitoring holes in the pavement structure. Laser pointers were used to ensure that the monitoring holes were aligned perfectly with the laser profiler and were drilled perpendicular to the surface. The monitoring holes were 1.5 inches (3.81 cm) in diameter. Steel conduit was inserted inside the monitoring holes to protect them from collapsing during loading. During loading, it was anticipated that the holes could become slightly skewed from their perpendicular orientation due to the shear failure of the asphalt layers. Because the holes were only 1.5 inches (3.81 cm) in diameter, any such skew might prohibit the laser profiler from correctly reading the bottom of the monitoring holes. To alleviate this possibility, steel rods were inserted in the monitoring holes such that the tops of the rods were 1 inch below the layer surface (see Figure 3.22).

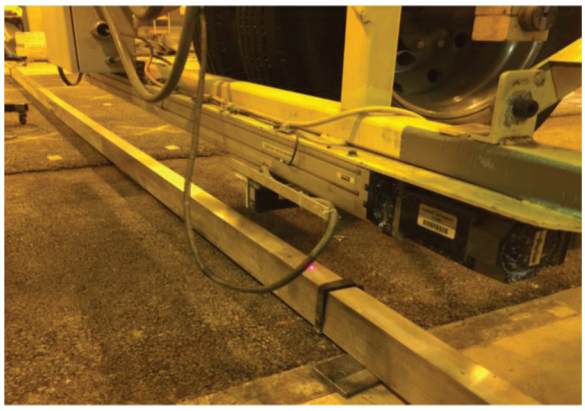

Figure 3.19 Automated laser profile system.

3.5.4 Pavement Structure Evaluation Using Falling Weight Deflectometer

The FWD is widely used to evaluate pavement structures and determine *in situ* modulus values. The FWD applies an impact force to a circular plate placed on the pavement's surface and measures the resulting deflections at the center of the load and fixed radii from the loading center. Deflections at the load center represent the overall structural capacity of the pavement. A set of pavement deflections can be used to back-calculate pavement layer modulus. In this study, the FWD test was performed following ASTM D4694-09,

TABLE 3.6
Profile measurement plan

Number	Load Application	Number	Load Application	Number	Load Application
1	0	13	900	25	17,500
2	25	14	1,000	26	20,000
3	50	15	1,500	27	22,500
4	75	16	2,000	28	25,000
5	100	17	2,500	29	27,500
6	200	18	3,000	30	30,000
7	300	19	4,000	31	35,000
8	400	20	5,000	32	40,000
9	500	21	7,500	33	45,000
10	600	22	10,000	34	50,000
11	700	23	12,500	–	–
12	800	24	15,000	–	–

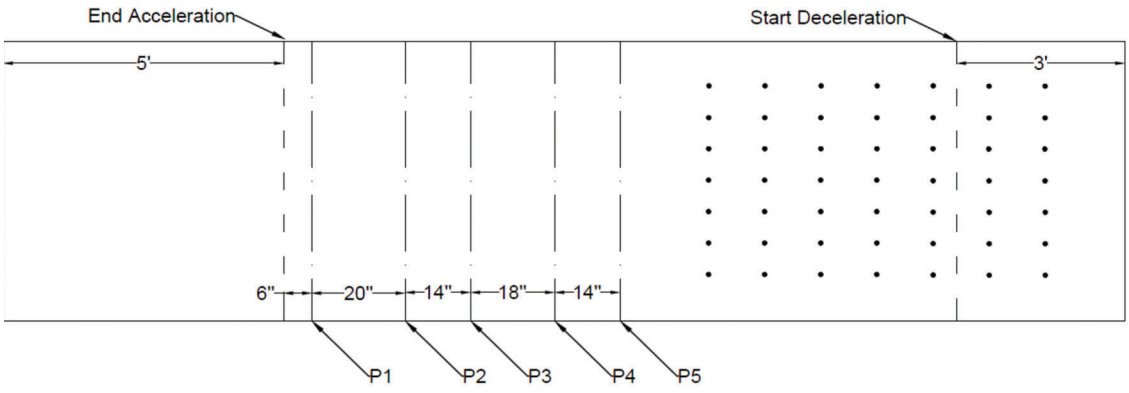

Figure 3.20 Transverse surface profile locations.

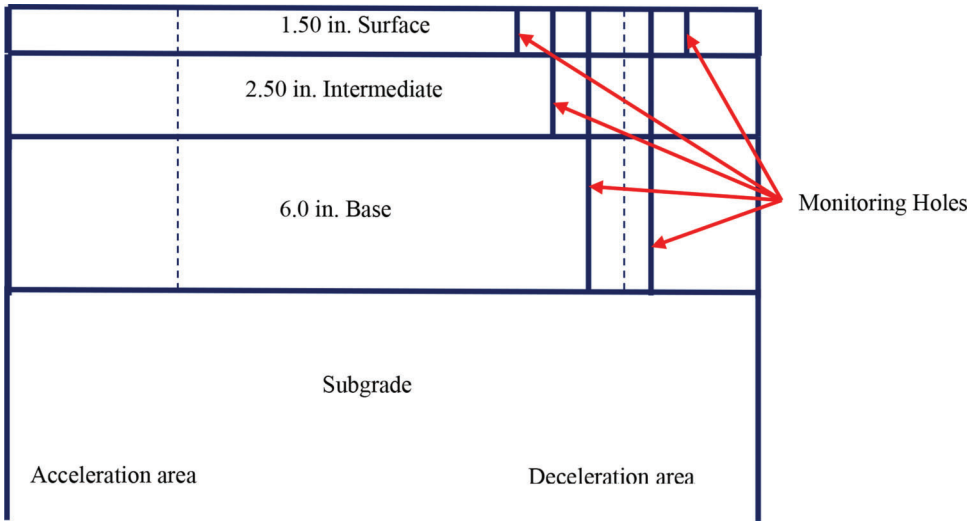

Figure 3.21 Longitudinal cross-section view of monitoring holes in the pavement structure.

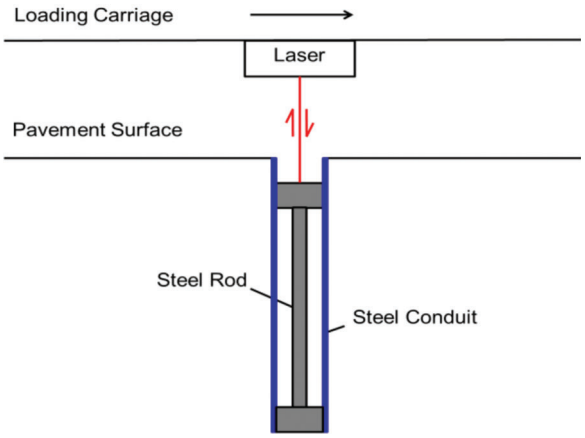

Figure 3.22 Laser measurements of monitoring holes.

Standard Test Method for Deflections with a Falling-Weight-Type Impulse Load Device (ASTM D4694-09, 2015), before and after APT trafficking at each test lane. Test locations were chosen at the sites where strain gauges or load cells were embedded. One set of FWD load drops consisted of three load levels (i.e., 7,000 lb., 9,000 lb., 11,000 lb., or 3,175 kg, 4,082 kg, and 4,989 kg), and three sets of FWD load drops were applied at each test location.

4. APT TEST RESULTS AND INTERPRETATION

4.1 Permanent Deformation at Surface

4.1.1 Rut Depth

Permanent deformation of pavement surface can be determined using the transverse profile of pavement surface. The transverse profile represents the pavement surface's elevation for an imaginary datum about 225 mm (8.86 inches) below the pavement surface. A laser scanner with a high resolution and accuracy of 0.15 mm (0.00590 inches) and 0.16 mm (0.00630 inches)/data point was used to collect the surface profile data. Figure 4.1 shows a sample of change in transverse profile for a different number of APT passes. In this study, two parameters are used to describe pavement surface rutting. As shown in Figure 4.1, the first parameter is rut depth defined and determined based on AASHTO R48, *Standard Practice for Determining Rut Depth in Pavements* (AASHTO R48-10, 2013). Local agencies have widely used this definition in their pavement management system (PMS) for pavement evaluation. In Figure 4.1, R_o and R_i are rut depths of outside and inside wheel paths, respectively. The second parameter is the permanent deformation, characterized as the maximum difference in elevation caused by APT loading between the original and deformed pavement surface. When the deformed surface is lower than the original surface, permanent deformation is negative; that is, depression is apparent.

Table 4.1 summarizes the total rut depth after 50,000 APT load applications obtained from five different measurement locations (P1 to P5) for all pavement lanes. The previous project (SPR-3307) results have been added to have a more comprehensive rut depth analysis (15.5-inch dense-graded, 15.5-inch SMA, 12.5-inch dense-graded, and 12.5-inch SMA).

Additionally, Figure 4.2 shows the rut depth results based on the surface layer type, i.e., dense-graded HMA and SMA. For SMA pavements, the pavement with higher thickness shows a better rutting performance. Although there is a considerable reduction in rut depth from 10-inch SMA to 12.5-inch SMA pavements, the rut depth difference between the 12.5 inches of SMA and the 15.5 inches of SMA is negligible. There is no specific trend for HMA pavements as the rut depth increases from pavement thickness of 7 inches to 10 inches and decreases from 10 inches to 12.5 inches. However, there is a noticeable reduction in rut depth when dense-graded HMA pavement thickness increases from 10 inches to 12.5 inches. Also, regardless of the

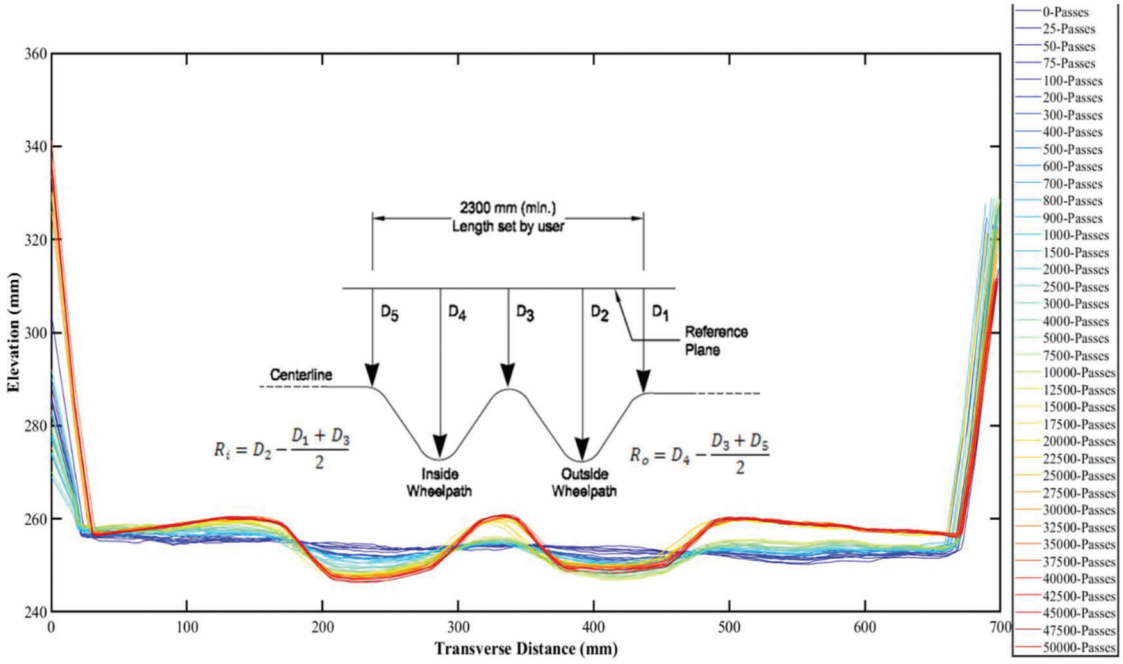

Figure 4.1 Sample transverse profile.

TABLE 4.1
Rut depth summary

		Rut Depth (mm)							
		Current Project (SPR-4212)				Previous Project (SPR-3307)			
Measurement Location		**10-inch Dense**	**10-inch SMA**	**7-inch SMA**	**7-inch Dense**	**15.5-inch Dense**	**15.5-inch SMA**	**12.5-inch SMA**	**12.5-inch Dense**
North Wheel	P1	-30.76	-13.92	-13.01	-24.44	-8.32	-4.55	-4.98	-8.37
	P2	-26.14	-12.83	-11.99	-19.3	-8.76	-4.25	-4.65	-8.18
	P3	-29.68	-12.26	-11.46	-16.97	-8.48	-4.53	-4.96	-7.59
	P4	-26.46	-11.69	-10.93	-21.33	-8.54	-5.26	-5.75	-8.86
	P5	-23.92	-9.53	-8.91	-20.13	-8.86	-4.68	-5.12	-8.99
South Wheel	P1	-29.05	-16.99	-15.88	-28.62	-8.41	-5.85	-6.4	-6.84
	P2	-24.74	-17.22	-16.09	-28.34	-8.17	-4.24	-4.64	-7.19
	P3	-31.3	-14.78	-13.81	-21.2	-7.23	-4.56	-4.99	-6.48
	P4	-24.26	-11.06	-10.34	-16.84	-7.35	-5.6	-6.13	-6.8
	P5	-17.62	-11.32	-10.58	-16.03	-7.91	-4.38	-4.79	-7.29
Mean		*-26.39*	*-13.16*	*-12.3*	*-21.32*	*-8.2*	*-4.79*	*-4.79*	*-5.24*
Standard Deviation		*3.892*	*2.417*	*2.264*	*4.299*	*0.552*	*0.661*	*0.552*	*0.627*

pavement thickness, there is a substantial difference between SMA and HMA pavements' rut depth values. The amount of reduction (%) in rut depth from HMA to SMA pavements for 7-inch, 10-inch, 12.5-inch, and 15.5-inch pavement thickness is 42%, 50%, 28%, and 42%, respectively (see Figure 4.3). Results of rut depth evolution with APT load passes for all test pavements are presented in Appendix B.

Moreover, to statistically compare the rut depth results obtained from all tested pavements, a t-test was performed. The results of the t-test indicate that except for two pair pavements of (15.5-inch and 12.5-inch dense-graded HMA pavements) and (15.5-inch and 12.5-inch SMA pavements), there is a significant difference between the values of rut depth for each pair of pavements.

4.1.2 Permanent Deformation for Individual Layers

Two parameters, including permanent deformation and percentage of layer contribution in total permanent deformation, characterize layer-wise deformation.

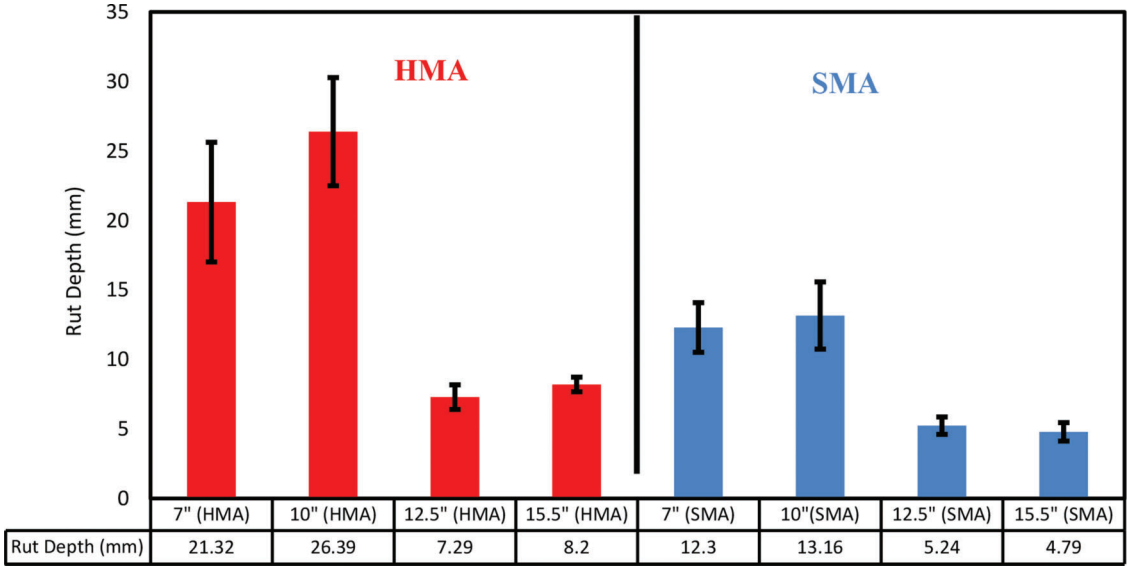

Figure 4.2 Results of rut depth.

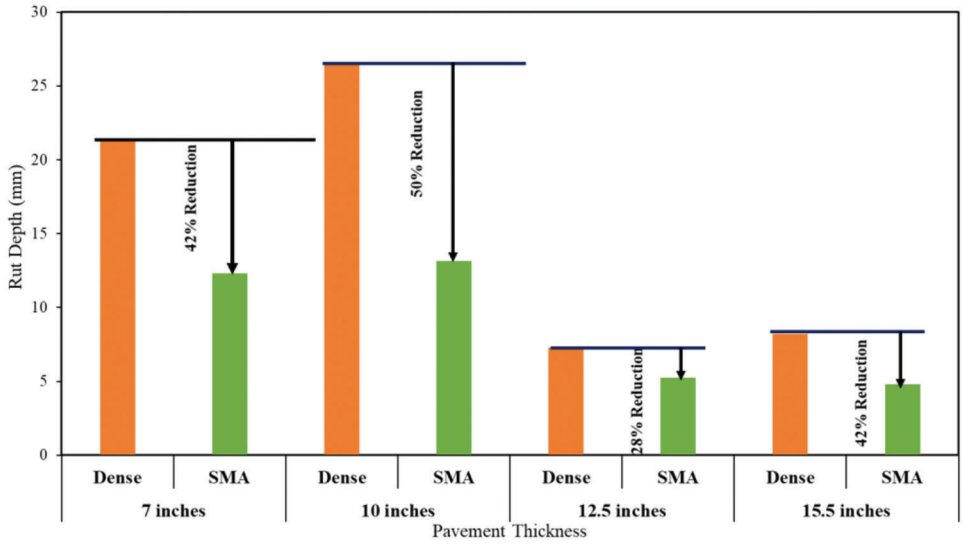

Figure 4.3 Reduction (%) in rut depth values from dense-graded HMA to SMA for different pavement thicknesses.

The mid-depth rut is defined as the difference in elevation between the original and the deformed interfaces at each depth. A negative value indicates depression, which means that the elevation has decreased. Layer permanent deformation values were obtained by subtracting the elevation change in the layer's bottom interface from the top interface. The layer contribution (%) represents how much each pavement layer contributes to each pavement lane's total permanent deformation. The subgrade permanent deformation was calculated based on the assumption that the bottom interface of the subgrade layer was not deformed at all.

Figures 4.4, 4.5, 4.6, and 4.7 provide the mid-depth rut data for 10-inch dense-graded HMA, 10-inch SMA, 7-inch SMA, and 7-inch dense-graded HMA pavements. A series of rutting prediction models based on logarithmic regression has also been developed and presented. These prediction models have been used to create each layer's permanent deformation evolution to minimize the effects of the measurement's accuracy-related error.

The results of permanent layer deformation are presented in Figure 4.8 for all pavement lanes. It shows that the surface layer's permanent deformation for SMA pavements is lower than that for HMA pavements with the same thickness. However, for other under layers, the amount of deformation in SMA pavement is higher than that in HMA pavements. For example, the permanent deformation of subgrade in SMA pavement is almost double that for the HMA pavement with the same thickness.

Figure 4.9 presents the distribution of the permanent deformation within the pavement layers. The surface layer has a higher contribution to the permanent

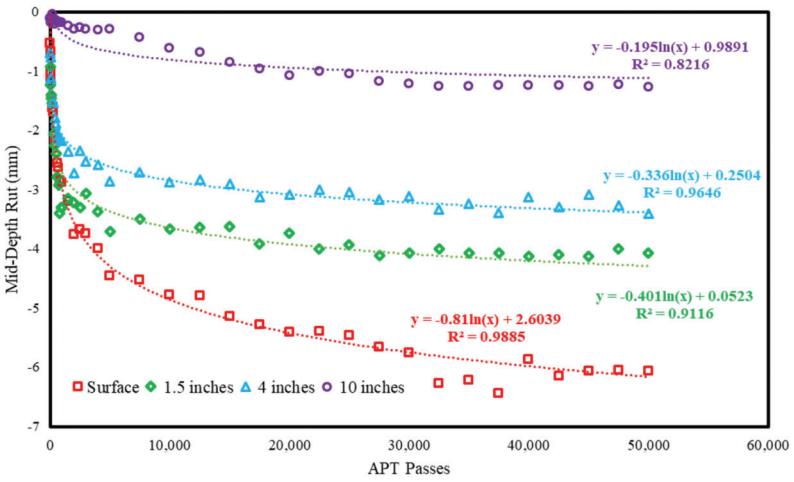

Figure 4.4 Mid-depth ruts for 10-inch dense-graded HMA lane (Lane 1).

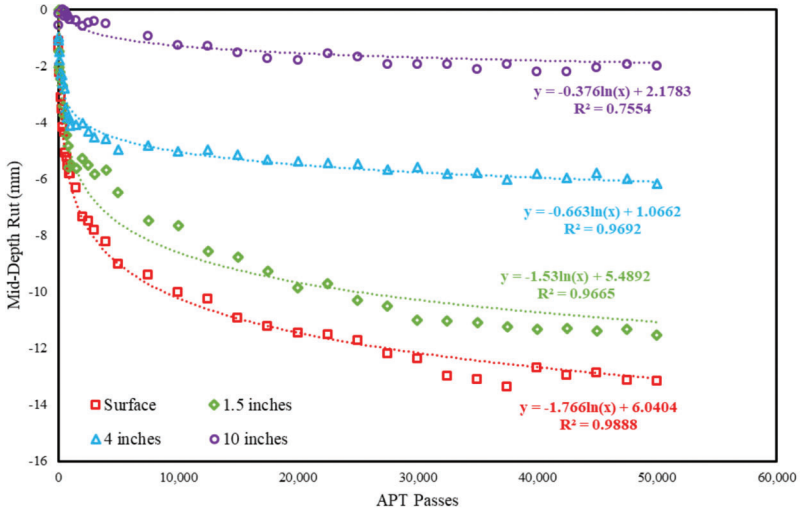

Figure 4.5 Mid-depth ruts for 10-inch SMA lane (Lane 2).

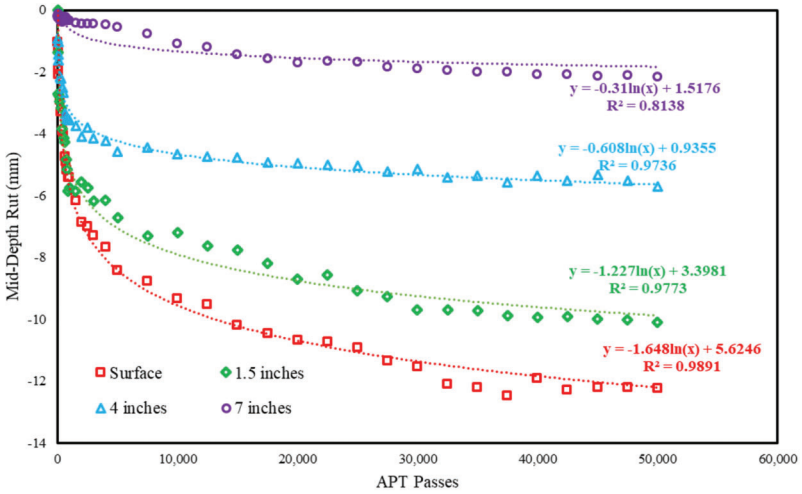

Figure 4.6 Mid-depth ruts for 7-inch SMA lane (Lane 3).

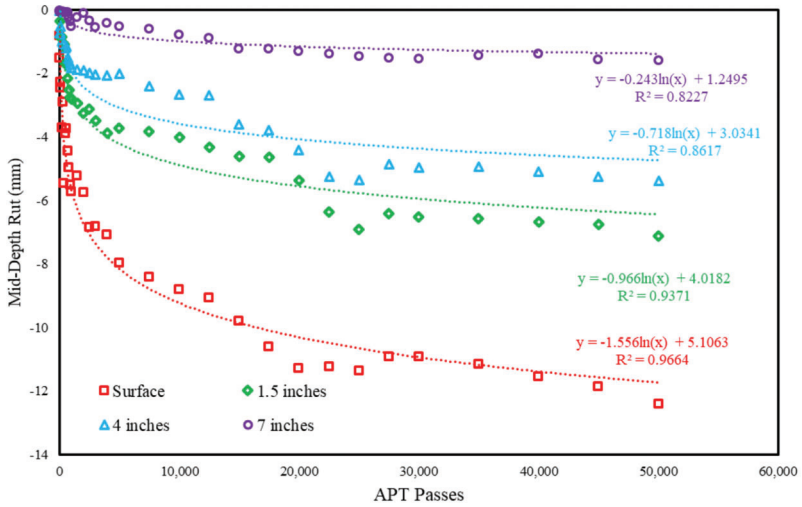

Figure 4.7 Mid-depth ruts for 7-inch dense-graded HMA lane (Lane 4).

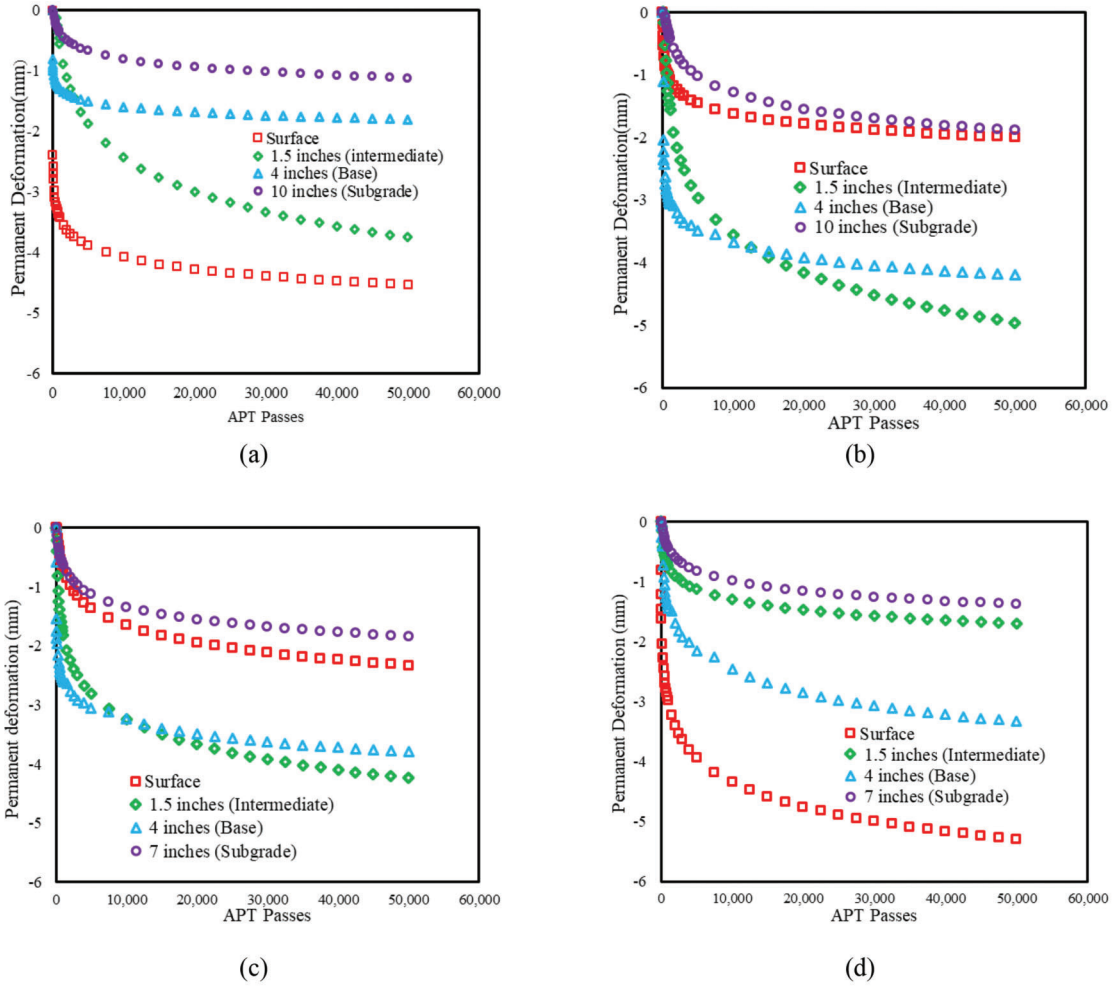

Figure 4.8 Permanent deformation evolution for (a) 10-inch dense-graded HMA, (b) 10-inch SMA, (c) 7-inch SMA, and (d) 7-inch dense-graded HMA pavement lanes.

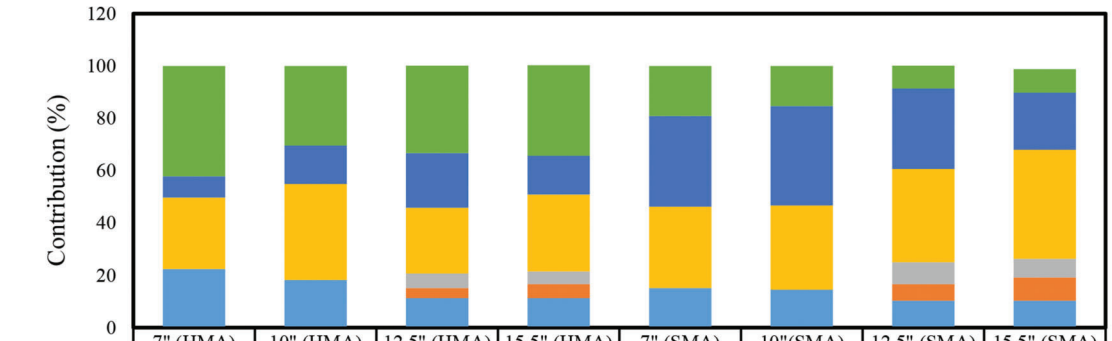

	7" (HMA)	10" (HMA)	12.5" (HMA)	15.5" (HMA)	7" (SMA)	10"(SMA)	12.5" (SMA)	15.5" (SMA)
Surface	42.2	30.4	33.4	34.6	19.1	15.3	8.7	9
Intermediate	8.1	14.7	20.9	14.8	34.7	38	30.8	21.8
Upper Base	27.3	36.7	25.1	29.4	31.1	32.2	35.6	41.7
OG			5.6	4.8			8.4	7.1
Lower base			3.8	5.4			6.3	8.9
Subgrade	22.4	18.2	11.3	11.3	15.1	14.5	10.3	10.3

Figure 4.9 Layer-wise permanent deformation distribution.

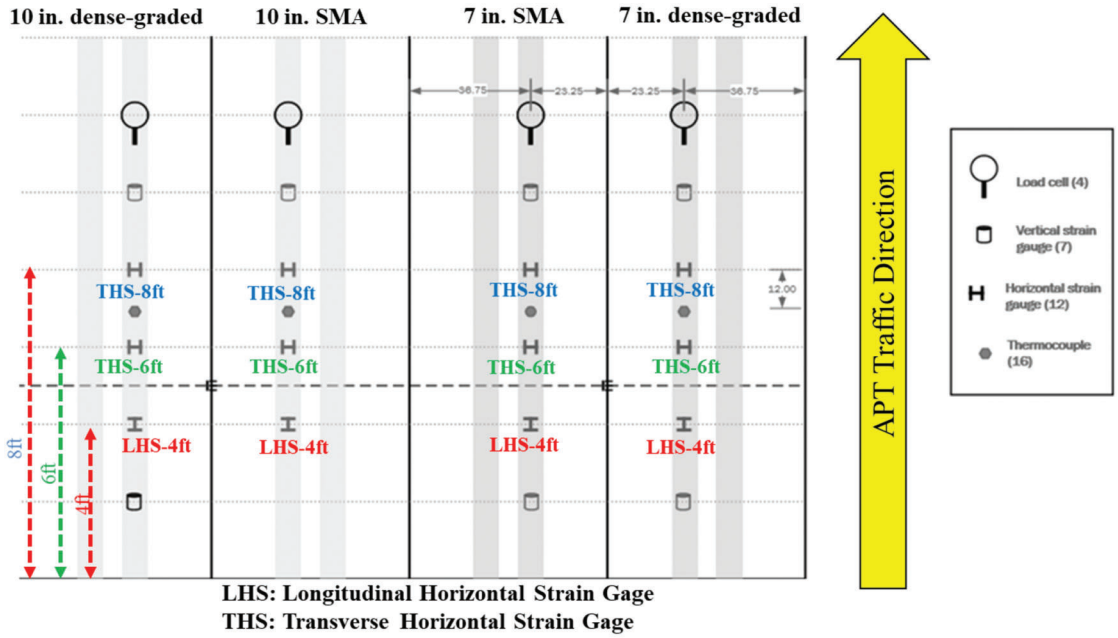

Figure 4.10 Location of strain gages.

deformation of HMA pavements than the other layers. The main rutting occurred at the upper asphalt concrete layers, with about half of the total rutting observed within the pavement's top 4 inches. However, in SMA pavements, the intermediate and base layers' contribution is the most, as it includes more than 50% of total rutting. SMA's have more excellent rutting resistance as a surface layer than the dense-graded HMA mix; the amount of rutting in the SMA surface courses is reduced by an average of 70% compared to HMA surface layers. Therefore, most of the rutting comes from the closest layer to the surface, i.e., the intermediate layer. The results also showed that the subgrade deformation persisted at a very low degree, regardless of pavement thickness and paving material; only about 12% of the subgrade rutting occurred.

4.2 Strain Data Analysis

As mentioned earlier, in this study, three horizontal and two vertical strain gages were installed on top of the subgrade soil for all pavement lanes. The distance of horizontal strain (HS) gages from the beginning of each lane was 4, 6, and 8 ft, while the vertical strain gages were at 2 and 10 ft from the beginning of the lane. HS's position at 4 ft was longitudinal (LHS), while HS's position located at 6 and 8 ft from the beginning of the lane was transverse (see Figure 4.10). After the

completion of construction, it was found that both two vertical strain gages for lanes were dead; therefore, the results of horizontal strain gages are presented and addressed in this report. The first part of this section covers the evolution of strain data during the APT test. The second part gives the strain results from the falling weight deflectometer (FWD) test conducted before and after the APT test at three load levels of 7, 9, and 11 kips.

4.2.1 Strain Evolution from the APT Test

For each APT test day, the strain data was collected at the first and last twenty APT passes. Table 4.2 shows the schedule that was followed for the APT test. Figure 4.11(a) shows a sample strain data obtained from LHS-4 ft of 10-inch dense-graded HMA pavement lane. Two envelope lines, peak and permanent residual strains are developed and used to calculate the absolute value of strain for each APT pass. The evolution of strain after 125 APT passes for LHS-4 ft of 10-inch dense-graded HMA pavement lane is also shown in Figure 4.11(b). The permanent residual strain is used to evaluate pavement behavior after the completion of 50,000 APT passes. Figures 4.12, 4.13, and 4.14 display the evolution of permanent residual strain. The polynomial curve fitting of degree 5 was applied to the original data to have a continuous and smooth evolution line. Compared to SMA pavements, the results indicated that the dense-graded HMA pavements demonstrate higher horizontal permanent residual strain.

4.2.2 Strain Results from FWD test

For the FWD test, the strain value is defined as a difference between the strain at unloading and loading conditions (see Figure 4.15). Results of horizontal strain from the FWD test before and after the APT test are shown in Figures 4.16, 4.17, 4.18, and 4.19. Additionally, the strain value from the first and last twenty APT passes are added as before and after the APT test, respectively. The test temperature for the FWD test was the same as the APT test (118°F at a 1.5-inch depth). It can be seen that SMA pavements have lower strain compared to HMA pavements. As expected, a higher load resulted in a higher strain. Regardless of pavement type and thickness, the APT test's strain values are higher than after the APT test. However, the FWD test results do not show any specific trend before and after the APT test condition. For 10-inch dense-graded HMA pavement, FWD's strain values before the APT test is higher than those after the APT test. However, the rest of the pavement lanes (10-inch SMA, 7-inch SMA, and 7-inch dense-graded HMA) display an opposite behavior (FWD's strain values before the APT test are lower than those after the APT test). A comparison between FWD (9 kips) and APT (9 kips) strain values indicates that the APT produces a higher strain than FWD does.

4.3 Pavement Structure Evaluation Using Falling Weight Deflectometer

The test sections were kept at a high temperature during the entire testing period. When a test lane was being loaded, eight heating panels were used to heat the test lane to 118°F (47.78°C) at a 1.5-inch (3.81 cm) depth. Leaving asphalt concrete in this environment for such a long time could cause the material to become aged or conditioned. As a result, the material could harden, and the degree of hardening varies and depends on the aging time. To account for the effect of hardening properly, FWD tests were performed to quantify the hardening amount during APT loading. All four lanes were used to evaluate the hardening effects at 118°F (47.78°C) due to the heating panels.

TABLE 4.2
APT test schedule for each pavement lane

APT Test Day	Passes Applied	Cumulative Passes	APT Test Day	Passes Applied	Cumulative Passes
1	25	25	8	500	3,000
1	25	50	9	1,000	4,000
1	25	75	10	1,000	5,000
1	25	100	11	2,500	7,500
2	100	200	12	2,500	10,000
2	100	300	13	2,500	12,500
3	100	400	14	2,500	15,000
3	100	500	15	2,500	17,500
4	100	600	16	2,500	20,000
4	100	700	17	2,500	22,500
4	100	800	18	2,500	25,000
4	100	900	19	2,500	27,500
5	100	1,000	20	2,500	30,000
5	500	1,500	21	5,000	35,000
6	500	2,000	22	5,000	40,000
7	500	2,500	23	5,000	45,000
8	500	3,000	24	5,000	50,000

It should be noted that the FWD tests were performed above the location of strain gauges and pressure cells of each test lane before and after APT loading. The results of deflection under the center of the FWD load plate are provided in Figure 4.20.

The results show that the deflection values before APT loading are higher than those after APT loading. Statistical analyses have also indicated that the difference between deflections before and after APT loading is significant for all lanes.

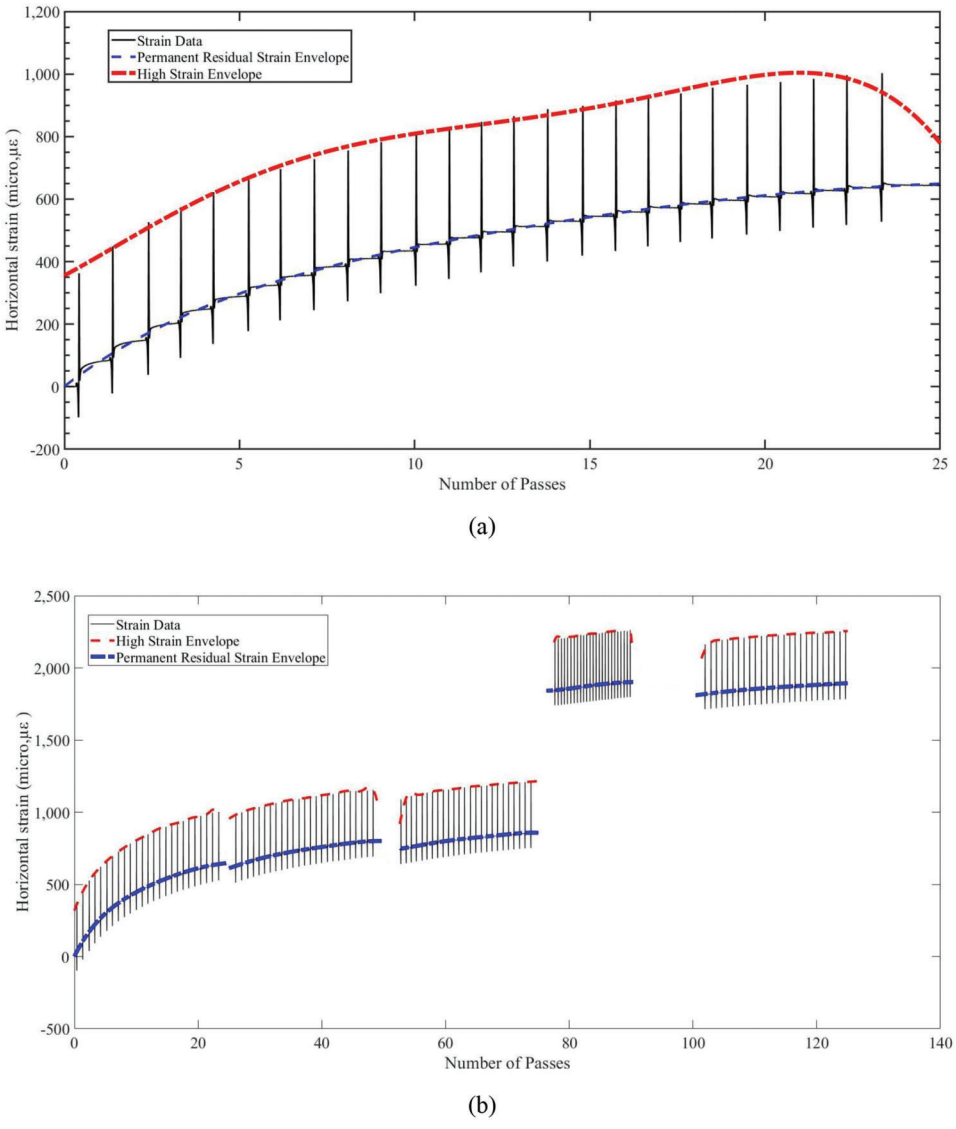

Figure 4.11 (a) A sample of strain data for the first twenty APT passes and (b) change in strain data after finishing 125 APT passes.

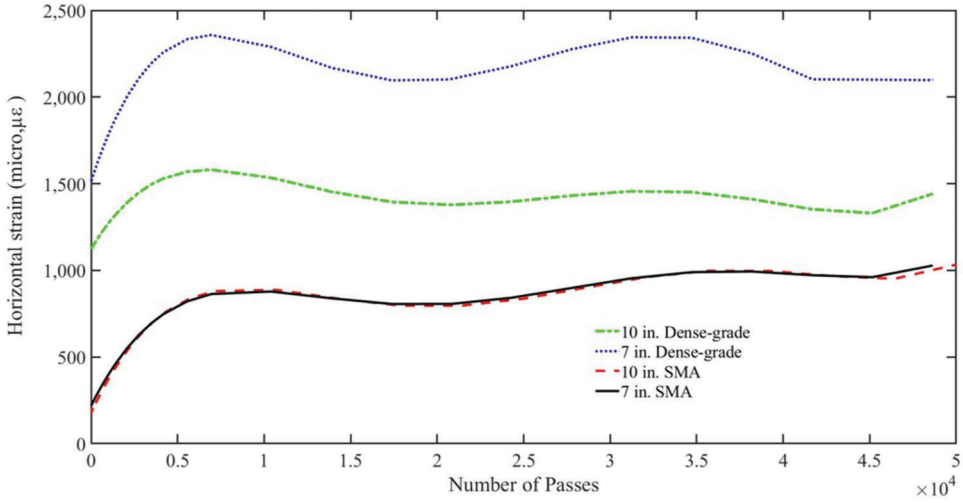

Figure 4.12 Permanent residual strain for LHS-4 ft.

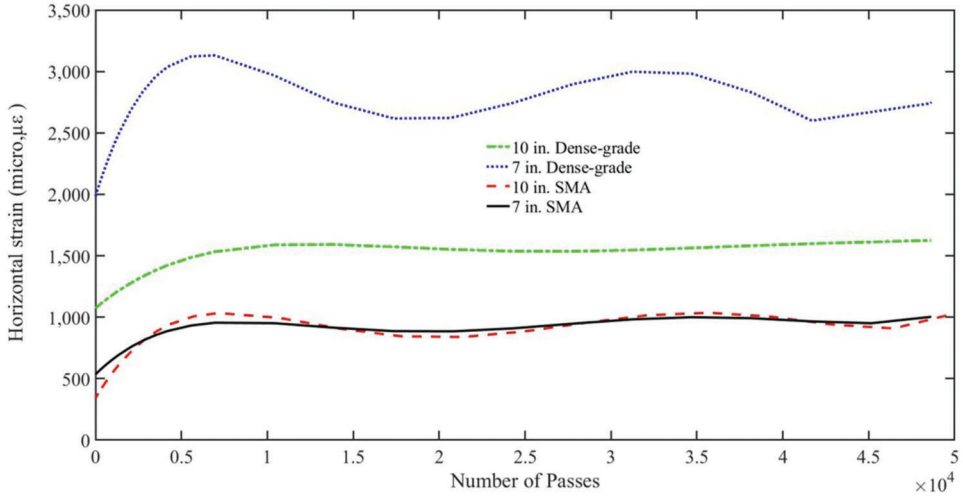

Figure 4.13 Permanent residual strain for THS-6 ft.

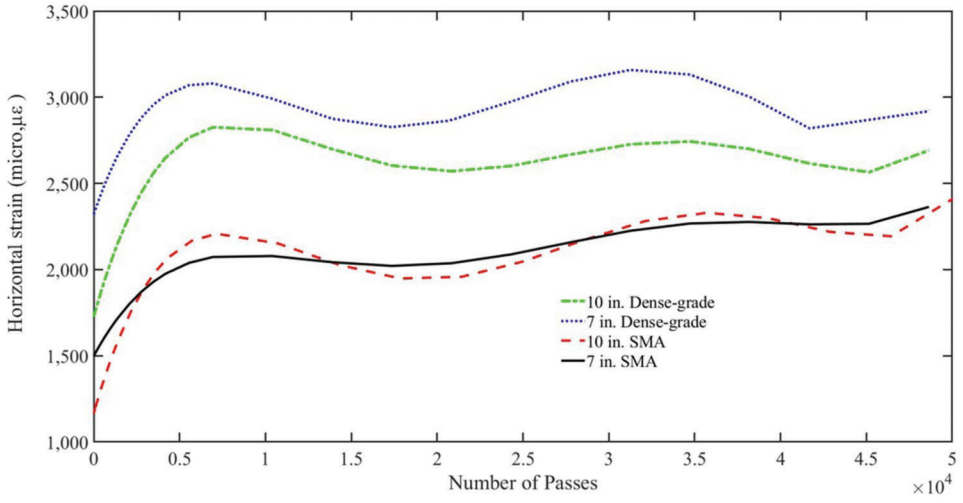

Figure 4.14 Permanent residual strain for THS-8 ft.

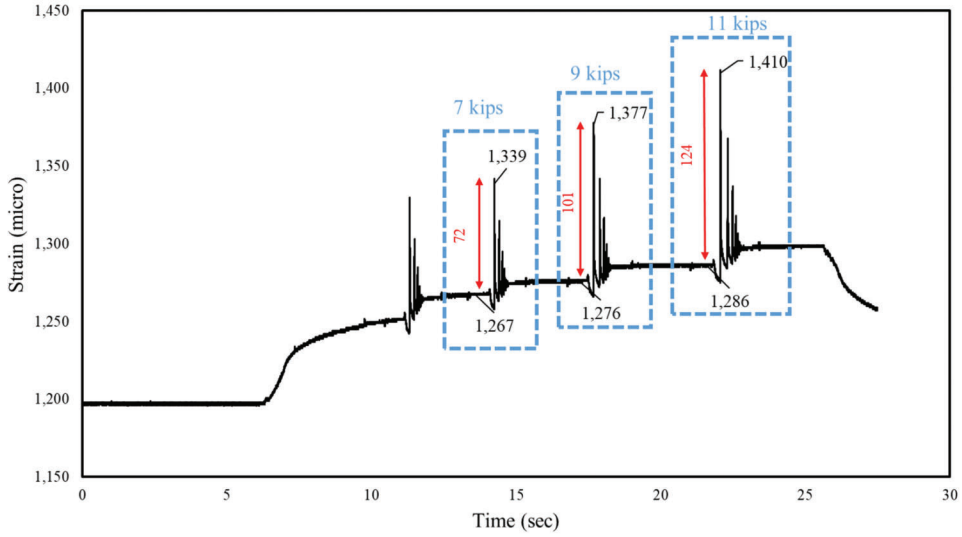

Figure 4.15 Example of strain calculation from FWD test.

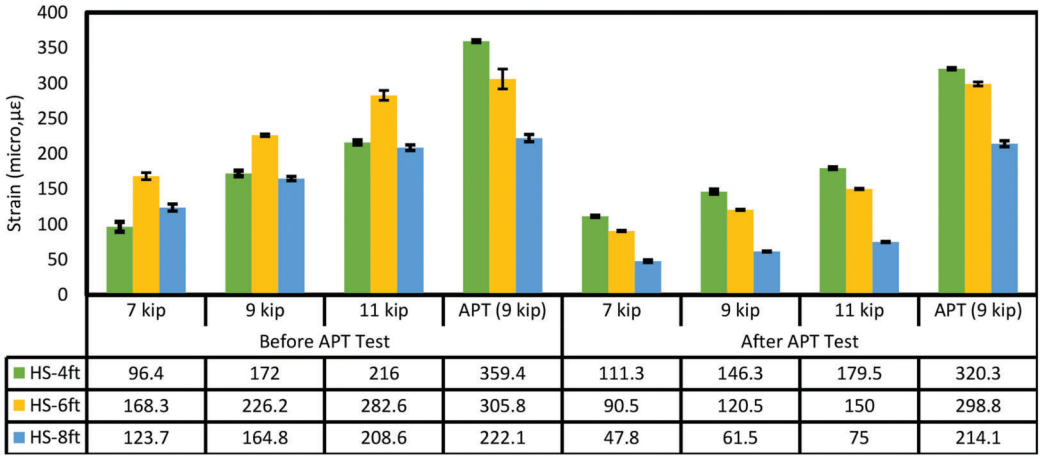

	7 kip	9 kip	11 kip	APT (9 kip)	7 kip	9 kip	11 kip	APT (9 kip)
	Before APT Test				After APT Test			
HS-4ft	96.4	172	216	359.4	111.3	146.3	179.5	320.3
HS-6ft	168.3	226.2	282.6	305.8	90.5	120.5	150	298.8
HS-8ft	123.7	164.8	208.6	222.1	47.8	61.5	75	214.1

Figure 4.16 Strain data from FWD and APT for 10-inch dense-graded HMA pavement.

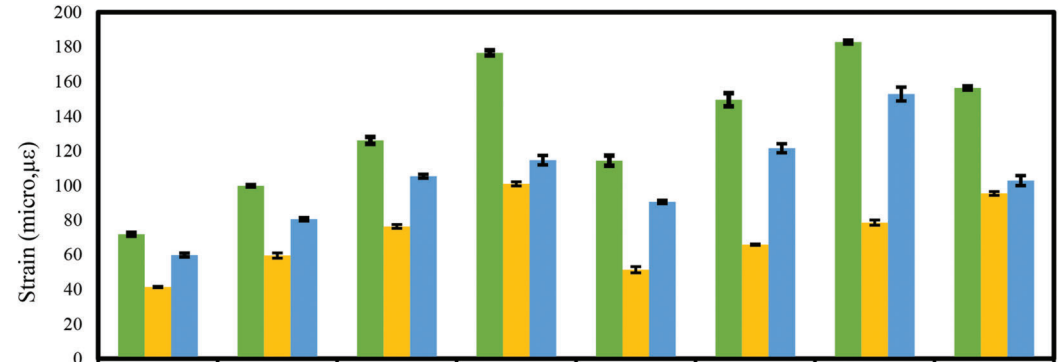

	7 kip	9 kip	11 kip	APT (9 kip)	7 kip	9 kip	11 kip	APT (9 kip)
	Before APT Test				After APT Test			
HS-4ft	71.8	99.8	126	176.6	114.3	149.5	182.8	156.3
HS-6ft	41.3	59.5	76.3	100.9	51.3	65.8	78.5	95.4
HS-8ft	59.8	80.5	105.3	114.6	90.5	121.5	152.8	102.8

Figure 4.17 Strain data from FWD and APT for 10-inch SMA pavement.

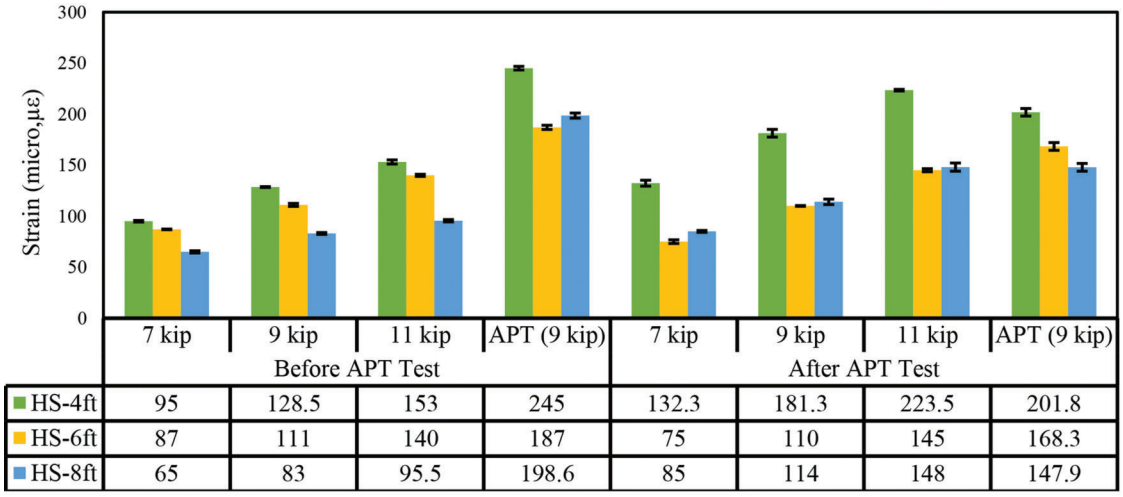

	7 kip	9 kip	11 kip	APT (9 kip)	7 kip	9 kip	11 kip	APT (9 kip)
	Before APT Test				After APT Test			
HS-4ft	95	128.5	153	245	132.3	181.3	223.5	201.8
HS-6ft	87	111	140	187	75	110	145	168.3
HS-8ft	65	83	95.5	198.6	85	114	148	147.9

Figure 4.18 Strain data from FWD and APT for 7-inch SMA pavement.

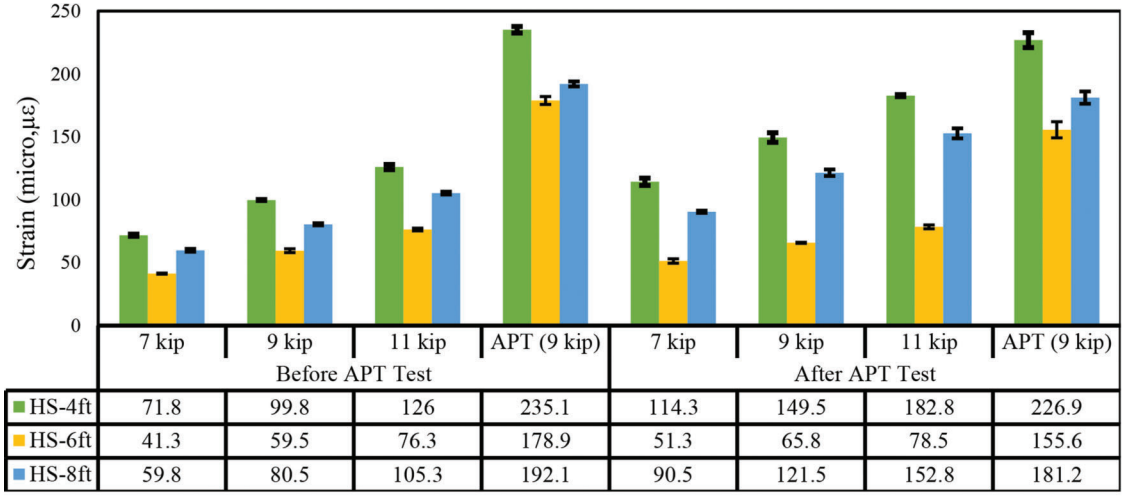

	7 kip	9 kip	11 kip	APT (9 kip)	7 kip	9 kip	11 kip	APT (9 kip)
	Before APT Test				After APT Test			
HS-4ft	71.8	99.8	126	235.1	114.3	149.5	182.8	226.9
HS-6ft	41.3	59.5	76.3	178.9	51.3	65.8	78.5	155.6
HS-8ft	59.8	80.5	105.3	192.1	90.5	121.5	152.8	181.2

Figure 4.19 Strain data from FWD and APT for 7-inch dense-graded HMA pavement.

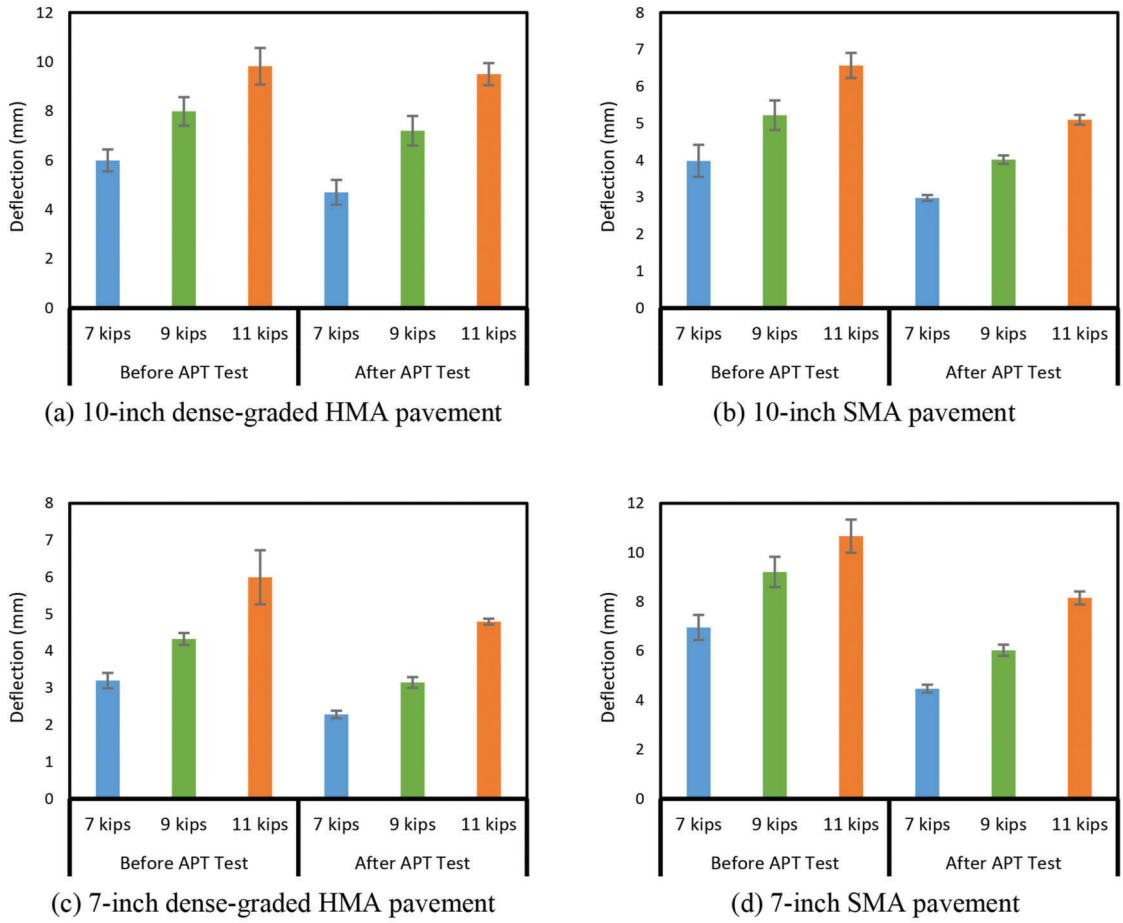

Figure 4.20 Falling weight deflectometer deflections under the center of FWD load plate for all tested lanes.

5. MEPDG VERIFICATION

5.1 Introduction

In SPR-3307, an effort to calibrate the MEPDG rutting model for Indiana pavements was made using eight local field projects and five APT sections. The APT sections were thick full-depth asphalt pavements with 12.5- and 15.5-inch' thickness. One of this study's objectives is to determine if the MEPDG calibrated model is applicable for thin full-depth pavements (i.e., the 7-inch and 10-inch thick full-depth pavements) using Pavement ME Design version 2.3.

As discussed in Chapter 1, the MEPDG uses hierarchical input levels based on the designer's knowledge and the input parameters' availability. The following three input levels are used to characterize the material and traffic properties (Applied Research Associates, 2004).

- Level 1 is the highest input level in which all parameters are measured directly from laboratory or field tests.
- Level 2 input parameters are calculated from other site-specific data or information using correlations or regression equations.
- Level 3 input parameters are estimated from global or regional default values.

The input level selection depends on current test capabilities, construction specifications, and data collection procedures. The input level for the local calibration process should be consistent with the future pavement design and analysis. The MEPDG local calibration is sensitive to input parameters and significantly influences the accuracy and precision of calibrated transfer functions.

5.2 Input Parameters

5.2.1 Climate Data

5.2.1.1 Input Data Requirements. The MEPDG considers the environmental effects on the material properties and pavement responses in a sophisticated manner. Because asphalt is a viscoelastic material, its properties depend directly on the temperature. The MEPDG can update HMA modulus values every hour due to real-time changes in temperature. It integrates a climatic model, the EICM, to calculate the temperature and moisture content within each pavement layer and the subgrade soil on an hourly basis throughout the pavement design life. The EICM consists of the following three primary models.

- The Climatic Materials Structural (CMS) Model developed at the University of Illinois (Dempsey et al., 1985).
- The CRREL Frost Heave and Thaw Settlement Model (CRREL Model) developed at the United States Army Cold Regions Research and Engineering Laboratory (Guymon et al., 1986).
- The Infiltration and Drainage (ID) Model developed at Texas A&M University (Lytton et al., 1990).

Both temperature and moisture content have a significant impact on unbound materials. The month when the material is frozen can be determined by calculating the temperatures within the unbound material. Its resilient modulus can thus be adjusted according to freeze or thaw periods. The resilient modulus also can be adjusted in terms of the average monthly moisture content relative to the optimum moisture content.

The EICM provides three outputs throughout the pavement design life for each pavement sublayer: (1) an unbound material resilient modulus adjustment factor, (2) the temperature at the surface and midpoint of each sublayer on an hourly basis, and (3) the average volumetric moisture content for each sublayer. To accomplish the climate analysis, the EICM requires six weather parameters on an hourly basis: (1) air temperature, (2) wind speed, (3) the percentage of sunshine, (4) precipitation, (5) relative humidity, and (6) groundwater table.

Also, shortwave absorptivity is required to determine the amount of solar energy absorbed by the pavement surface. This parameter is used to define the heat flux boundary condition in the CMS model. The pavement surface color affects shortwave absorptivity, and the MEPDG suggests using 0.9–0.98 (black) for fresh asphalt pavement and 0.8–0.9 (gray) for aged asphalt pavement.

5.2.1.2 Data Collection. The APT sections have a well-controlled environment, so separate weather data were created to reflect the APT conditions. It would be ideal if the MEPDG could assign the temperature at each sublayer according to the APT sections' measured values and force them to be constant throughout the analysis period. However, the MEPDG simulates realistic environmental conditions by considering daily and seasonal temperature and moisture variations. The controlled climate condition in the APT facility challenged the EICM. The most faithful simulation of the APT conditions was not allowed in the MEPDG because the MEPDG does not allow the user to manually turn off the EICM feature or modify the EICM output file to bypass this climate model.

To obtain the best simulations of the APT conditions, the author generated a virtual weather station and adjusted the climatic parameters to achieve a constant representative temperature at all depths. Because the top portion of pavement is more susceptible to rutting than its lower layers, it seemed logical to use the temperature at this upper portion as the representative temperature. The selected temperature was 118°F (47.77°C), which was the temperature 1.5 inches (3.81 cm) deep in the APT lanes. The APT weather data were then created using a constant air temperature of 118°F (47.77°C), and the wind speed, percentage of sunshine, and precipitation were always zero. The relative humidity was 1%, according to the measurement. The groundwater table was set as 18 ft (5.49 m) because no water was introduced into the pavement system. Shortwave absorptivity was set to zero to maintain a constant temperature throughout the pavement depth.

5.2.2 Traffic Data

5.2.2.1 Input Data Requirements. Before developing the MEPDG model, traffic typically was considered based on the concept of the equivalent single-axle load (ESAL). The ESAL concept was developed from the AASHTO road test to establish a damage relationship between the effects of various axle types or amounts of loading and the standard axle load (i.e., 18,000 lb or 8.16-ton single axle with dual tires). The MEPDG, however, handles traffic using a more comprehensive process called *axle load spectra* that analyzes traffic directly via the axle configuration and load magnitude. The axle load spectra approach requires detailed and complete traffic information to characterize traffic properly. The traffic input parameters for this approach include.

- *Initial two-way average annual daily truck traffic (AADTT)*, which is obtained directly from weigh-in-motion (WIM) data or INDOT traffic survey data by multiplying the average annual daily traffic (AADT) by the truck percentage.
- *Percentage of trucks ("percent trucks")* in the design lane and design direction. "Percent trucks" is the percentage of truck traffic in the designed lane or direction relative to all truck traffic in one direction or both directions.
- *Operational speed*, which is the truck speed, determines the loading frequency underneath the pavement structure; hence, operating speed significantly impacts the predicted dynamic modulus value(s) of HMA material.
- *Growth of truck traffic*, whereby the MEPDG can assign various growth rates to each vehicle class; however, those growth rates are constant over time.
- *Axle load distribution* is the percentage of the total load repetitions within each load group for each axle type. Single, tandem, tridem, and quad axles are considered in the MEPDG, and axle loads are grouped with 1,000-lb (0.45 ton) intervals.
- *Normalized truck volume distribution*, which is the percentage of each truck traffic class. The MEPDG provides nine truck traffic classes according to the FHWA's vehicle classification system.
- *Axle load configuration*, which is the axle spacing in each truck traffic class.
- *Monthly distribution factors*, which distribute the truck traffic within each class throughout the year. These factors were set to be one in the global calibration.
- *Hourly distribution factors*, which distribute the truck traffic within each class throughout one day.
- *Dual tire spacing information* can be obtained from WIM data; a default value of 12 inches (30.48 cm) was used in the global calibration.

- *Tire pressure* was set to a constant value in this study because individual tire pressure for each truck traffic class is not considered in the MEPDG.
- *Lateral wander of axle load*, which the MEPDG simulates as a normal distribution. Standard deviation is used to characterize lateral wander. One distribution is used for all truck traffic classes. The default value of 10 inches (25.4 cm) was used in the global calibration.
- These traffic parameters can be input into the following three hierarchical input levels.

  - Level 1 requires site-specific traffic data, including traffic count, axle load, and truck traffic class distribution measured at or near the to-be-designed/analyzed roadway segments.
  - Level 2 requires site-specific traffic count and truck traffic class distribution data, whereas axle load data are normally averaged in neighborhood areas or regions.
  - Level 3 is used when only traffic count data are available for the desired roadway segments; global default values are assumed for the other traffic parameters.

5.2.2.2 Data Collection. APT traffic can be simulated using the unique axle configuration feature offered by the MEPDG to customize and define the APT wheel's assembly. The dual tires can be simulated using two tires with each tire load of 4,500 lb. (2.04 ton), the dual tire spacing was 13.5 inches (34.29), and the tire inflation pressure was 100 psi (0.69 MPa). Lateral wander standard deviation was set to zero so that the load could be applied repeatedly along with the same location.

5.2.3 Material Characterization

5.2.3.1 Input Data Requirements. In this study, Level 3 input data were used for the HMA mixtures and unbound materials. Level 1 input requires laboratory characterization of the materials used in the construction of each roadway segment. The required laboratory tests typically are not needed for construction. Level 1 input was excluded from this study's scope to be consistent with the future implementation of this calibration product. Table 5.1 and Table 5.2

Table 5.2 summarize the data requirements for the three input levels for the HMA mixture volumetric and thermal properties and HMA mixture mechanical properties.

TABLE 5.1
Data requirements for HMA mixture volumetric and thermal properties

Mixture Volumetric	**Unit Weight**
	Effective Binder Content by Volume
	Air Void Content
	Poisson's Ratio
Thermal	Thermal Conductivity (ASTM E1952)
	Heat Capacity (ASTM D2766)
	Thermal Contraction

The unit weight of HMA can be calculated as shown in Equation 5.1.

$$\gamma_{HMA} = \gamma_w \times G_{mb} = \gamma_w \times G_{mm} \times \%G_{mm} \qquad \text{(Eq. 5.1)}$$

where:

G_{mb} = bulk specific gravity of the mix;
G_{mm} = theoretical maximum specific density; and
$\%G_{mm}$ = percentage of theoretical maximum specific density.

The calculation of the effective binder content by volume is shown in Equation 5.2.

$$v_{beff} = G_{mb}\left[\frac{P_b}{g_b} - (100 - P_b) \times \frac{(G_{se} - G_{sb})}{G_{se} \times G_{sb}}\right] \qquad \text{(Eq. 5.2)}$$

where:

P_b = binder content by weight;
G_b = specific gravity of binder;
G_{se} = effective specific gravity of mix; and
G_{sb} = bulk specific gravity of aggregate.

The effective specific gravity of the mix is calculated as Equation 5.3.

$$g_{se} = \frac{100 - P_b}{\frac{100}{G_{mm}} - \frac{P_b}{G_b}} \qquad \text{(Eq. 5.3)}$$

The thermal properties are not utilized during rutting analysis; global default values are used. The dynamic modulus is the most critical parameter that is used to describe HMA. It is a function of temperature and loading frequency. Factors such as aggregate gradation, binder viscosity, binder content, and air void content significantly impact the dynamic modulus value. The dynamic modulus is measured directly for Level 1 input. For Level 2 and Level 3 inputs, the dynamic modulus is predicted using a revised Witczak model, as shown in Equation 5.4.

$$\begin{aligned} \log E = {} & 3.750063 + 0.02932\rho_{200} - 0.001767(\rho_{200})^2 \\ & - 0.002841\rho_4 - 0.058097 v_a \\ & - 0.802208\left(\frac{v_{beff}}{v_{beff} + v_a}\right) \\ & + \frac{3.871977 - 0.0021\rho_4 + 0.003958\rho_{38} - 0.000017(\rho_{38})^2 + 0.005470\rho_{34}}{1 + e^{(-0.303313 - 0.313351\log(f) - 0.3933532\log(\eta))}} \end{aligned} \qquad \text{(Eq. 5.4)}$$

where:

E^* = dynamic modulus, psi;
= binder viscosity, $10^6 Poise$;
f = loading frequency, Hz;
v_a = air void content, %;
v_{beff} = effective binder content by volume;

TABLE 5.2
Data requirements for HMA mixture mechanical properties

		Dynamic Modulus (AASHTO T 342)	
Mechanical Properties	Level 1		**OR**
		Shear Modulus (AASHTO T49)	Softening Point (AASHTO T202) Absolute Viscosity (AASHTO T201) Kinematic Viscosity (AASHTO T228)
		Phase Angle (AASHTO T49)	Specific Gravity Penetration (AASHTO T53) Brookfield Viscosity (AASHTO T316)
		Indirect Tensile Strength (AASHTO T322) Creep Compliance (AASHTOT 322)	
	Level 2	Percent Passing 3/4-inch sieve Percent Passing 3/8-inch sieve Percent Passing No. 4 sieve Percent Passing No. 200 sieve	
			OR
		Shear Modulus (AASHTO T49)	Softening Point (AASHTO T202) Absolute Viscosity (AASHTO T201) Kinematic Viscosity (AASHTO T228)
		Phase Angle (AASHTO T49)	Specific Gravity Penetration (AASHTO T53) Brookfield Viscosity (AASHTO T316)
		Indirect Tensile Strength (AASHTO T322) Creep Compliance (AASHTOT322)	
	Level 3	Percent Passing 3/4-inch sieve Percent Passing 3/8-inch sieve Percent Passing No. 4 sieve Percent Passing No. 200 sieve Performance Grade or Viscosity Grade or Penetration Grade	

ρ_{34} = cumulative percentage retained on 3/4 inch sieve;
ρ_{38} = cumulative percentage retained on 3/8-inch sieve;
ρ_4 = cumulative percentage retained on No. 4 sieve; and
ρ_{200} = percentage passing the No. 200 sieve.

Binder viscosity is a critical parameter for dynamic modulus predictions. It is usually expressed as a function of temperature, as shown in Equation 5.5. When the dynamic modulus is provided using Level 1 or Level 2 input, the A and VTS parameters can be estimated using a dynamic shear rheometer test following AASHTO T315 or a series of conventional tests include viscosity, softening point, and penetration. When the dynamic modulus is provided using Level 3 input, the binder PG, viscosity grade, or penetration grade can be used for estimation.

$$\log\log\eta = A + VTS\log T_R \qquad \text{(Eq. 5.5)}$$

where:

= binder viscosity, cP;
T_R = temperature, Rankine; and
A,VTS = regression parameters.

The indirect tensile strength and creep compliance are measured directly following AASHTO T322 at input Levels 1 and 2. At input Level 3, these parameters are estimated based on the air void content, voids filled with asphalt, asphalt penetration at 77°F (25°C), and parameter A.

The required parameters of all the input levels for the unbound subgrade material are the Poisson's ratio, coefficient of lateral earth pressure, and AASHTO soil classification. The material stiffness is defined using the resilient modulus. For Level 2 input analysis, the resilient modulus value is estimated using the California bearing ratio value, R-value, DCP rate, gradation, and Atterberg limit. For Level 3 input analysis, the

resilient modulus value is estimated based on the soil classification.

5.2.4 Conditions Simulation

Once asphalt concrete is placed and exposed to the environment, it begins to age as the material starts to oxidize. As a result, the asphalt binder's viscous properties change over time and, thus, so do the HMA mixtures. HMA mixtures tend to become stiffer and more brittle with time. Such an impact plays a vital role in material behavior and pavement long-term performance. The MEPDG incorporates aging using the GAS developed by Mirza and Witczak (Mirza & Witczak, 1995). The system consists of four models: the original to mix/lay-down model, the surface aging model, air void adjustment, and the viscosity-depth model.

The GAS predicts the binder viscosity at any time and any depth in the pavement system. The predicted viscosity is then incorporated into the determination of the dynamic modulus. A realistic aging effect is then simulated. However, such a feature challenges the most faithful simulation of an APT. APTs usually are performed within a few months of pavement placement, whereas MEPDG simulations typically are conducted over a much more extended analysis period to evaluate the rutting evolution. As a result, more asphalt aging is simulated in the MEPDG than occurs during APTs. Also, the MEPDG does not allow users to turn off the GAS manually. The minimum analysis period in the MEPDG is 1 year, which means that a minimum of 1 year of aging must be enforced.

The FWD test was used to quantify the amount of increase in the modulus value. The analysis period (referred to as the "aging analysis period") under the amount of increase could be determined for each test lane. The aging analysis period is used in the calibration process if the aging analysis period is less than 1 year, which is the minimum analysis period allowed in the MEPDG. APT load applications were stretched within the aging analysis period, and only the simulation results within the aging analysis period were used. The complete APT load application is 50,000 passes, which must be applied during the 4 months. Thus, 12,500 passes per month were used in the MEPDG 1-year simulation. In short, 6-month analysis results were used, although a 1-year simulation was performed.

5.3 MEPDG Verification

The transfer function of asphalt concrete layers, as shown in Equation 5.6, has three calibration coefficients (i.e., β_{r1}, β_{r2}, and β_{r3}), whereas the transfer function for unbound materials, as shown in Equation 5.7, has only one calibration coefficient (i.e., β_{s1}).The local calibration calculates the calibration coefficients to eliminate or minimize bias and standard errors of estimates. In the previous APT study (SPR-3307), the local calibration of MEPDG was performed using 13 sections (eight local field projects and five APT sections) for each combination. The results indicated that the combination of $\beta_{r2} = 1.9$ and $\beta_{r3} = 0.4$ yielded the lowest SSEs. Table 5.3 provides a summary of the selected calibration coefficients.

TABLE 5.3
Selected calibration coefficients

β_{r1}	β_{r2}	β_{r3}	β_{s1}
0.079	1.9	0.4	0.110

TABLE 5.4
Summary of statistical parameters

Layer	Pavement Type	Bias (%)	SSE1 (mm^2)	Se (mm)	R^2
AC Layer	Thin	88	214	4.23	78
	Thick	82	216	4.25	45
SG	Thin	-244	0.24	0.14	88
	Thick	-343	0.11	0.01	90
Total	Thin	82	217	4.25	76
	Thick	75	224	4.33	40

[1]SSE = sum of squares error.

$$\frac{\varepsilon_p}{\varepsilon_r} = K_Z \beta_{r1} 10^{k_{r1}} (T)^{k_{r2}\beta_{r2}} (N)^{k_{r3}\beta_{r3}} \quad \text{(Eq. 5.6)}$$

$$\delta_a(N) = \beta_{s1} k_1 \varepsilon_v h \left(\frac{\varepsilon_0}{\varepsilon_r}\right) e^{-\left(\frac{\rho}{N}\right)^{\beta}} \quad \text{(Eq. 5.7)}$$

In this study, the local calibrated MEPDG model is used to determine if it is applicable to predict thin full-depth flexible pavements rutting. A set of predicted rutting performance was calculated for the thin full-depth asphalt pavements using the local calibrated model. Statistical analyses were performed to evaluate the predictions.

Table 5.4 summarizes the statistical parameters at the 95% confidence level to compare the measured and predicted rutting values of thin and thick full-depth asphalt pavements based on the local calibrated model. In this table, the bias is the percentage of relative residual error between the predicted and measured values that cause the model to overestimate (i.e., when bias is positive) or underestimate (i.e., when bias is negative). SSE is the sum of the squares error. The error is defined as the difference between the observed and predicted values. The results show that the local calibrated model for total and AC layers overestimate the rutting, while for subgrade, it underestimates that. Additionally, it can be seen that there is no significant difference between the statistical parameters of thin and thick full-depth asphalt pavements.

6. CONCLUSIONS AND RECOMMENDATIONS

This study investigated the rutting behavior for HMA and SMA full-depth pavements using APT. A mid-depth rut monitoring and automated laser

profile system were utilized to reconstruct each pavement layer interface's transverse profiles. The rutting distributions throughout the pavement layers were monitored closely during APT loading. The pavement mechanical behavior was observed using responses from the strain gauges and the pressure cells. The findings were then used to verify the MEPDG local calibrated rutting coefficients for the thin full-depth asphalt pavements. To conduct MEPDG verification, simulations of the APT conditions, including climate, traffic, and aging conditions, were performed using virtual weather station generation, a particular traffic configuration, and FWD evaluation.

6.1 Conclusions

The following conclusions were drawn from this study.

- The developed mid-depth rut monitoring and automated laser profile system successfully captured the evolution of permanent deformation for each pavement structural layer.
- Comparison between rut-depth results for thin (7 and 10 inches) and thick (12.5 and 15.5 inches) full-depth flexible pavements showed that the permanent deformation within asphalt concrete highly depends on pavement thickness. A significant decrease was in rut depth when the pavement thickness increases from 10 inches (25.4 cm) to 12.5 inches (31.75 cm). However, no significant change in total rut depth was observed when the thickness increased from 12.5 inches (31.75 cm) to 15.5 inches (39.37 cm).
- The primary contribution to HMA rutting was from the upper part of the asphalt layers, with about half of the rutting observed within the pavement layer's top 4 inches.
- The rut depth in the SMA course was 70% less than that in the HMA surface course. The SMA lanes reduced the HMA total rut depth by 42%. Additionally, the most contribution to the rutting on the SMA lanes was from the intermediate course.
- The subgrade deformation under the SMA lanes remained low (i.e., approximately 12% of total rutting) regardless of the pavement thickness and the surface course type. However, the permanent deformation of subgrade in SMA pavements was almost twice that in HMA pavements. The SMA surface course having a higher modulus behaves possibly as a rigid layer and conveys the load from the surface to the sublayers with less dissipation. The pressure cells' results also confirm it, as the amount of pressure on top of the SMA pavement's subgrade was approximately double that on the subgrade of HMA pavements.
- Results of horizontal stain bottom of the base course showed that for HMA pavements, the horizontal strain in both longitudinal and transverse direction was higher than that for SMA pavements. This finding indicates that the SMA pavements have a better potential of bottom-up fatigue cracking resistance.
- The current rutting local calibration coefficients with the thin asphalt full-depth pavements were verified using Pavement ME Design version 2.3. No significant difference was found between the verification statistics of the calibrated models for thin and thick full-depth asphalt pavements.

6.2 Implementation

- A new version MEPDG (i.e., Pavement ME Design version 2.6) is available, and INDOT has a plan for the implementation. However, the current local model is not applicable to version 2.6, and a re-calibration for the rutting model in version 2.6 is needed. The ongoing study, SPR-4447: *MEPDG Implementation*, performs local calibrations for the version 2.6 implementation. The rutting distributions in terms of pavement layers found in this study will be provided to SPR-4447 for the re-calibration process.
- The INDOT Pavement Design Office will implement the study findings in the pavement design process.

6.3 Recommendations

The work completed in this study examined the rutting behavior of thin full-depth flexible pavement and verified the current local MEPDG predictions. Several recommendations are provided for future research and MEPDG implementation.

- Only two types of surface course material, i.e., an HMA mixture and an SMA mixture, were tested in this study. Future research should expand the material database and cover new materials such as warm-mix asphalt, recycled asphalt pavement, and polymer-modified asphalt.
- Future research should be conducted for other pavement types, such as asphalt overlays. When constructing asphalt overlays, the deteriorated surface is commonly milled to a certain depth; the new surface is then placed over the milled surface. Without knowing the rutting distribution in the existing pavement, the amount of rutting that has already occurred within the remaining layers of the existing pavement will be hidden, increasing the difficulty of designing the new surface layer. Thus, the findings of this study would be valuable for the analysis and design of asphalt overlays.
- Future research should expand the APT sections with additional pavement structures and subgrade types to develop a more comprehensive relationship between the rutting distribution and the paving material, pavement thickness, and subgrade.
- Forensic studies should be conducted for field roadways to confirm the findings from this APT study.

Finally, it is also recommended that any pavement condition evaluation be performed with extra caution because most of the precision problems in this study seemed to come from the distress measurements.

REFERENCES

AASHTO R48-10. (2013). *Standard practice for determining rut depth in pavements*. American Association of State Highway and Transportation Officials.

Applied Research Associates, Inc. (2004, February). *Guide for mechanistic-empirical design of new and rehabilitated pavement structures* (NCHRP Project 1-37A). National Cooperative Highway Research Program.

ASTM D4694-09. (2015). *Standard test method for deflections with a falling-weight-type impulse load device*. American Society for Testing and Materials International.

ASTM D6951. (2015). *Standard test method for use of the dynamic cone penetrometer in shallow pavement applications*. American Society for Testing and Materials International.

Azari, H., Mohseni, A., & Gibson, N. (2008). Verification of rutting predictions from mechanistic-empirical pavement design guide by use of accelerated loading facility data. *Transportation Research Record: Journal of the Transportation Research Board*, *2057*(1), 157–167. https://doi.org/10.3141/2057-19

Ceylan, H., Kim, S., Gopalakrishnan, K., & Ma, D. (2013, June). *Iowa calibration of MEPDG performance prediction models* (InTrans Project 11-401). Iowa Department of Transportation. http://publications.iowa.gov/14895/1/IA_DOT_InTrans_MEPDG_Iowa_calibration_w_cvr.pdf

Dempsey, B. J., Herlach, W. A., & Patel, A. J. (1985). *The climatic-material-structural pavement analysis program* (Report No. FHWA/RD-84/115). Federal Highway Administration.

Gibson, N., Li, S., & Kutay, M. E. (2010). Rutting resistance of laboratory-prepared and field-compacted asphalt mixtures. *Transportation Research Record: Journal of the Transportation Research Board*, *2181*(1), 109–116. https://doi.org/10.3141/2181-12

Gibson, N., Qi, X., Shenoy, A., Al-Khateeb, G., Kutay, M. E., Andriescu, A., Stuart, K., Youtcheff, J., & Harman, T. (2011). *Performance testing for superpave and structural validation*. Federal Highway Administration.

Guymon, G. L., Berg, R. L., & Johnson, T. C. (1986). *Mathematical model of frost heave and thaw settlement in pavement*. U. S. Army Cold Region Research and Engineering Laboratory.

Hall, K. D., Xiao, D. X., & Wang, K. C. P. (2011). Calibration of the mechanistic–empirical pavement design guide for flexible pavement design in Arkansas. *Transportation Research Record: Journal of the Transportation Research Board*, *2226*(1), 135–141. https://doi.org/10.3141/2226-15

Hong, F., & Chen, D.-H. (2008). Calibrating mechanistic-empirical design guide permanent deformation models based on accelerated pavement testing. *Journal of Testing and Evaluation*, *37*(1), 31–39. https://doi.org/10.1520/JTE101854

Immanuel, S., & Timm, D. H. (2007). *A field-calibrated shear strain rut prediction model* [Paper presentation]. 86th Annual Meeting of the Transportation Research Board, Washington, DC.

Kim, Y. R., Jadoun, F. M., Hou, T., & Muthadi, N. (2011, October). *Local calibration of the MEPDG for flexible pavement design* (Report No. FHWA\NC\2007-07). North Carolina State University Department of Civil, Construction, & Environmental Engineering.

Li, Q., Lee, H., & Lee, S. (2011). *Development and calibration of a permanent deformation model based on shear properties of asphalt mixtures* [Paper presentation]. 90th Annual Meeting of the Transportation Research Board, Washington, DC.

Lytton, R. L., Pufahl, D. E., Michalak, C. H., Liang, H. S., & Dempsey, B. J. (1990). *An integrated model of the climatic effects on pavement* (Report No. FHWA-RD-90-033). Federal Highway Administration.

Metcalf, J. B. (1996). *Synthesis of highway practice 235: Application of full-scale accelerated pavement testing*. Transportation Research Board.

Mirza, M. W., & Witczak, M. W. (1995). Development of a global aging system for short and long term aging of asphalt cements. *Journal of the Association of Asphalt Paving Technologists*, *64*, 393–430.

Monismith, C., Popescu, L., & Harvey, J. T. (2006). Use of shear test data for mix design, performance analysis, and rut depth prediction. *Proceedings of the 10th International Conference on Asphalt Pavements*, *2*, 694–706.

Nabhan, P. (2015). *Calibration of the AASHTO MEPDG for flexible pavements to fit Nevada's conditions* [Masters thesis, University of Nevada]. ScholarWorks. http://hdl.handle.net/11714/2615

Nantung, T., Lee, J., & Tian, Y. (2018). *Efficient pavement thickness design for Indiana* (Joint Transportation Research Program Publication No. FHWA/IN/JTRP-2018/06). West Lafayette, IN: Purdue University. https://doi.org/10.5703/1288284316649

Onyango, M. A., & Romanoschi, S. A. (2010). *Verification of mechanistic prediction models for permanent deformation in asphalt mixes using accelerated pavement testing* [Paper presentation]. Transportation Research Board 89th Annual Meeting. https://trid.trb.org/view/910008

Park, D.-W., Martin, A. E., & Masad, E. (2004, September 26–29). Simulation of permanent deformation using an elastic-viscoplastic constitutive relation. *Proceedings of the 2nd International Conference on Accelerated Pavement Testing*.

Saeed, A., Hammons, M. I., & Bianchini, A. (2010). *Airfield repairs in austere locations using pelletized asphalt technology* [Paper presentation]. Transportation Research Board 89th Annual Meeting, Washington, DC.

Sivasubramaniam, S., & Haddock, J. E. (2006). *Validation of superpave mixture design and analysis procedures using the NCAT test track* (Joint Transportation Research Program Publication FHWA/IN/JTRP-2005/24). Indiana Department of Transportation and Purdue University. West Lafayette, IN. https://doi.org/10.5703/1288284313375

Souliman, M. I., Mamlouk, M. S., El-Basyouny, M. M., & Zapata, C. E. (2010, January 10–14). *Calibration of the AASHTO MEPDG for flexible pavement for Arizona conditions* [Paper presentation]. Transportation Research Board 89th Annual Meeting, Washington, DC.

Ugé, P., & Van de Loo, P. (1974). *Permanent deformation of asphalt mixes*. Shell Research Laboratories.

Villiers, C., Roque, R., & Dietrich, B. (2005). Interpretation of transverse profiles to determine the source of rutting within asphalt pavement system. *Transportation Research Record: Journal of the Transportation Research Board*, *1905*(1), 73–81. https://doi.org/10.1177/0361198105190500108.

Williams, R. C., & Shaidur, R. (2013, January). *Mechanistic-empirical pavement design guide calibration for pavement rehabilitation*. Oregon Department of Transportation. https://www.oregon.gov/ODOT/Programs/ResearchDocuments/spr718_mechempiricalpvmtdesign.pdf

Xu, Q., & Mohammad, L. N. (2008). Modeling asphalt pavement rutting under accelerated testing. *Road Materials and Pavement Design*, *9*(4), 665–687. https://doi.org/10.1080/14680629.2008.9690144

APPENDICES

Appendix A. Subgrade DCP Profiles

Appendix B. Rut Depth Evolution Trends

Appendix C. Material Inputs

APPENDIX A. SUBGRADE DCP PROFILES

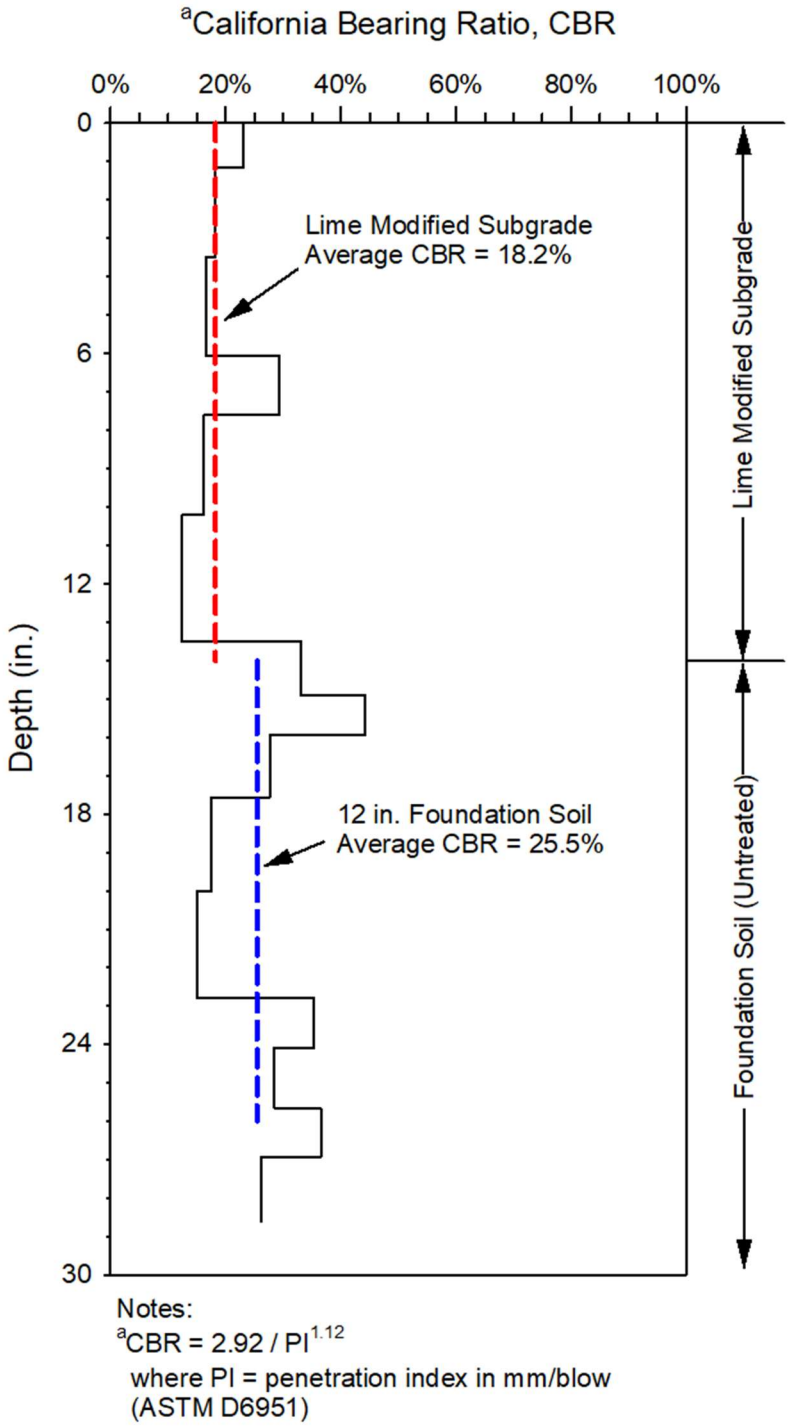

Figure A.1 California bearing ratio DCP profile for 14 -inch thick lime modified subgrade sections (Lanes 1 & 2) measured 1-day after placement—Test No. 1.

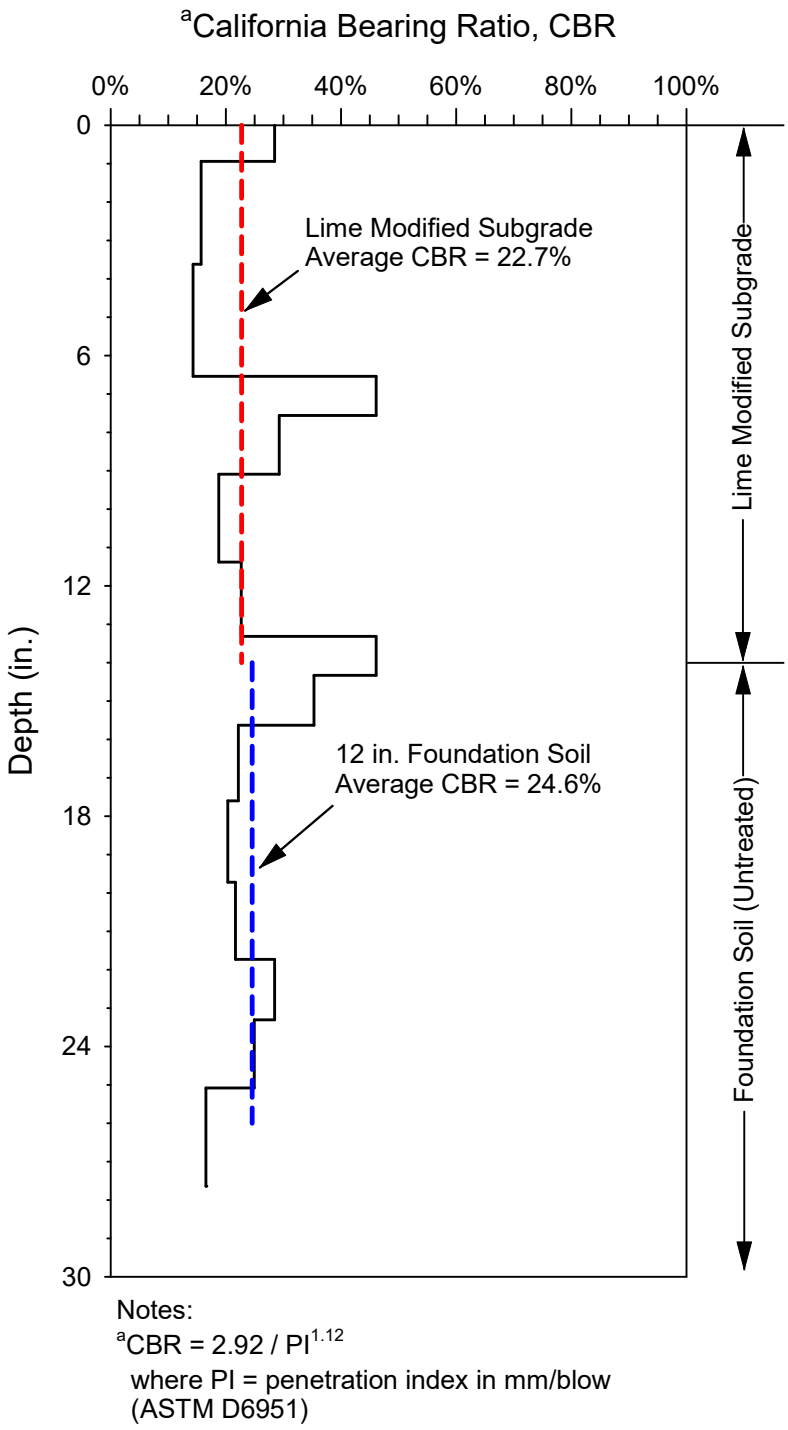

Figure A.2 California bearing ratio DCP profile for 14-inch thick lime modified subgrade sections (Lanes 1 & 2) measured 1-day after placement—Test No. 2.

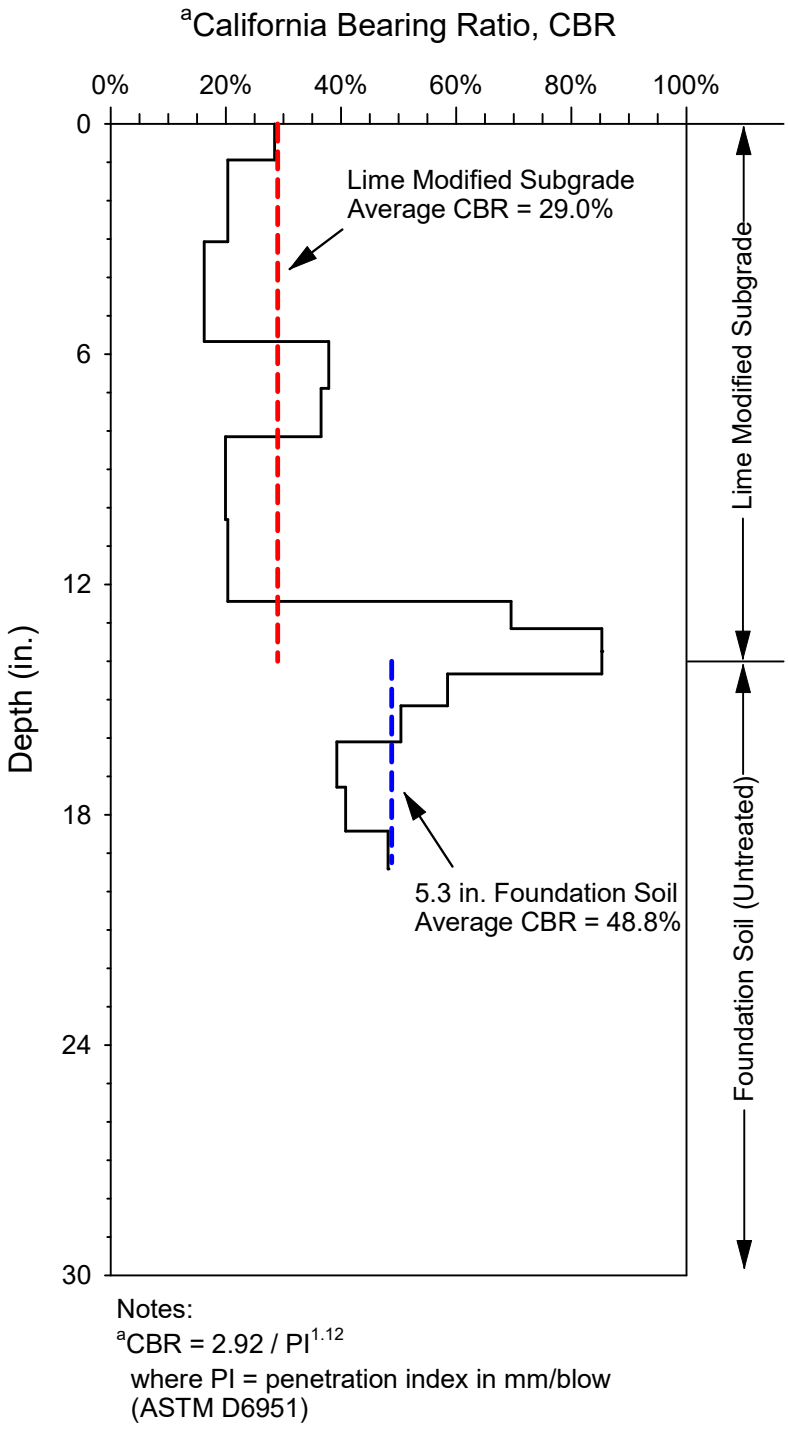

Figure A.3 California bearing ratio DCP profile for 14-inch thick lime modified subgrade sections (Lanes 1 & 2) measured 1-day after placement—Test No. 3 .

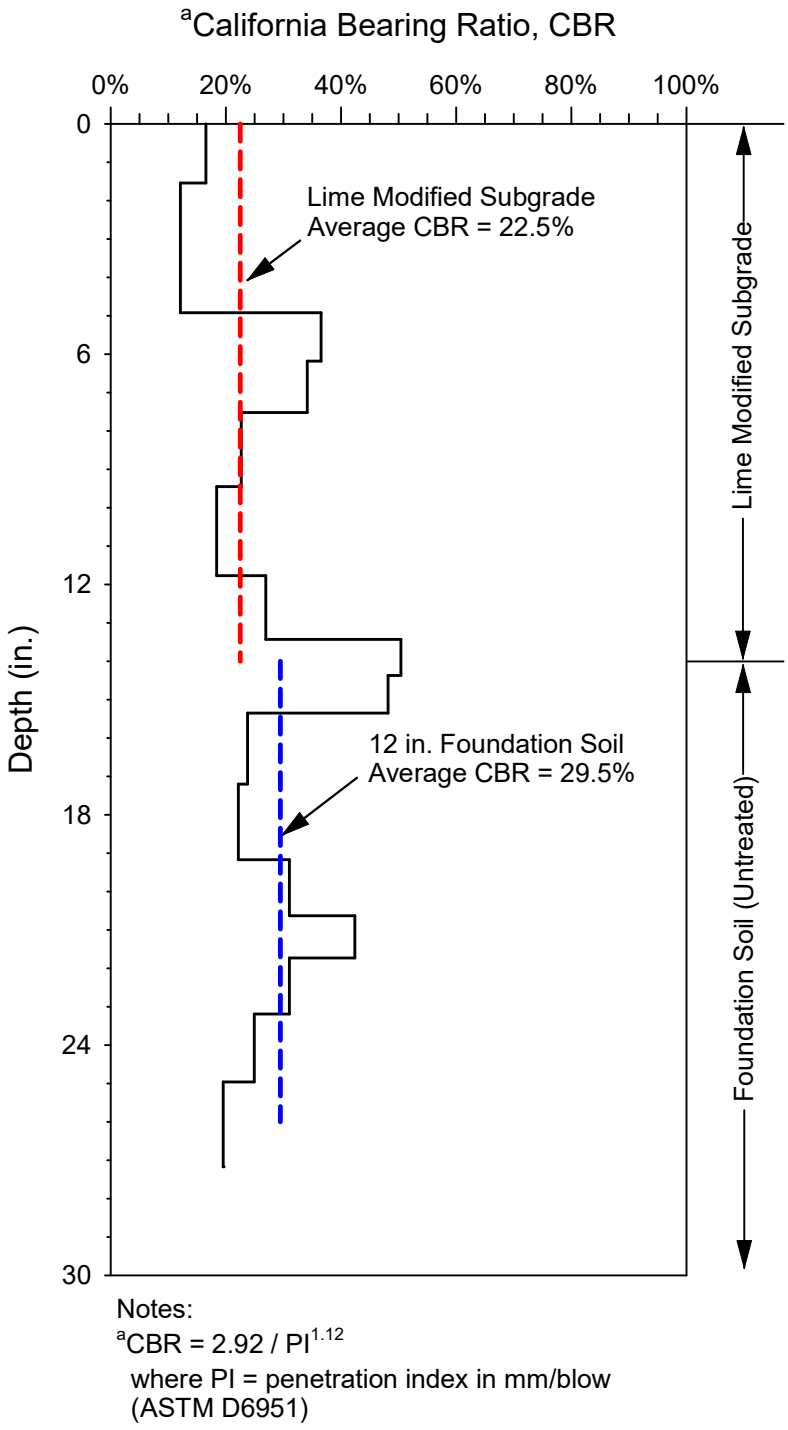

Figure A.4 California bearing ratio DCP profile for 14-inch thick lime modified subgrade sections (Lanes 1 & 2) measured 1-day after placement—Test No. 4.

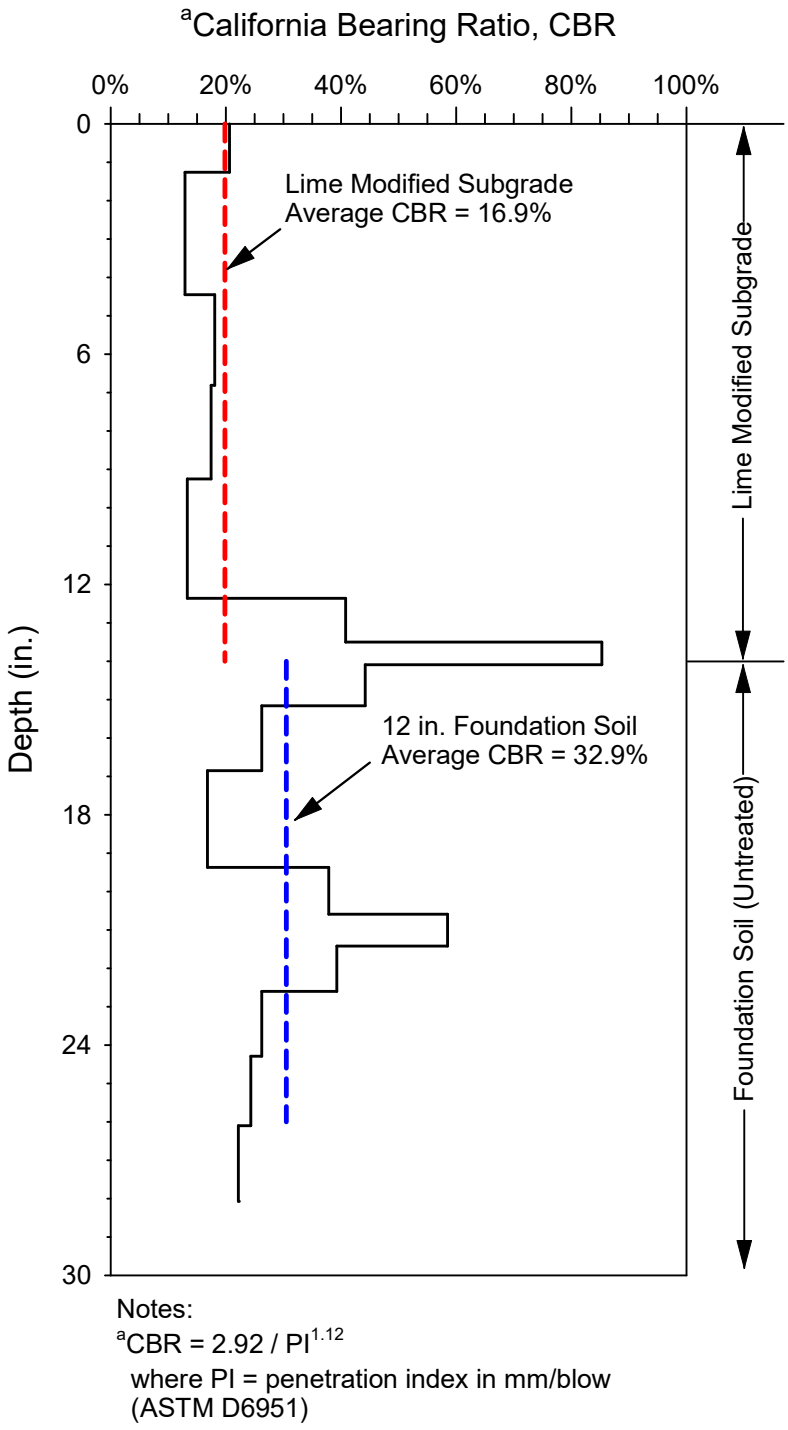

Figure A.5 California bearing ratio DCP profile for 14-inch thick lime modified subgrade sections (Lanes 1 & 2) measured 1-day after placement—Test No. 5.

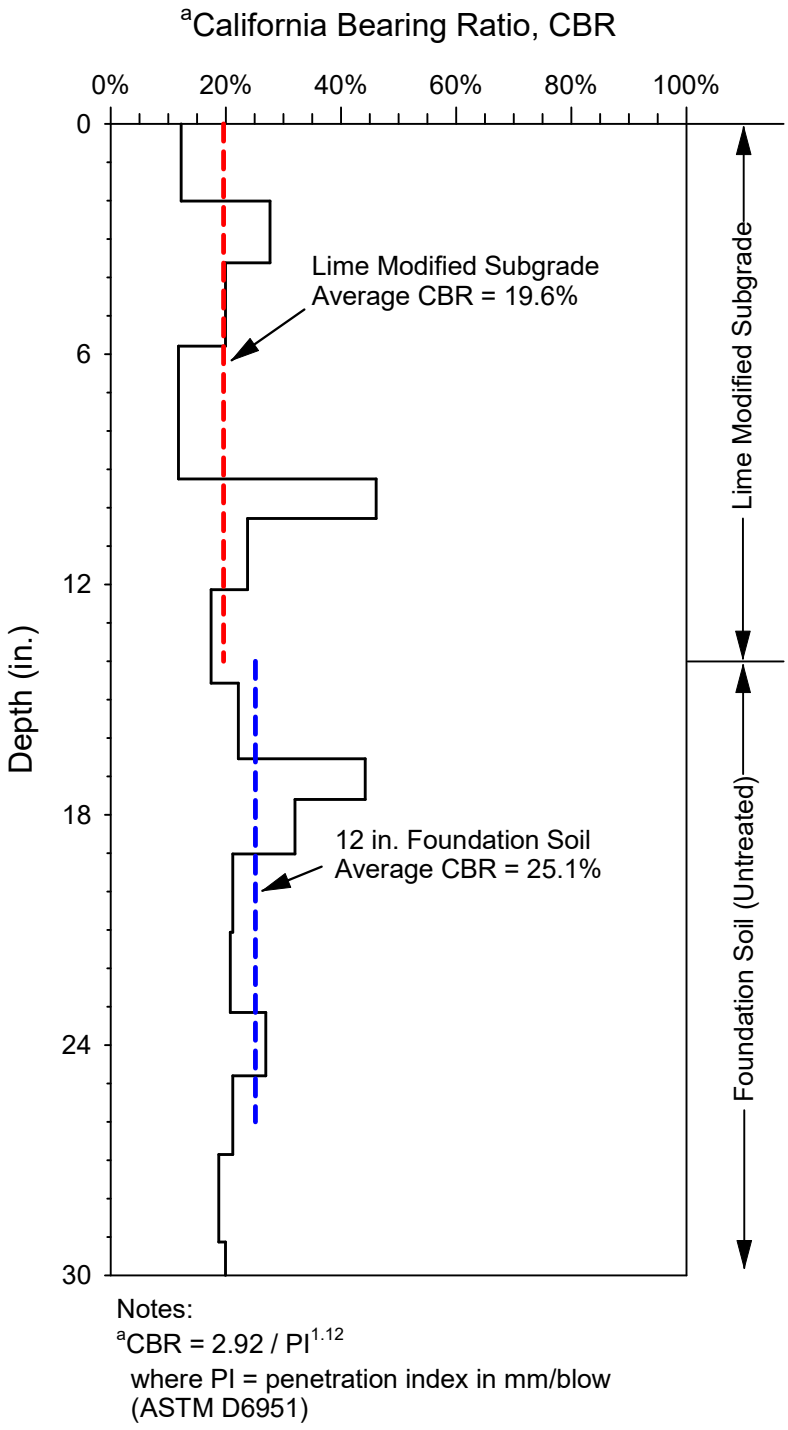

Figure A.3 California bearing ratio DCP profile for 14-inch thick lime modified subgrade sections (Lanes 1 & 2) measured 2-day after placement—Test No. 1.

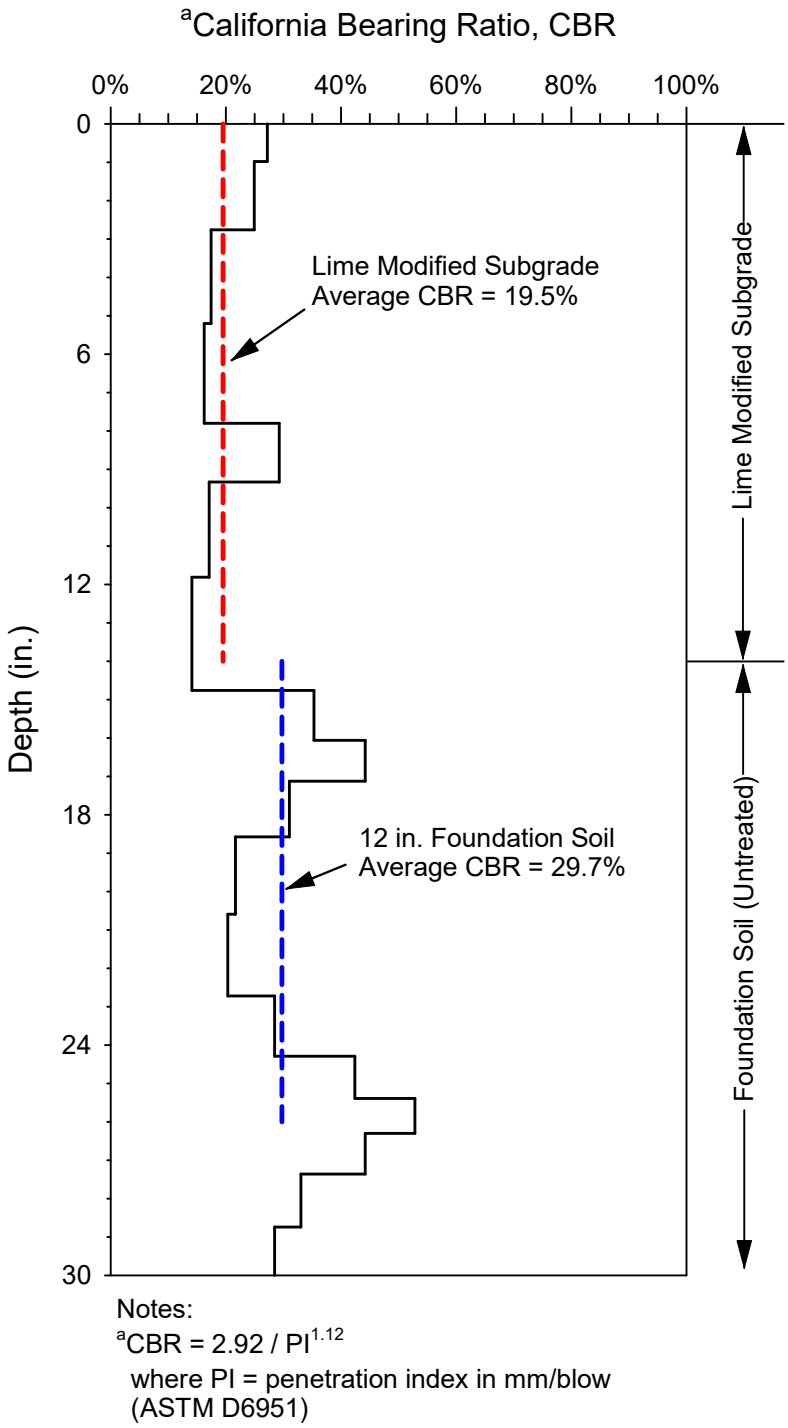

Figure A.4 California bearing ratio DCP profile for 14-inch thick lime modified subgrade sections (Lanes 1 & 2) measured 2-day after placement—Test No. 2.

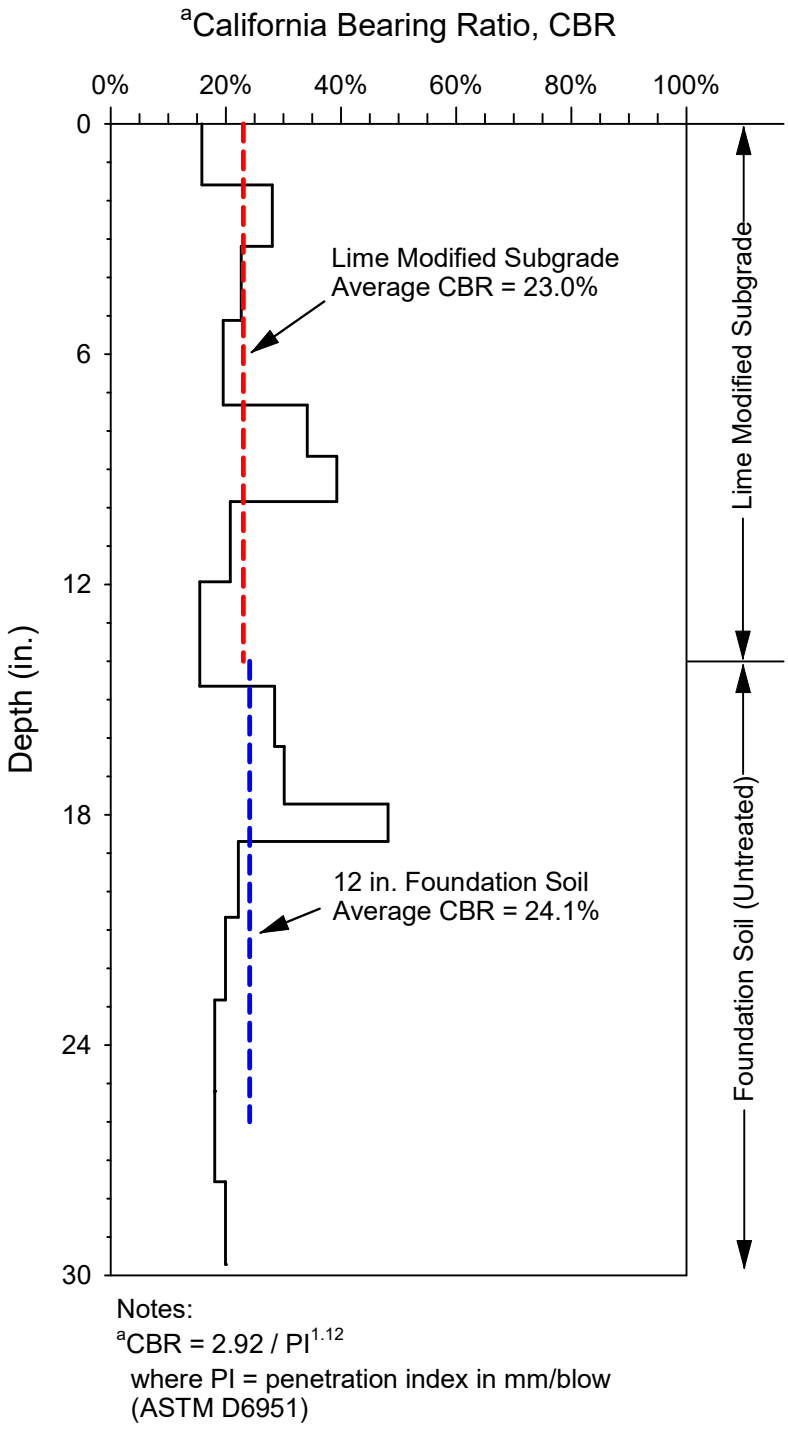

Figure A.8 California bearing ratio DCP profile for 14-inch thick lime modified subgrade sections (Lanes 1 & 2) measured 2-day after placement—Test No. 3.

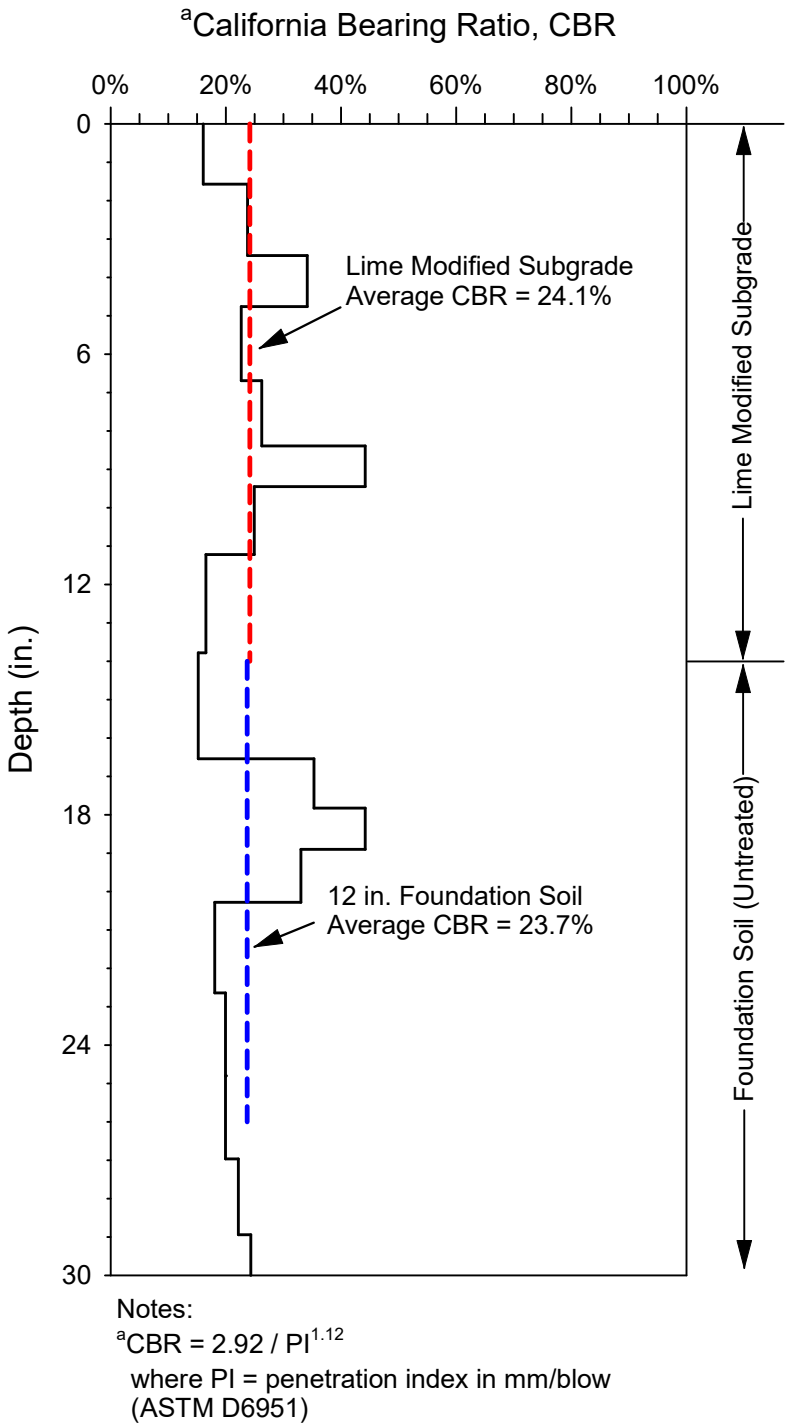

Figure A.9 California bearing ratio DCP profile for 14-inch thick lime modified subgrade sections (Lanes 1 & 2) measured 2-day after placement—Test No. 4.

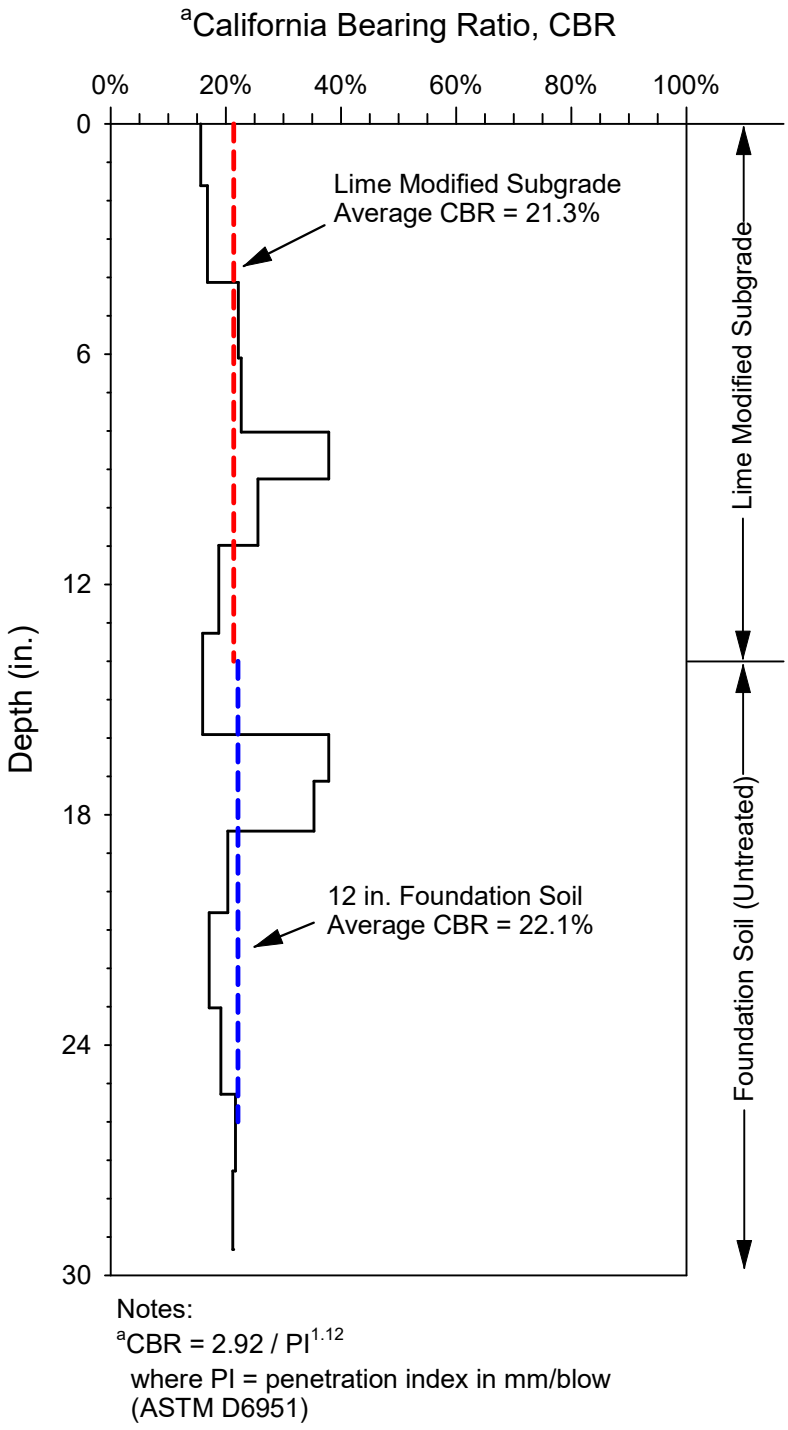

Figure A.10 California bearing ratio DCP profile for 14-inch thick lime modified subgrade sections (Lanes 1 & 2) measured 2-day after placement—Test No. 5.

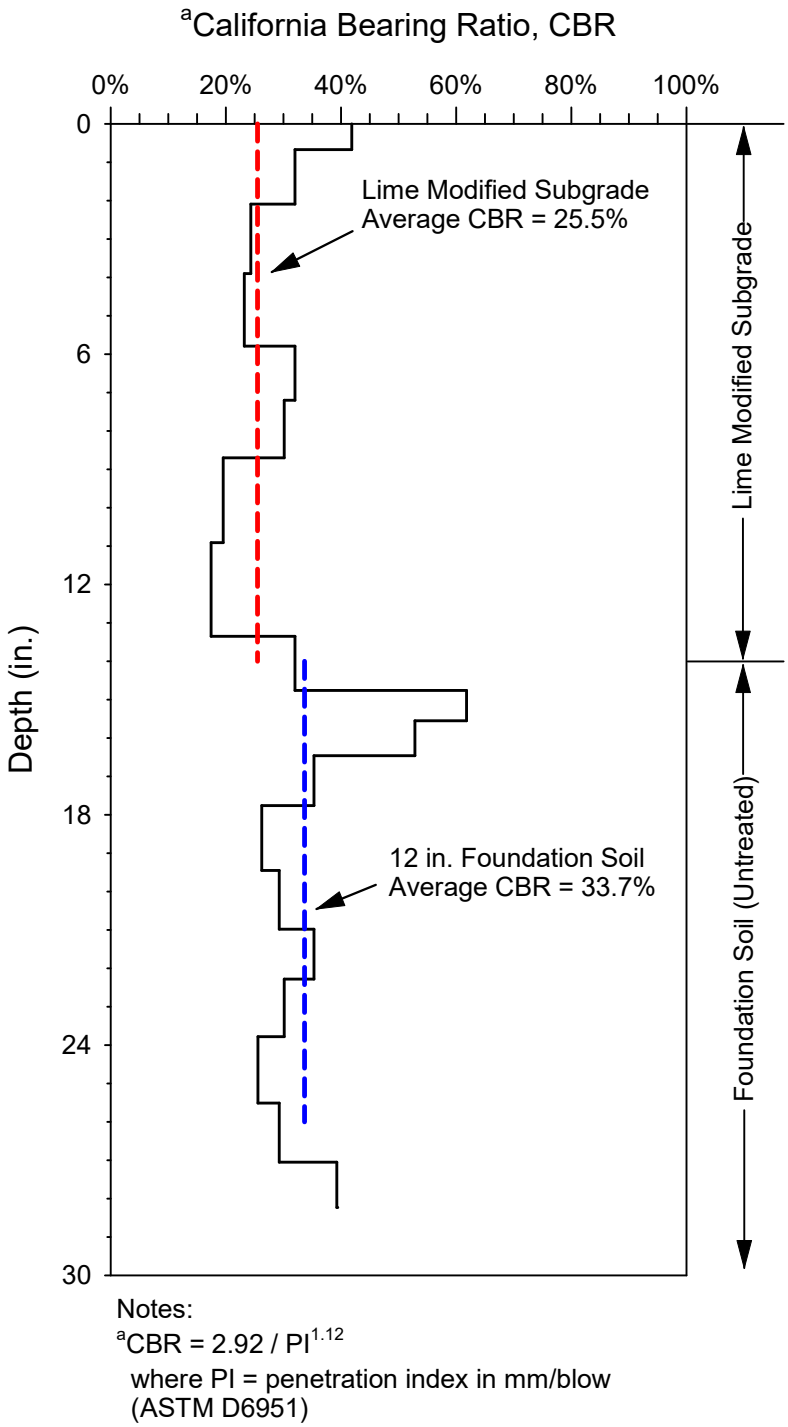

Figure A.11 California bearing ratio DCP profile for 14-inch thick lime modified subgrade sections (Lanes 1 & 2) measured 4-day after placement—Test No. 1.

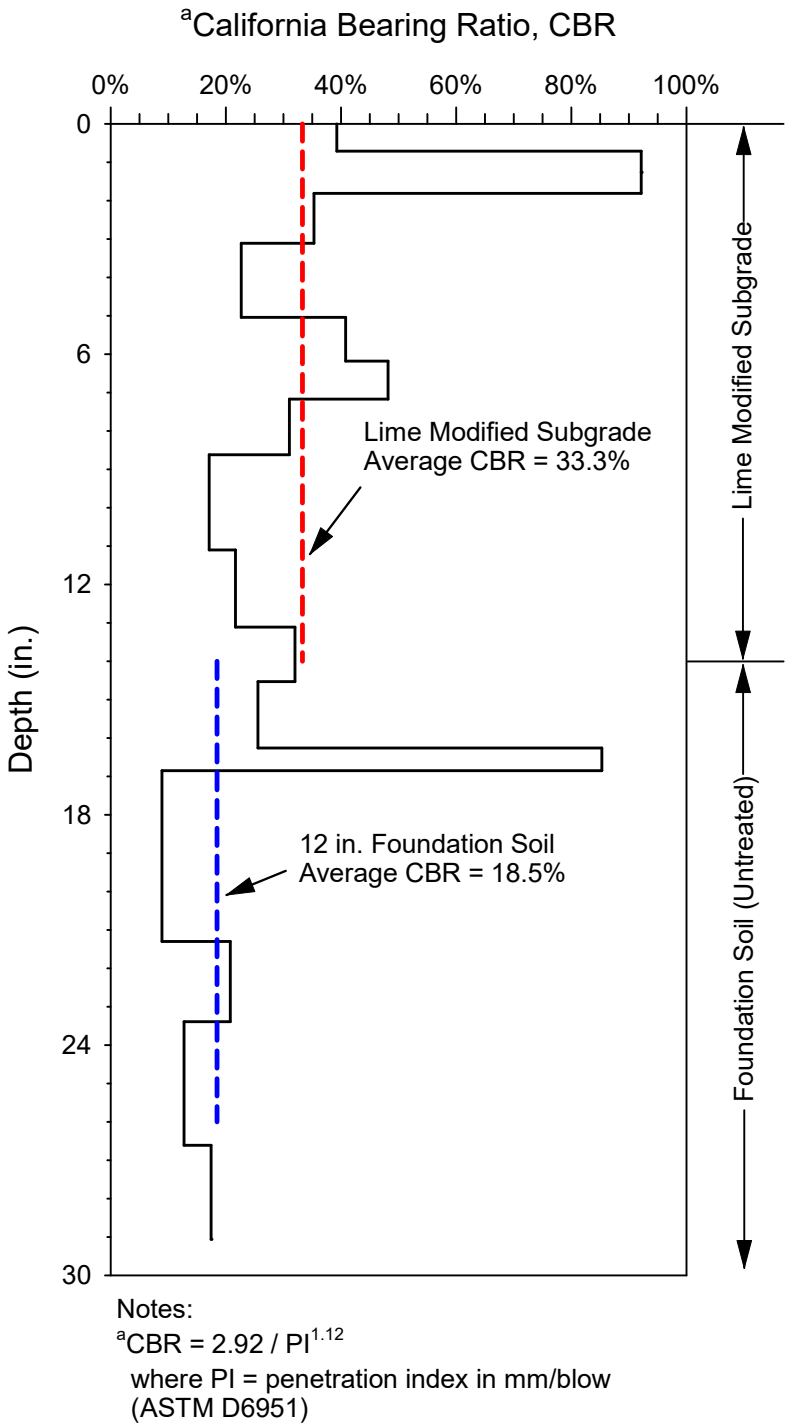

Figure A.12 California bearing ratio DCP profile for 14-inch thick lime modified subgrade sections (Lanes 1 & 2) measured 4-day after placement—Test No. 2.

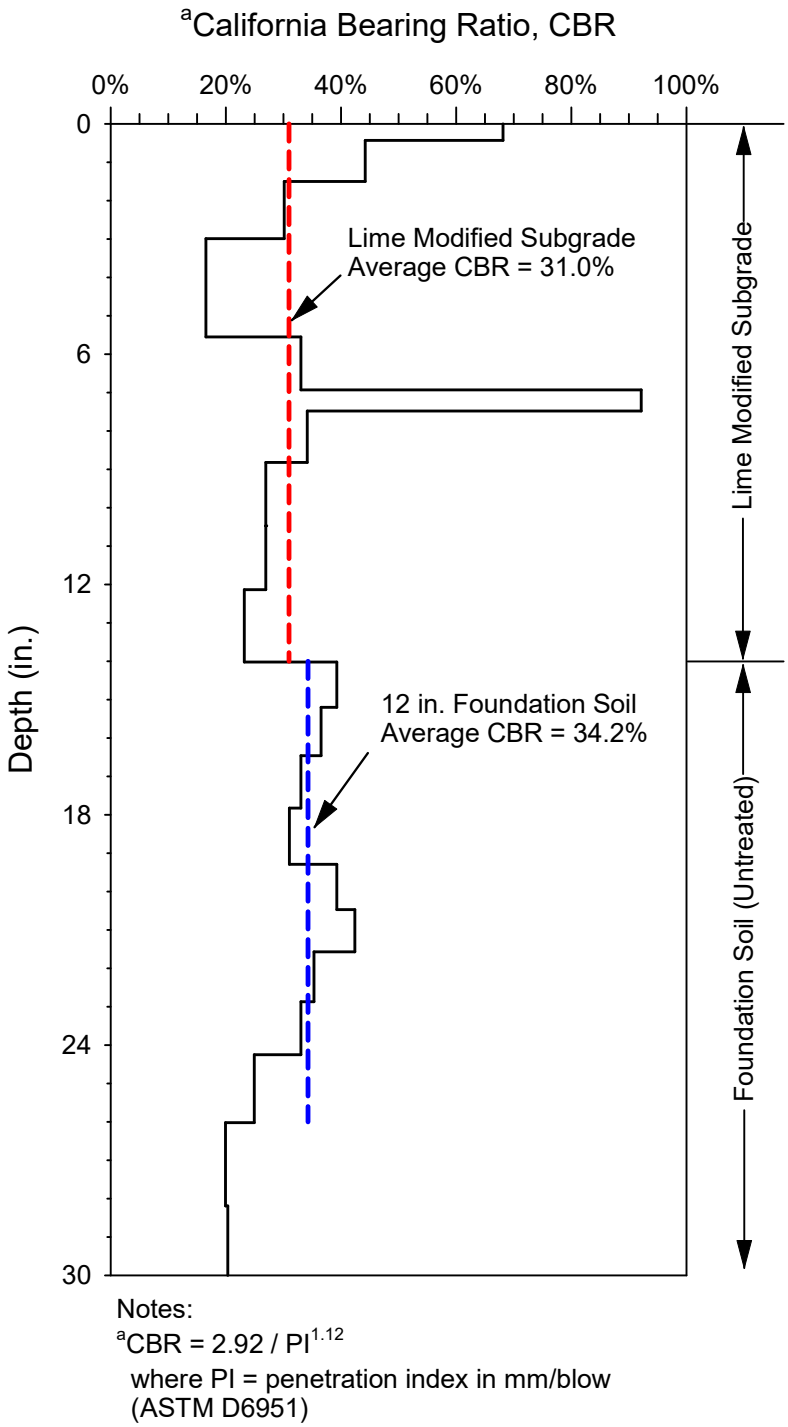

Figure A.13 California bearing ratio DCP profile for 14-inch thick lime modified subgrade sections (Lanes 1 & 2) measured 4-day after placement—Test No. 3.

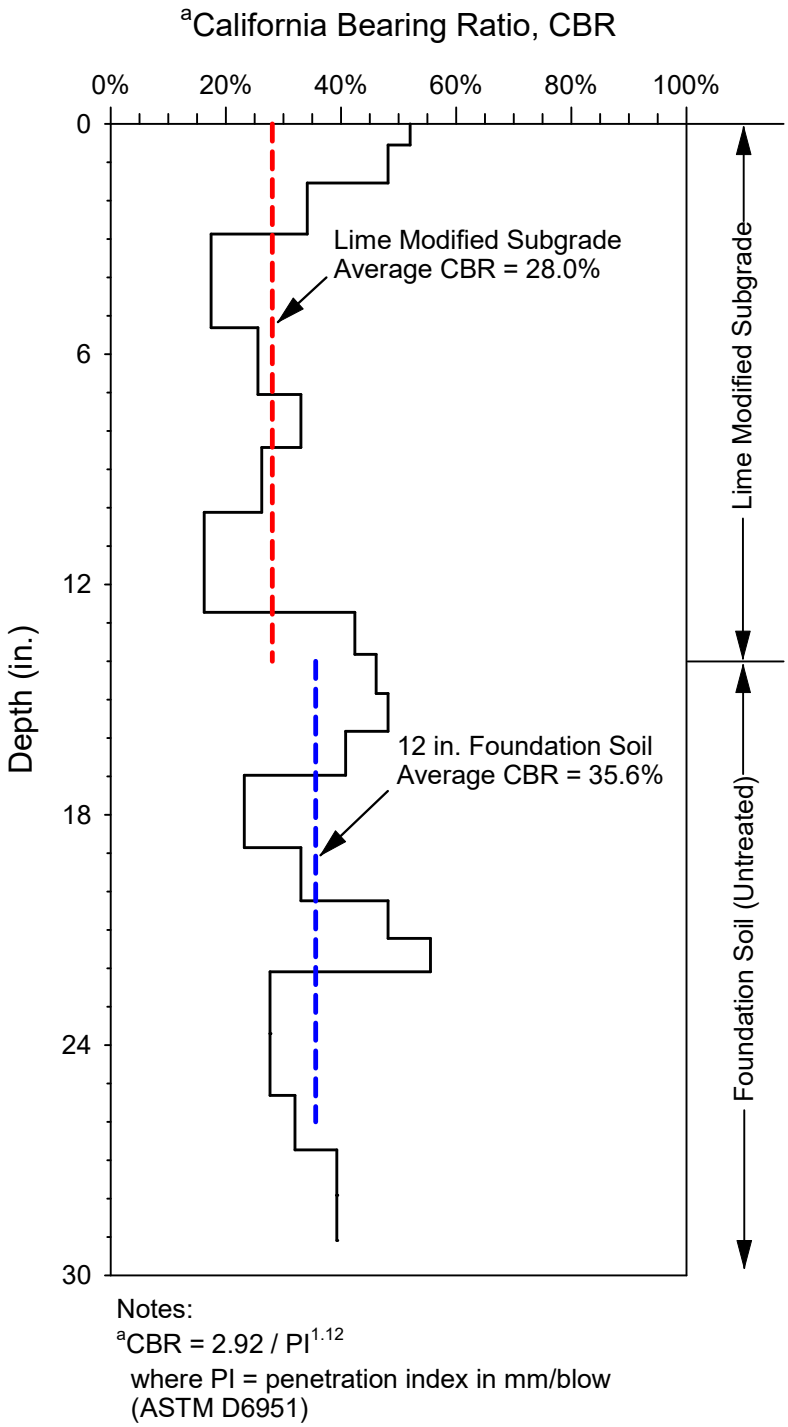

Figure A.14 California bearing ratio DCP profile for 14-inch thick lime modified subgrade sections (Lanes 1 & 2) measured 4-day after placement—Test No. 4.

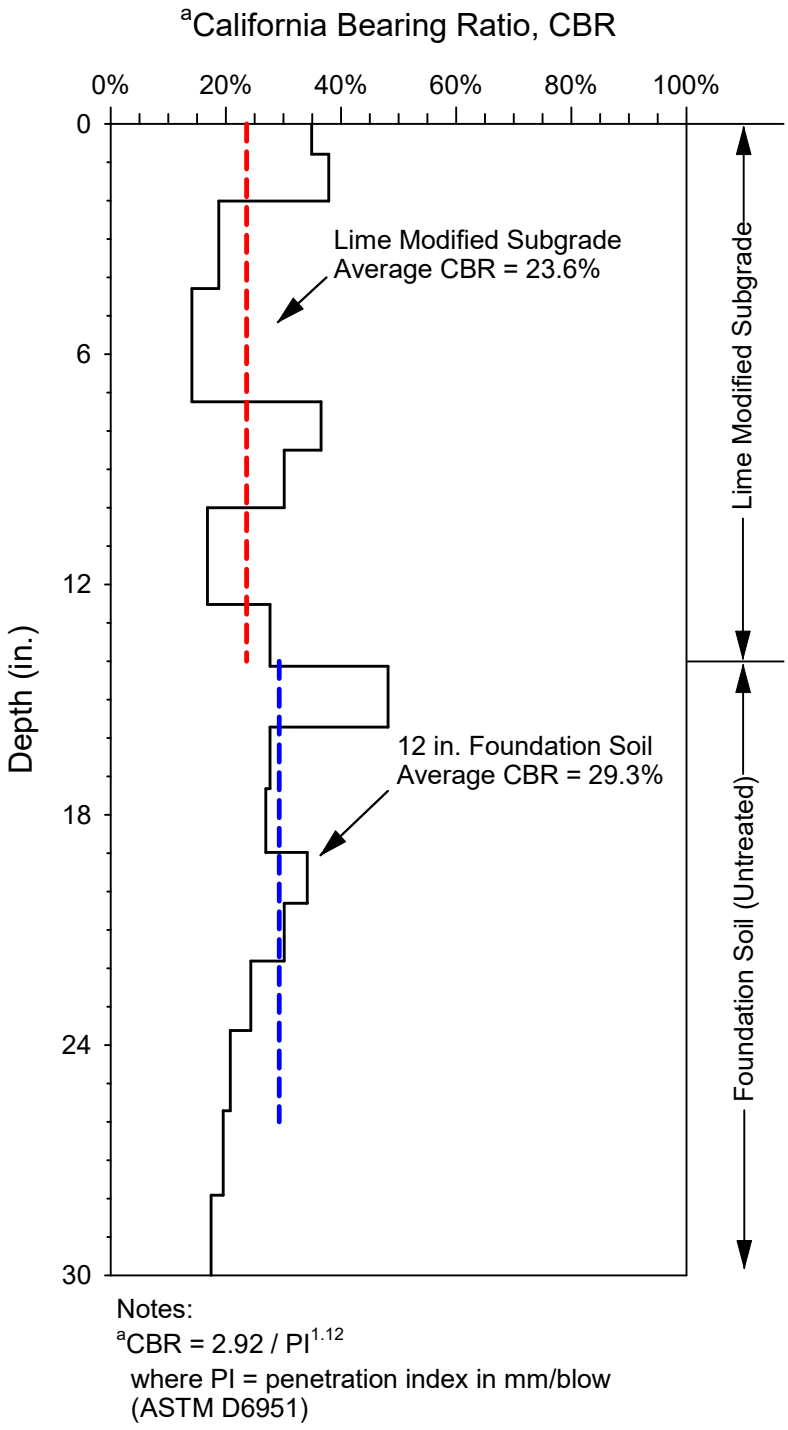

Figure A.15 California bearing ratio DCP profile for 14-inch thick lime modified subgrade sections (Lanes 1 & 2) measured 4-day after placement—Test No. 5.

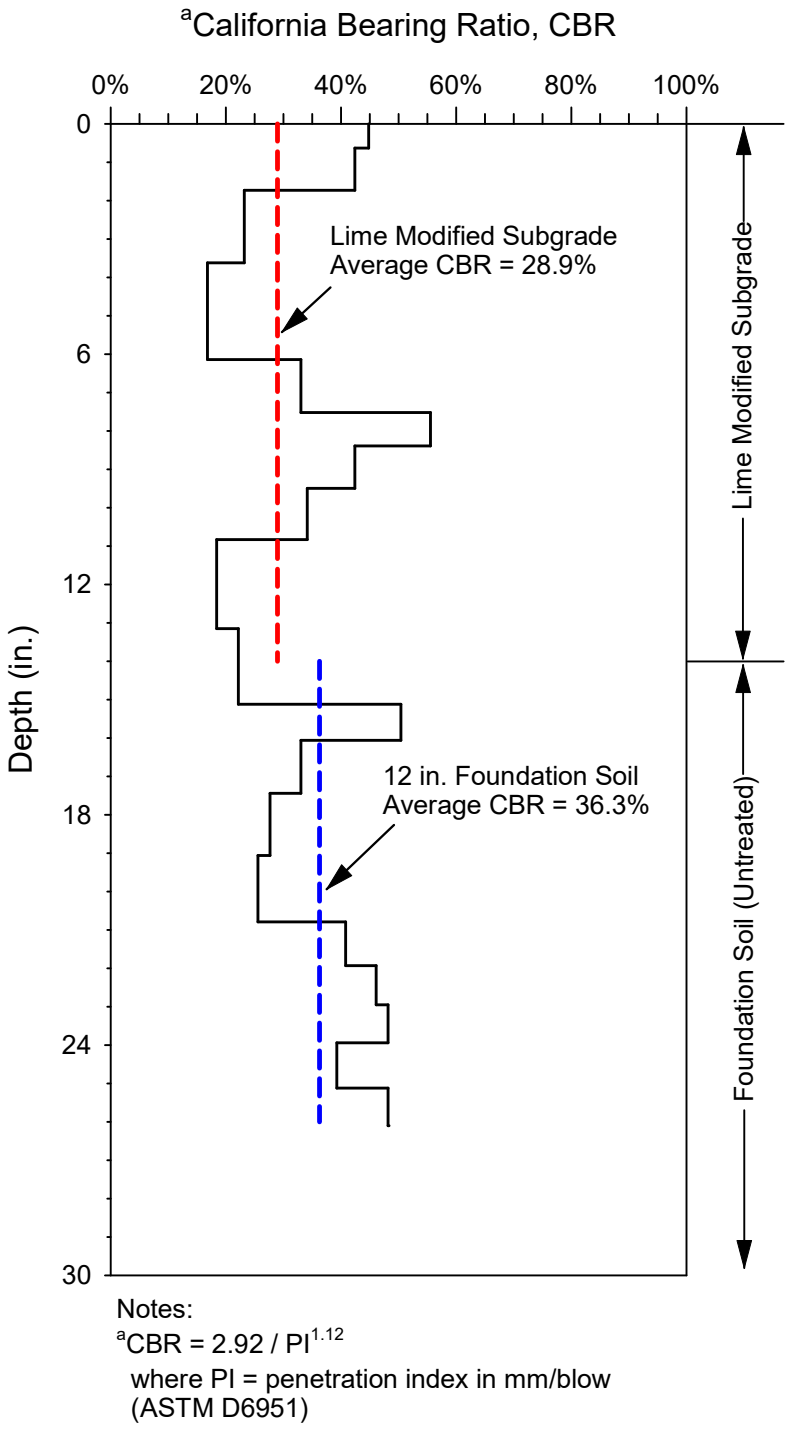

Figure A.16 California bearing ratio DCP profile for 14-inch thick lime modified subgrade sections (Lanes 1 & 2) measured 7-day after placement—Test No. 1.

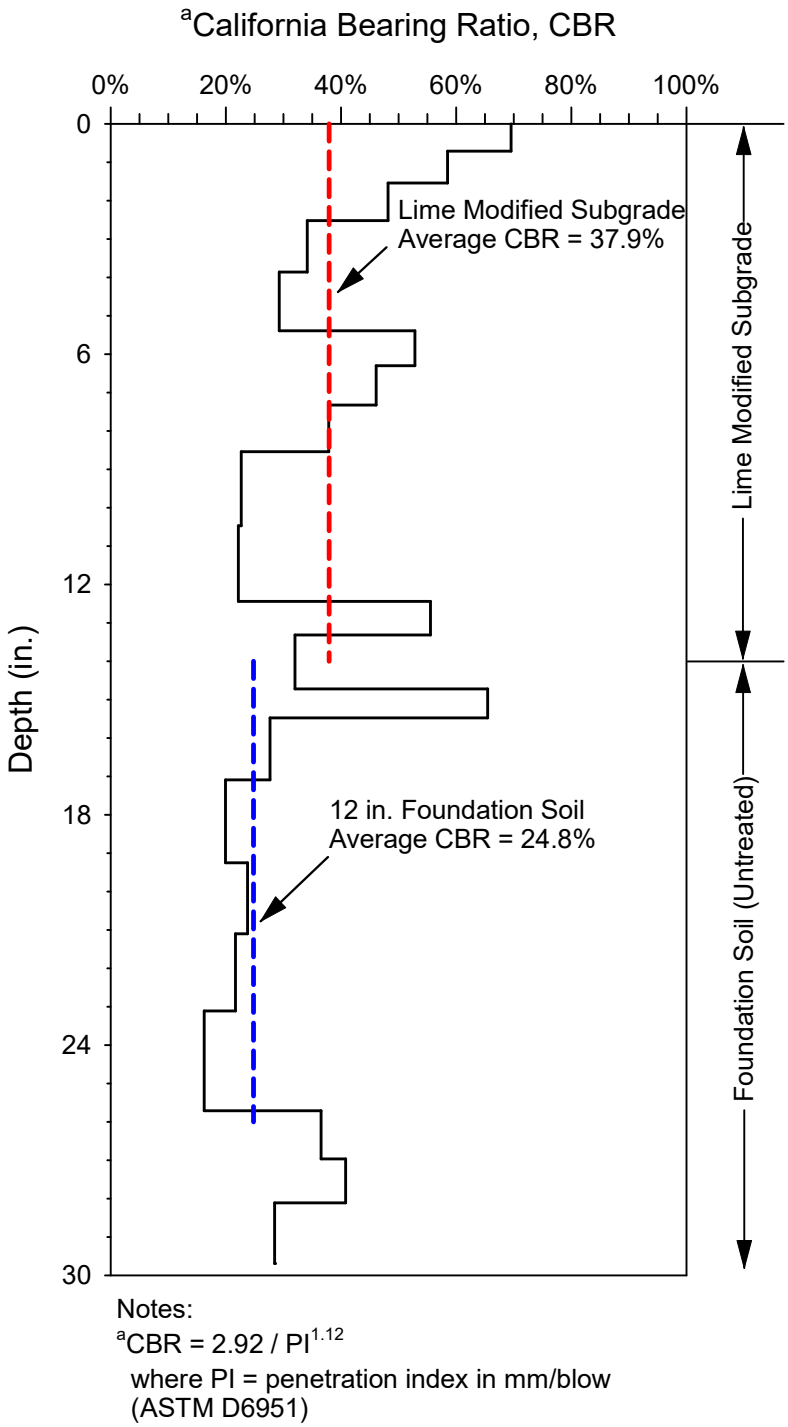

Figure A.17 California bearing ratio DCP profile for 14-inch thick lime modified subgrade sections (Lanes 1 & 2) measured 7-day after placement—Test No. 2.

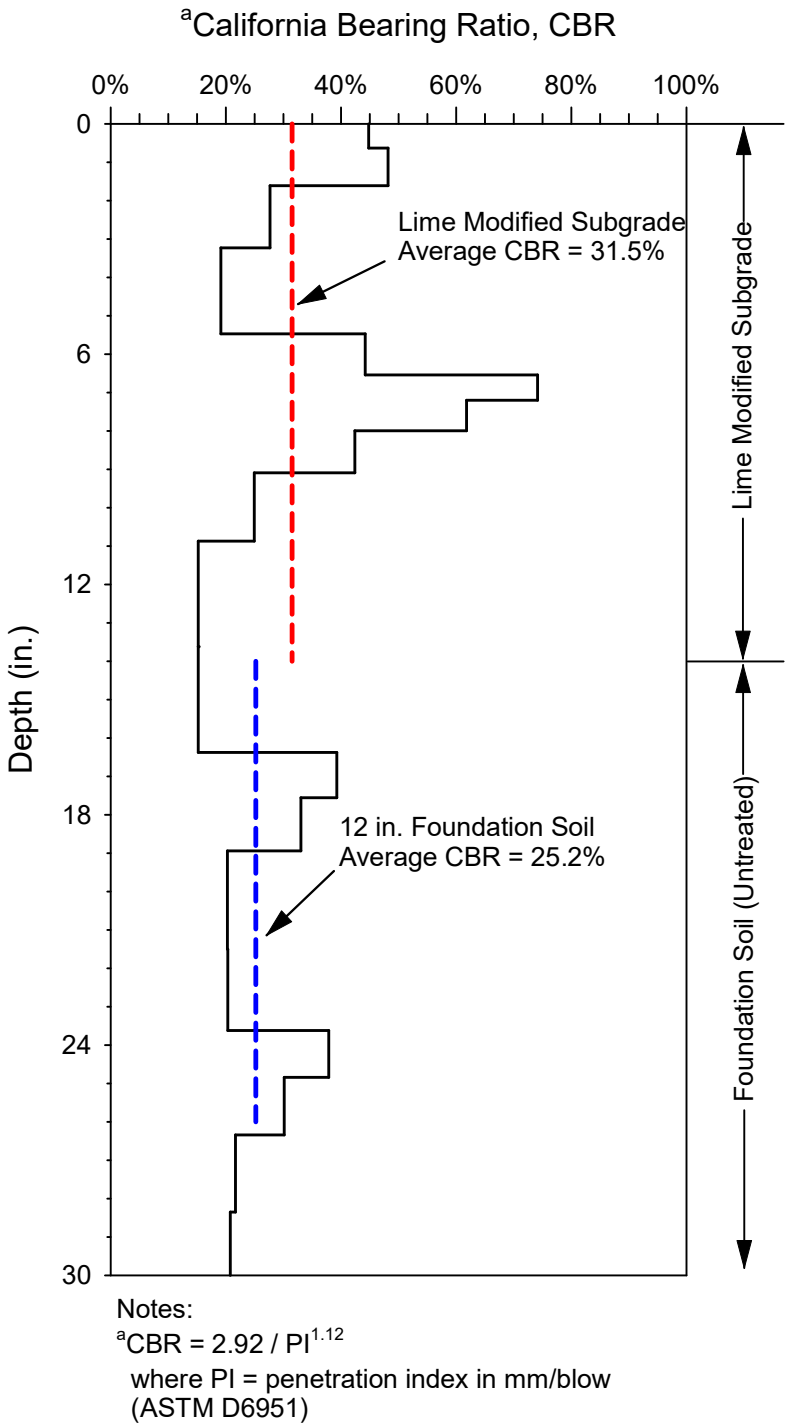

Figure A.18 California bearing ratio DCP profile for 14-inch thick lime modified subgrade sections (Lanes 1 & 2) measured 7-day after placement—Test No. 3.

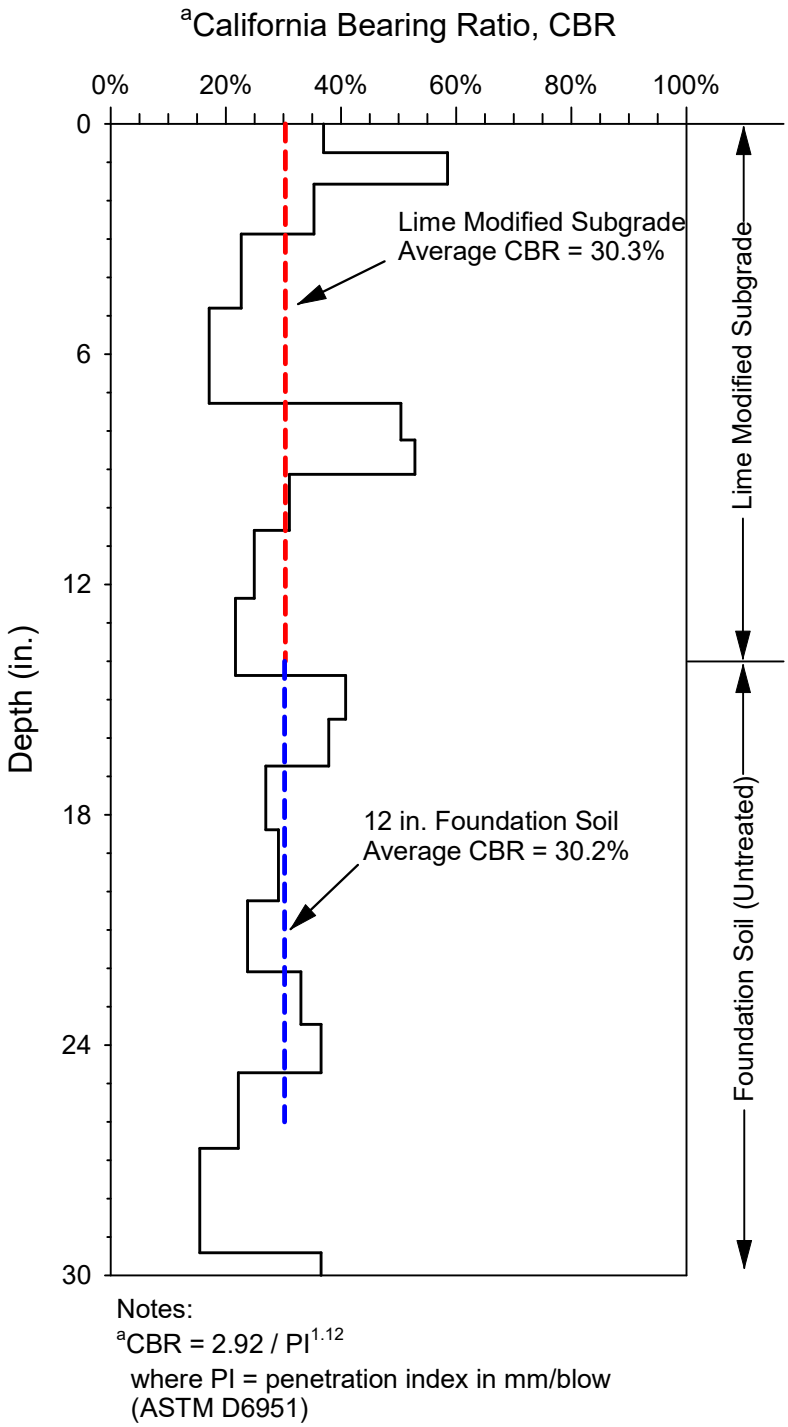

Figure A.19 California bearing ratio DCP profile for 14-inch thick lime modified subgrade sections (Lanes 1 & 2) measured 7-day after placement—Test No. 4.

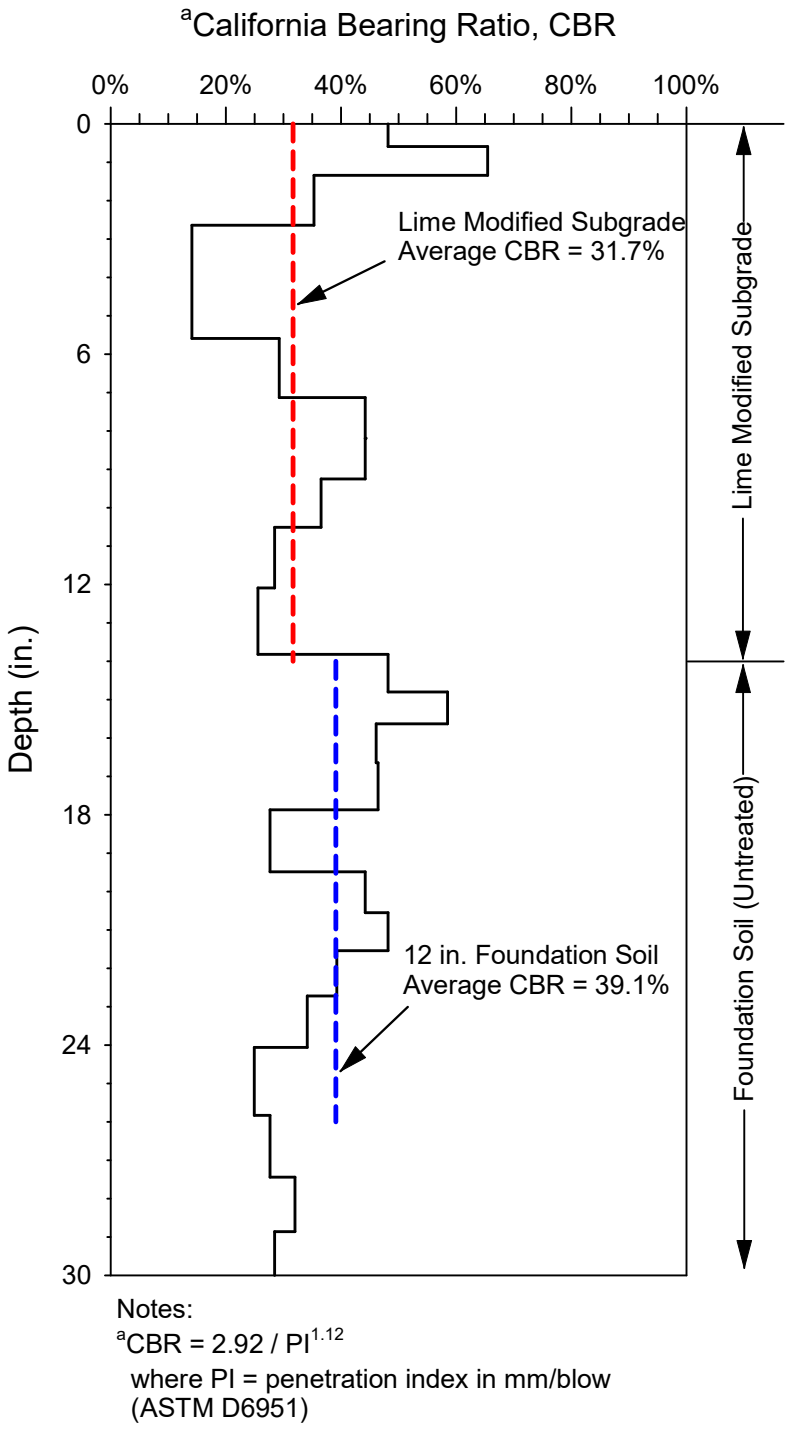

Figure A.20 California bearing ratio DCP profile for 14-inch thick lime modified subgrade sections (Lanes 1 & 2) measured 7-day after placement—Test No. 5.

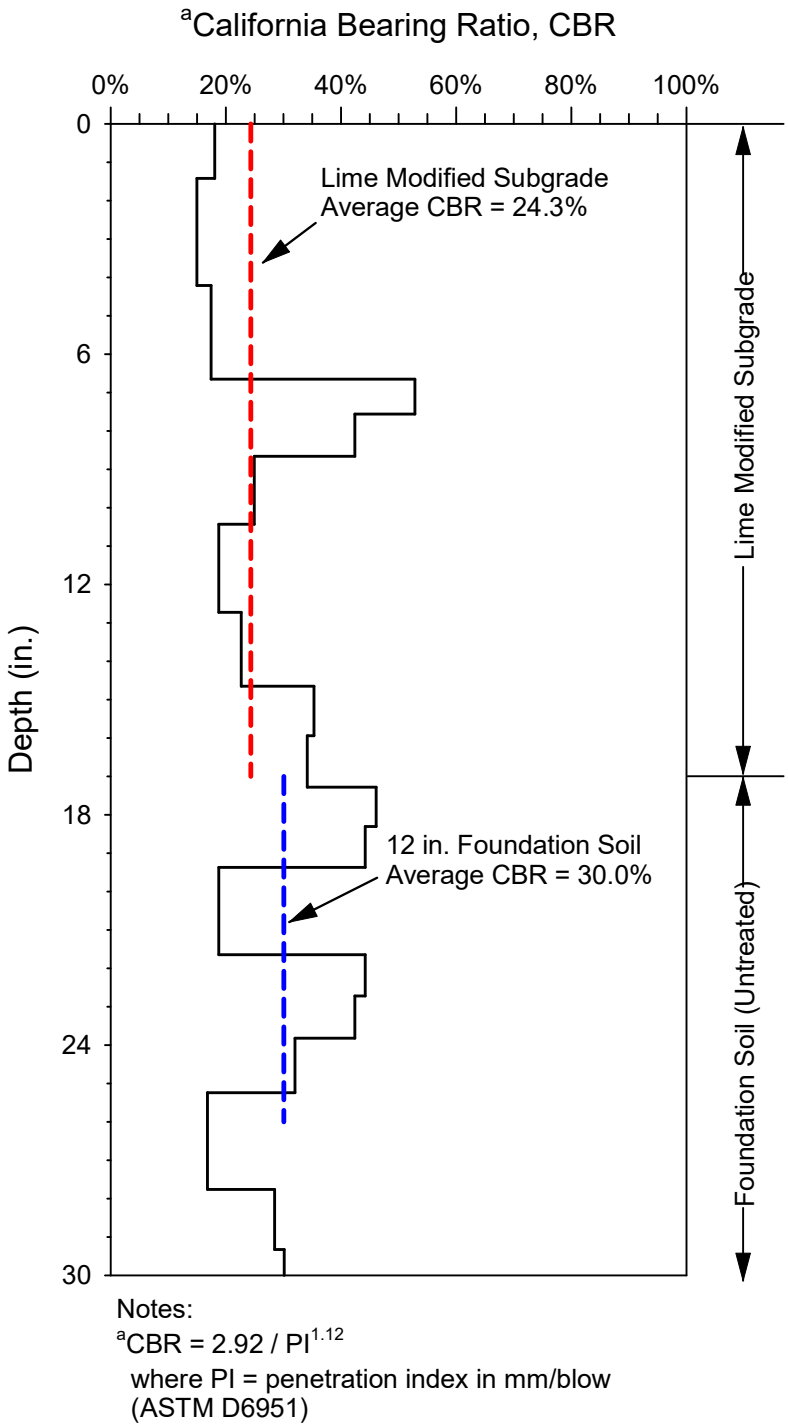

Figure A.21 California bearing ratio DCP profile for 17-inch thick lime modified subgrade sections (Lanes 3 & 4) measured 1-day after placement—Test No. 1.

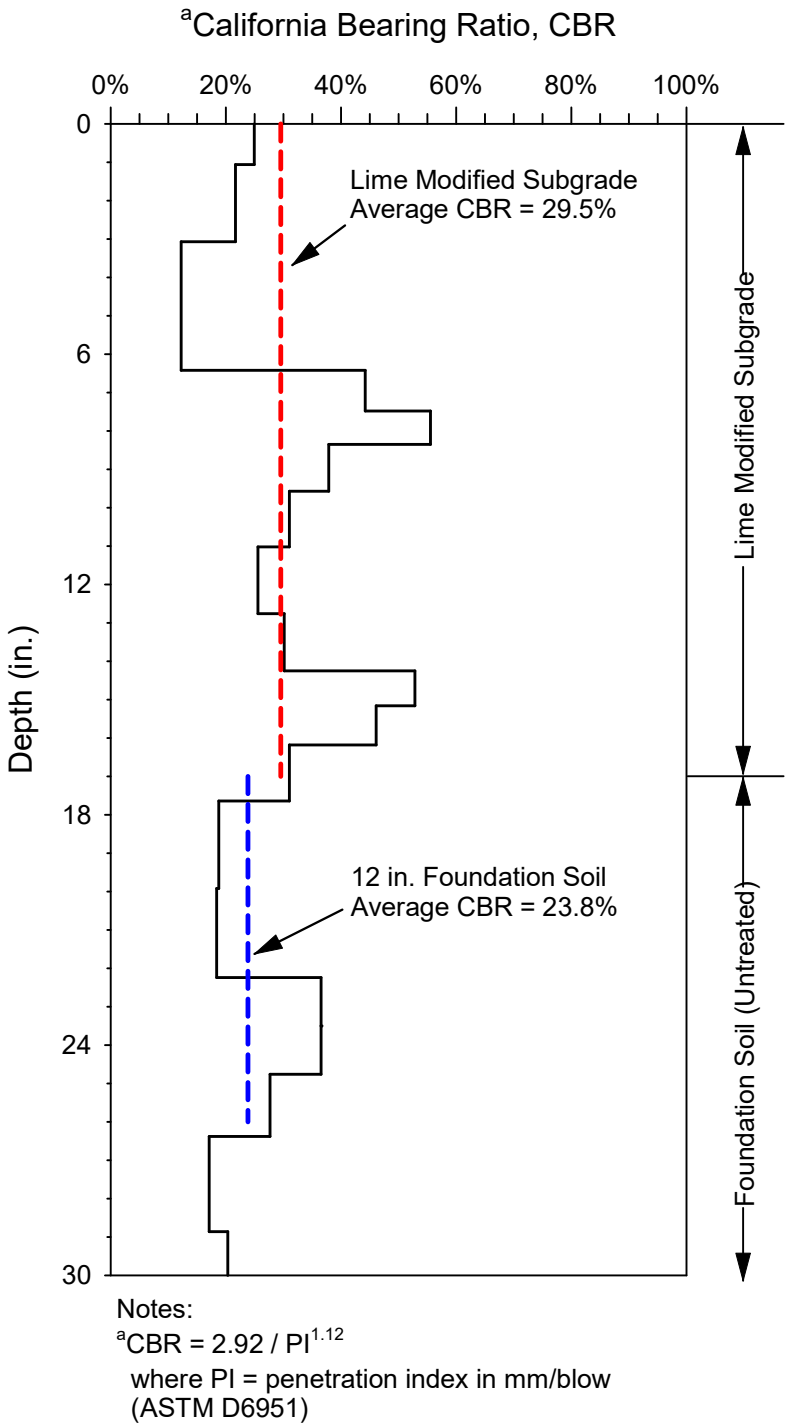

Figure A.22 California bearing ratio DCP profile for 17-inch thick lime modified subgrade sections (Lanes 3 & 4) measured 1-day after placement—Test No. 2.

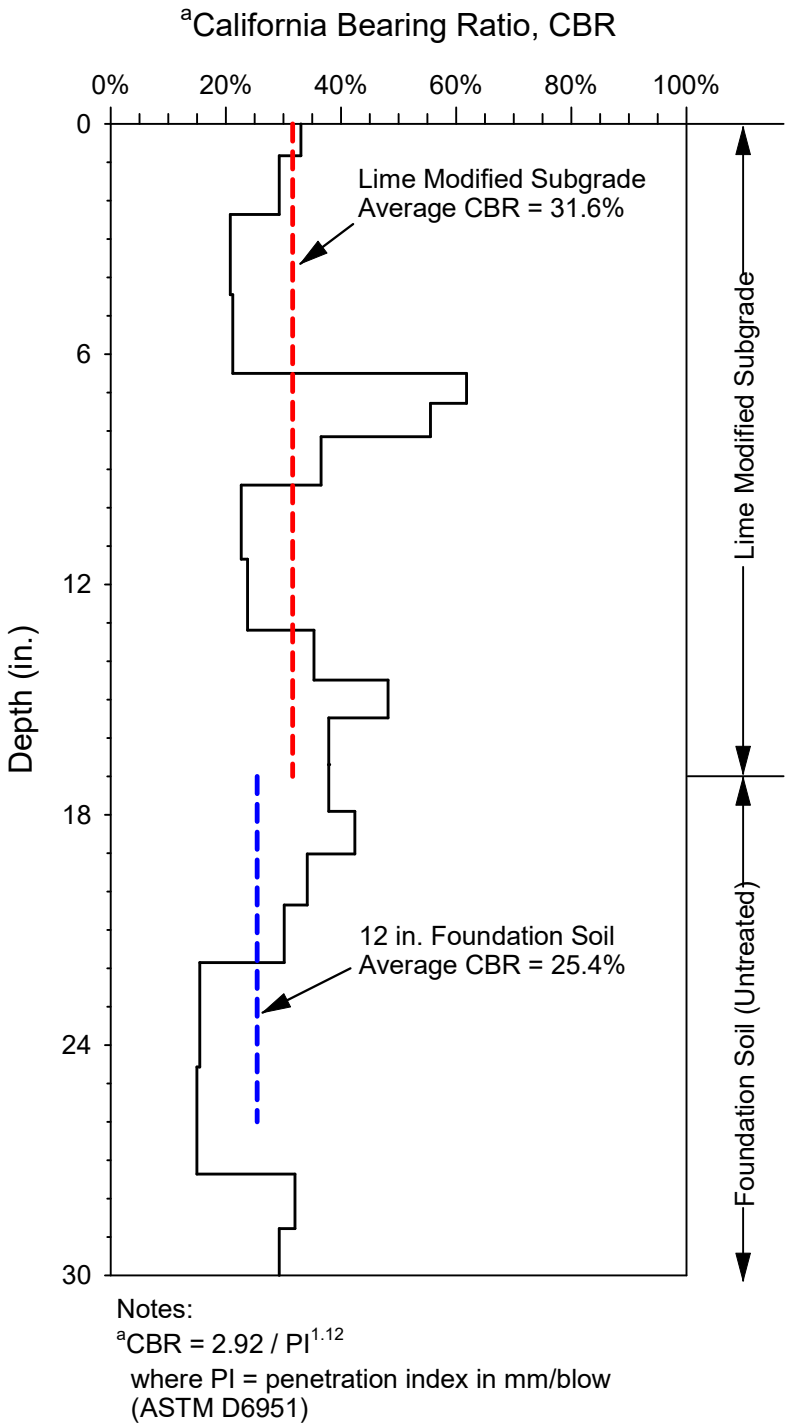

Figure A.23 California bearing ratio DCP profile for 17-inch thick lime modified subgrade sections (Lanes 3 & 4) measured 1-day after placement—Test No. 3.

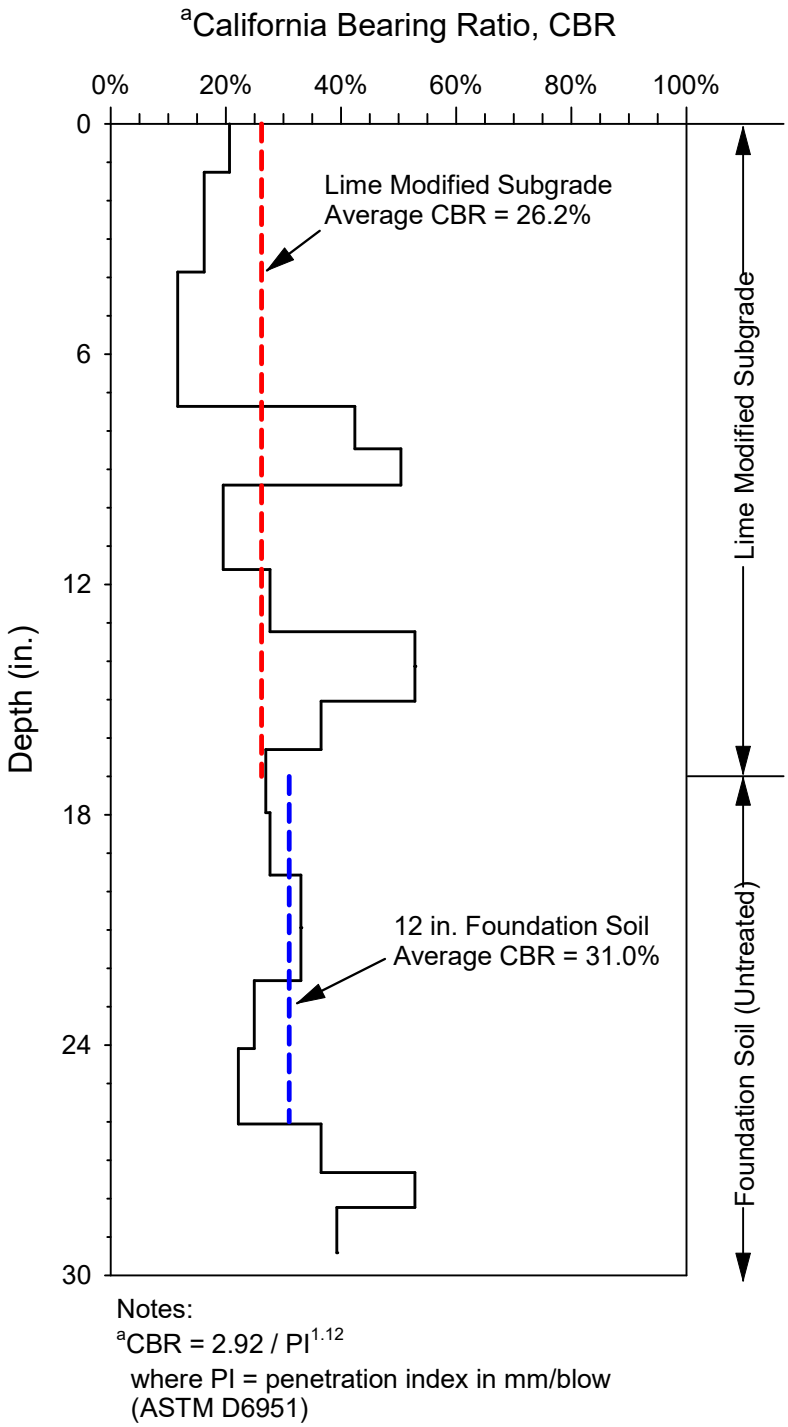

Figure A.24 California bearing ratio DCP profile for 17-inch thick lime modified subgrade sections (Lanes 3 & 4) measured 1-day after placement—Test No. 4.

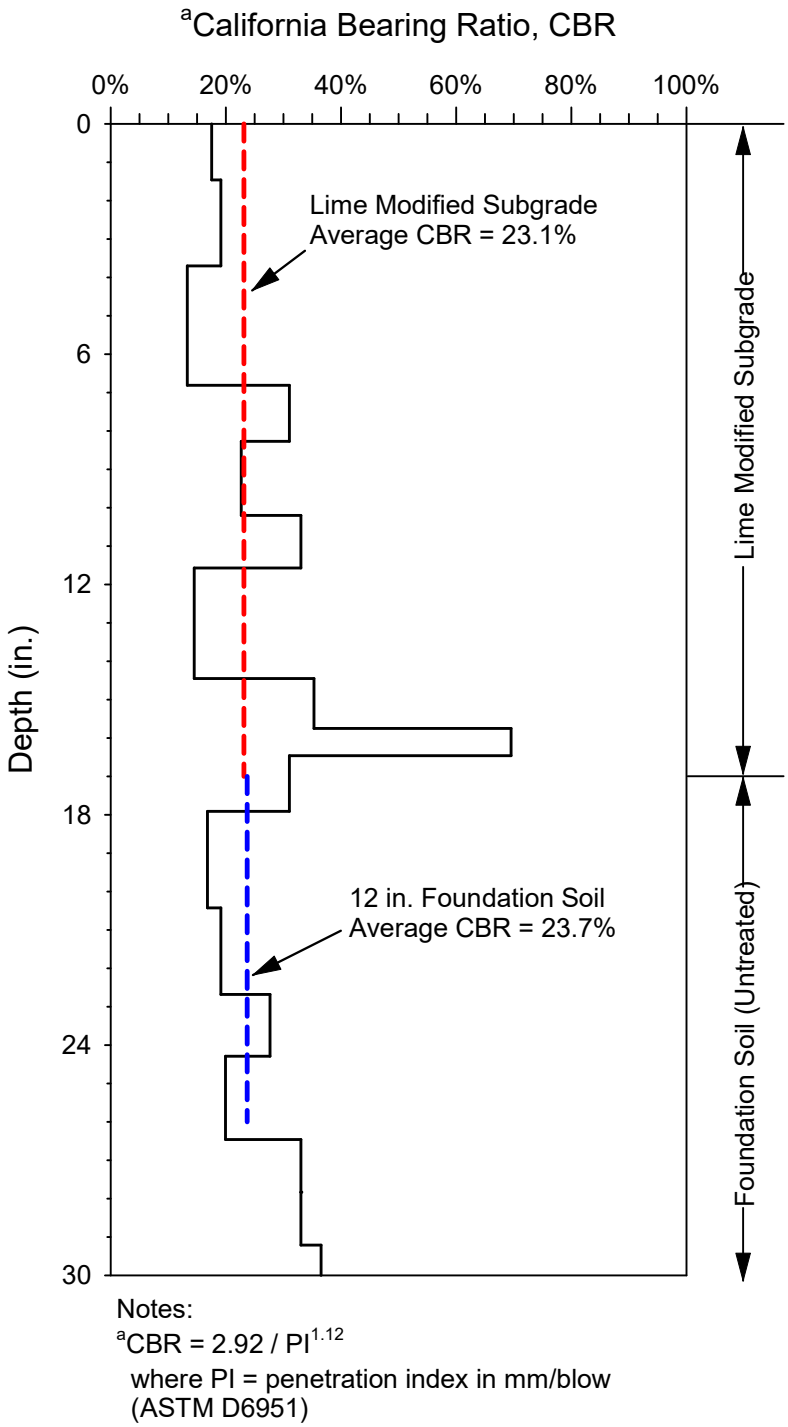

Figure A.25 California bearing ratio DCP profile for 17-inch thick lime modified subgrade sections (Lanes 3 & 4) measured 1-day after placement—Test No. 5.

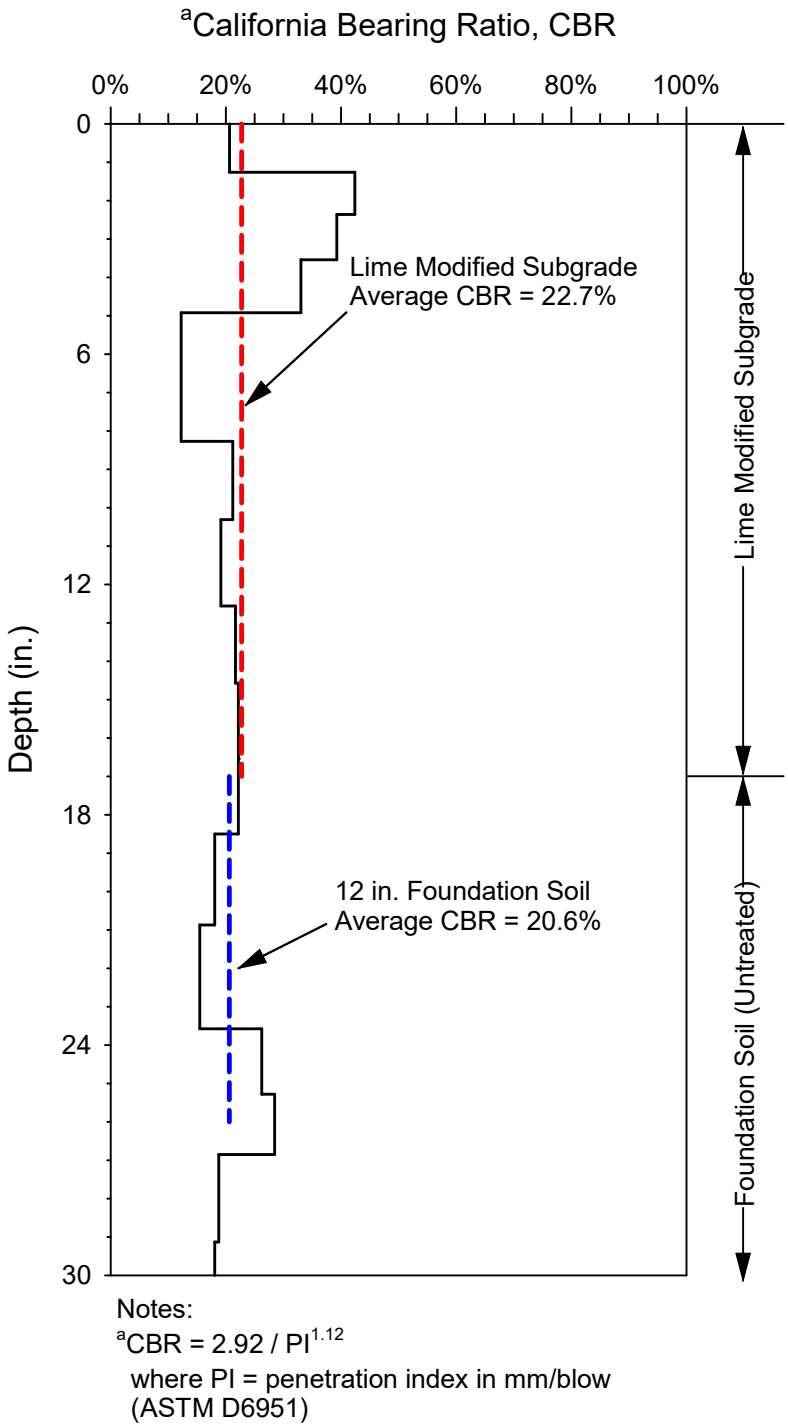

Figure A.26 California bearing ratio DCP profile for 17-inch thick lime modified subgrade sections (Lanes 3 & 4) measured 3-day after placement—Test No. 1.

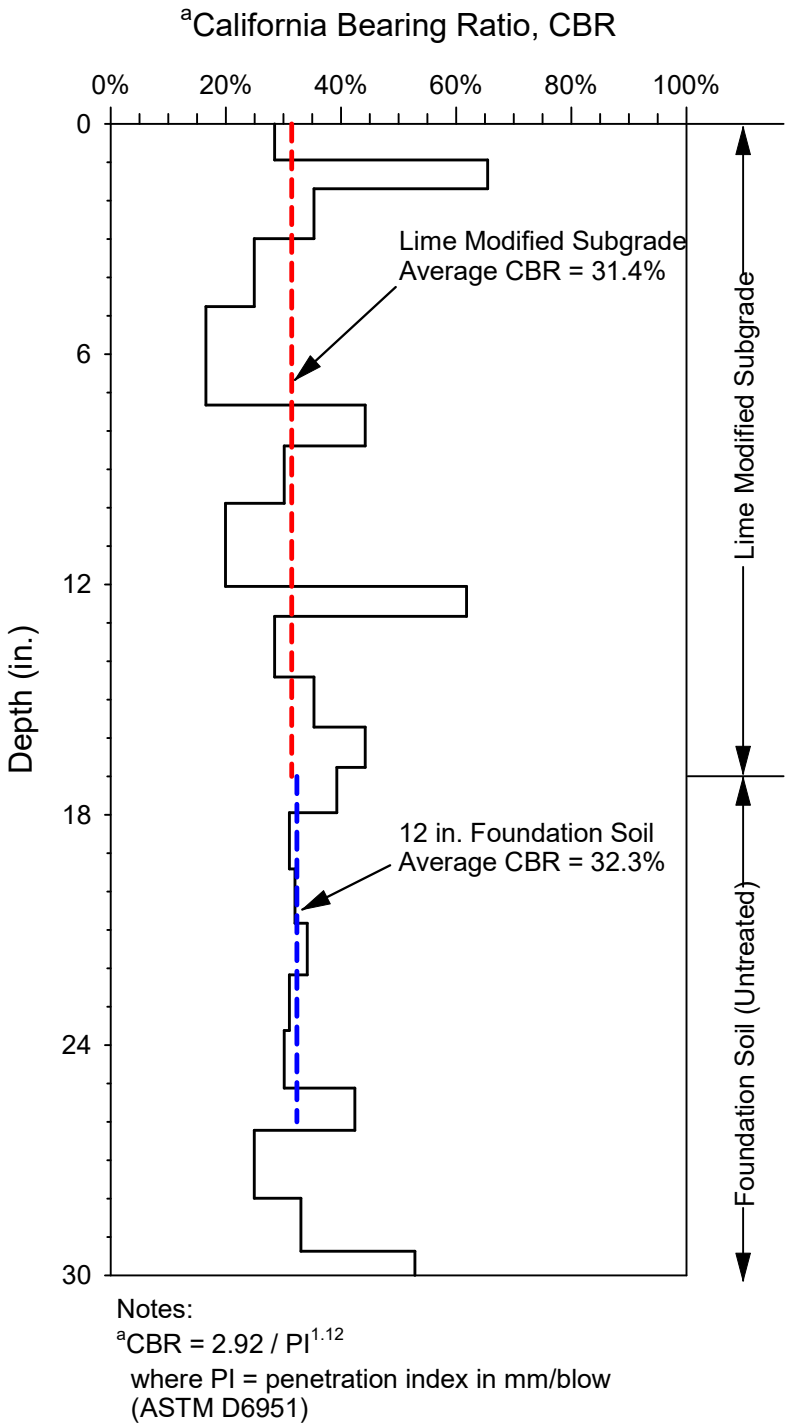

Figure A.27 California bearing ratio DCP profile for 17-inch thick lime modified subgrade sections (Lanes 3 & 4) measured 3-day after placement—Test No. 2.

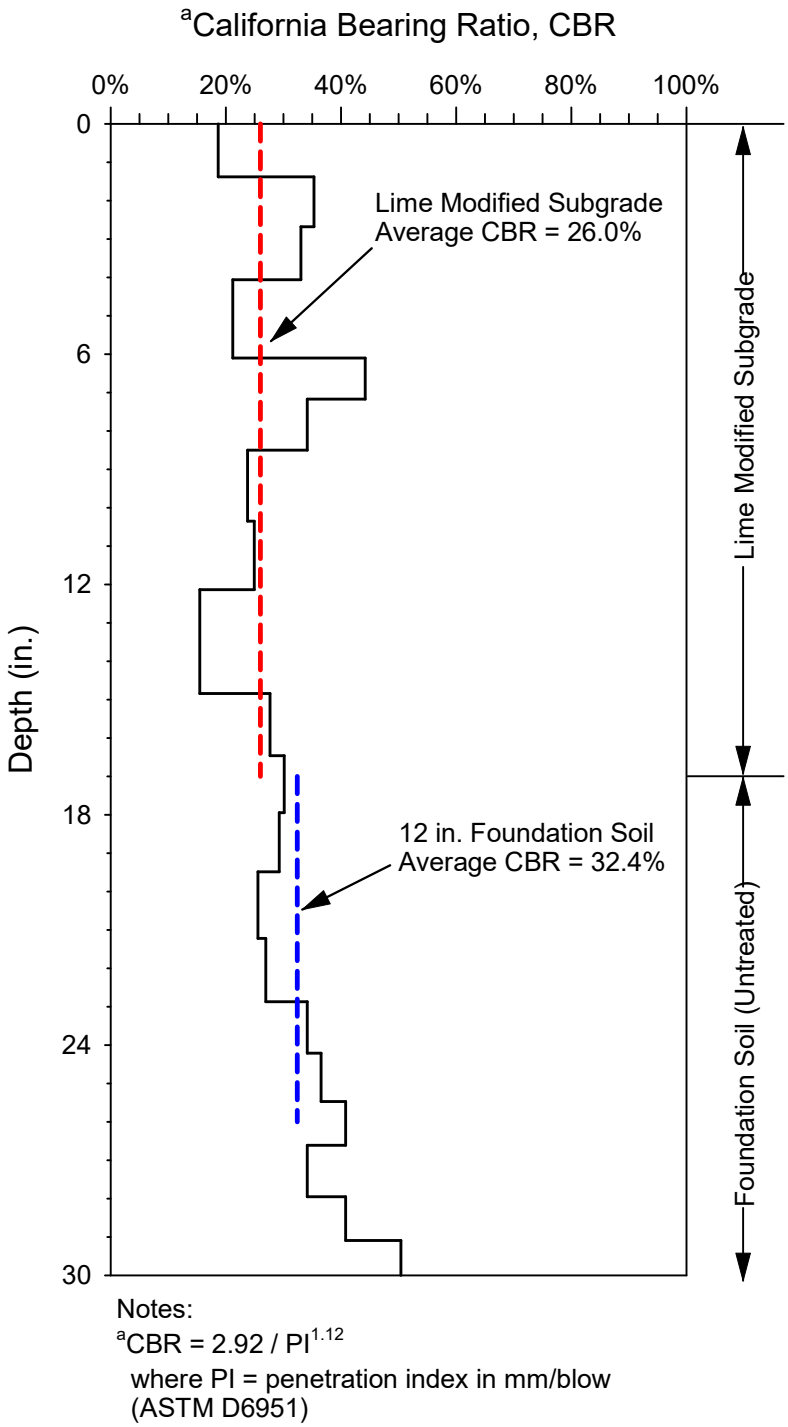

Figure A.28 California bearing ratio DCP profile for 17-inch thick lime modified subgrade sections (Lanes 3 & 4) measured 3-day after placement—Test No. 3.

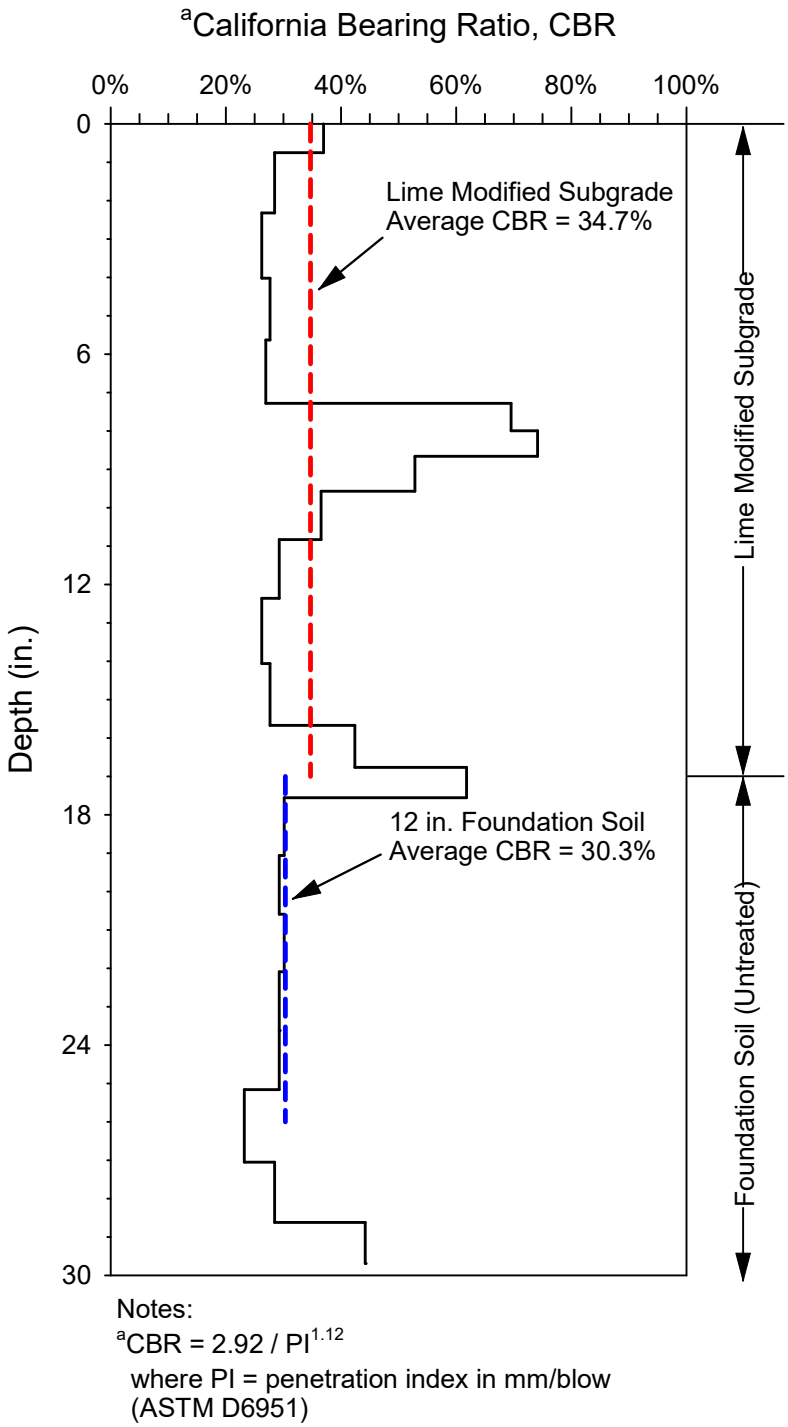

Figure A.29 California bearing ratio DCP profile for 17-inch thick lime modified subgrade sections (Lanes 3 & 4) measured 3-day after placement—Test No. 4.

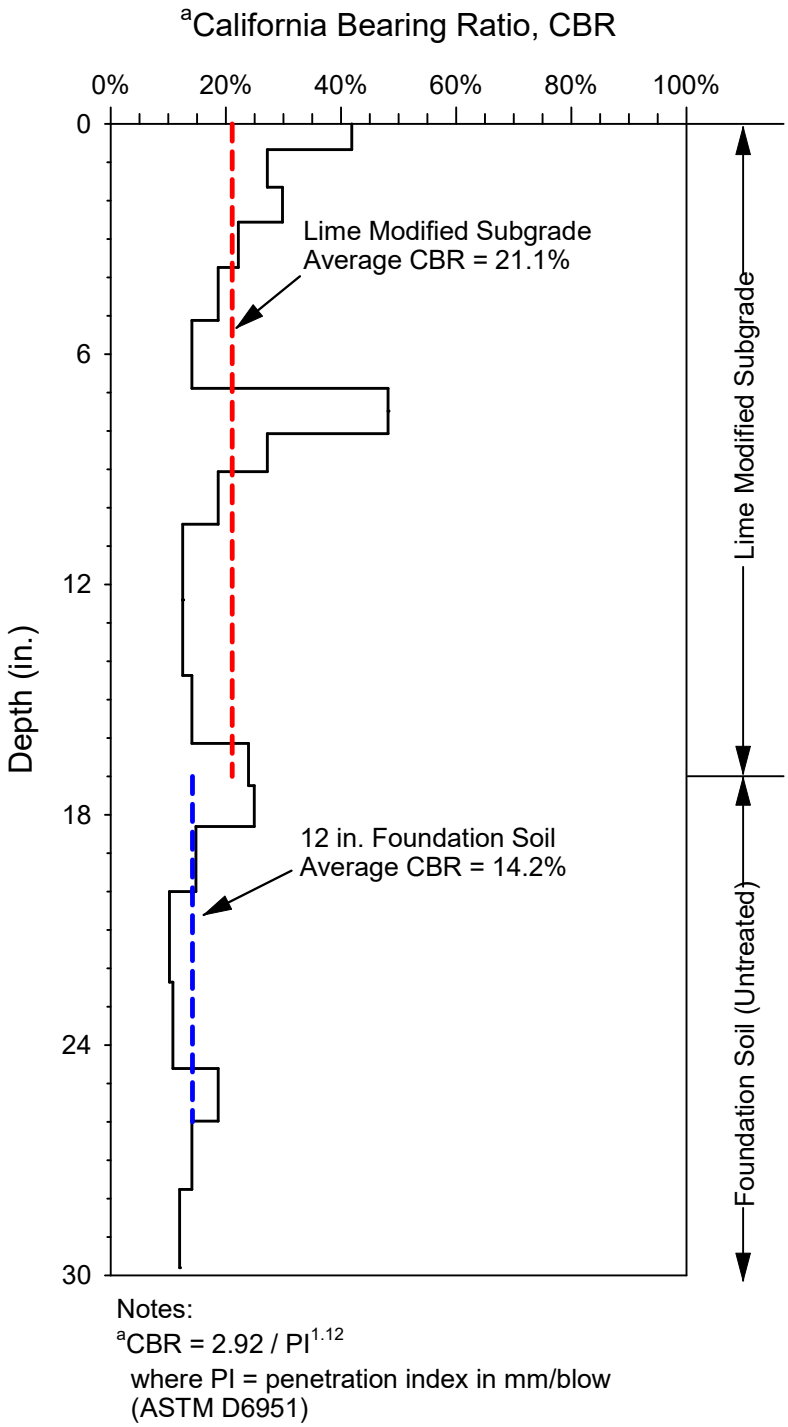

Figure A.30 California bearing ratio DCP profile for 17-inch thick lime modified subgrade sections (Lanes 3 & 4) measured 3-day after placement—Test No. 5.

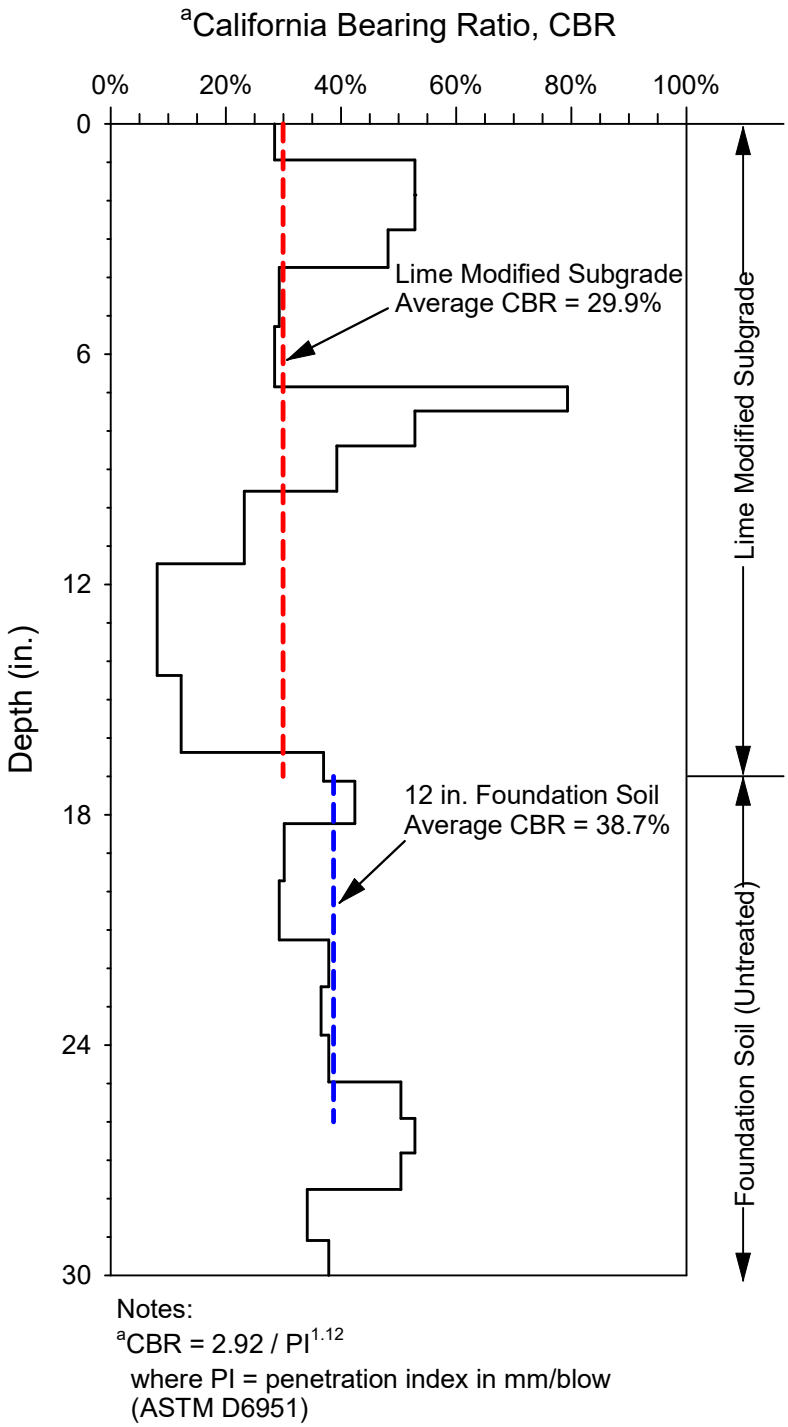

Figure A.31 California bearing ratio DCP profile for 17-inch thick lime modified subgrade sections (Lanes 3 & 4) measured 6-day after placement—Test No. 1.

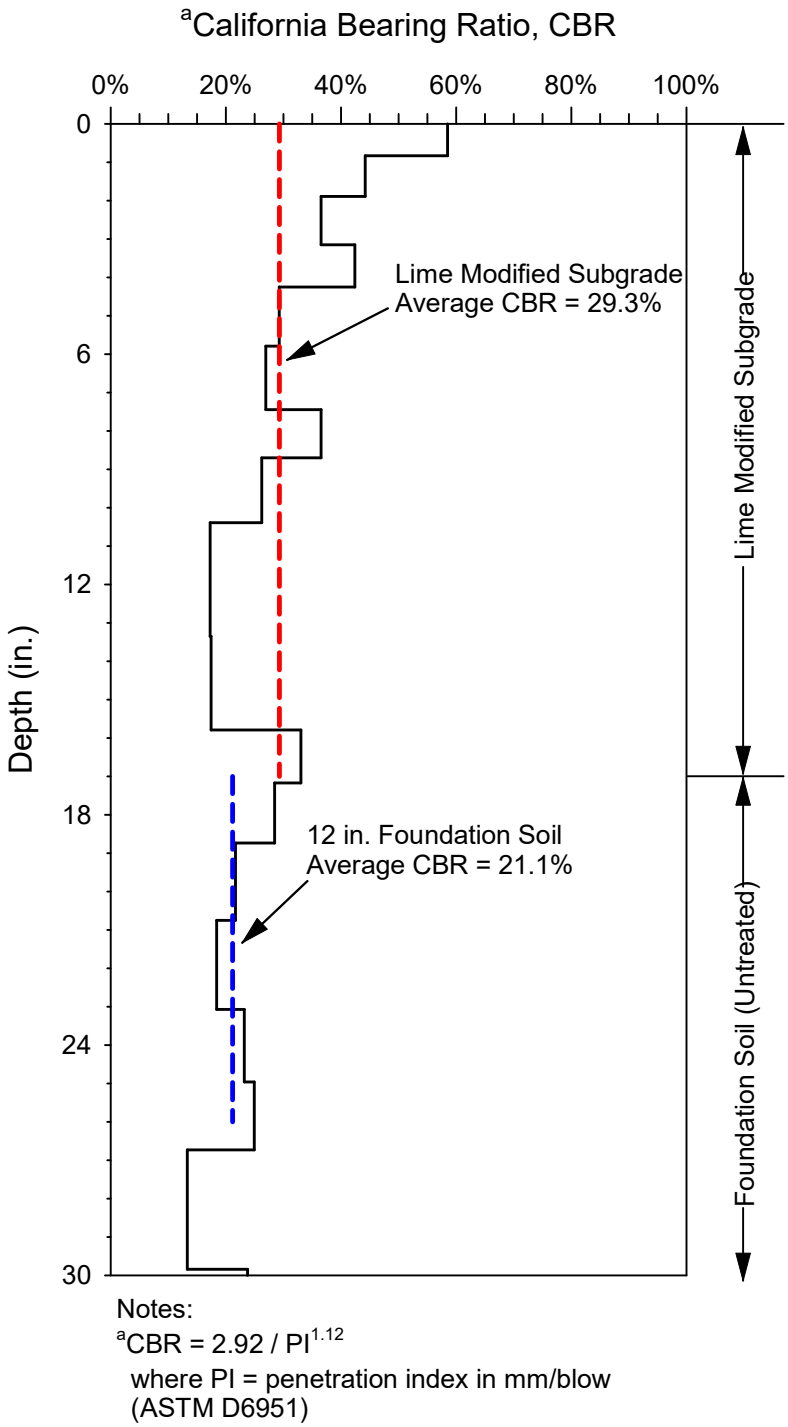

Figure A.32 California bearing ratio DCP profile for 17-inch thick lime modified subgrade sections (Lanes 3 & 4) measured 6-day after placement—Test No. 2.

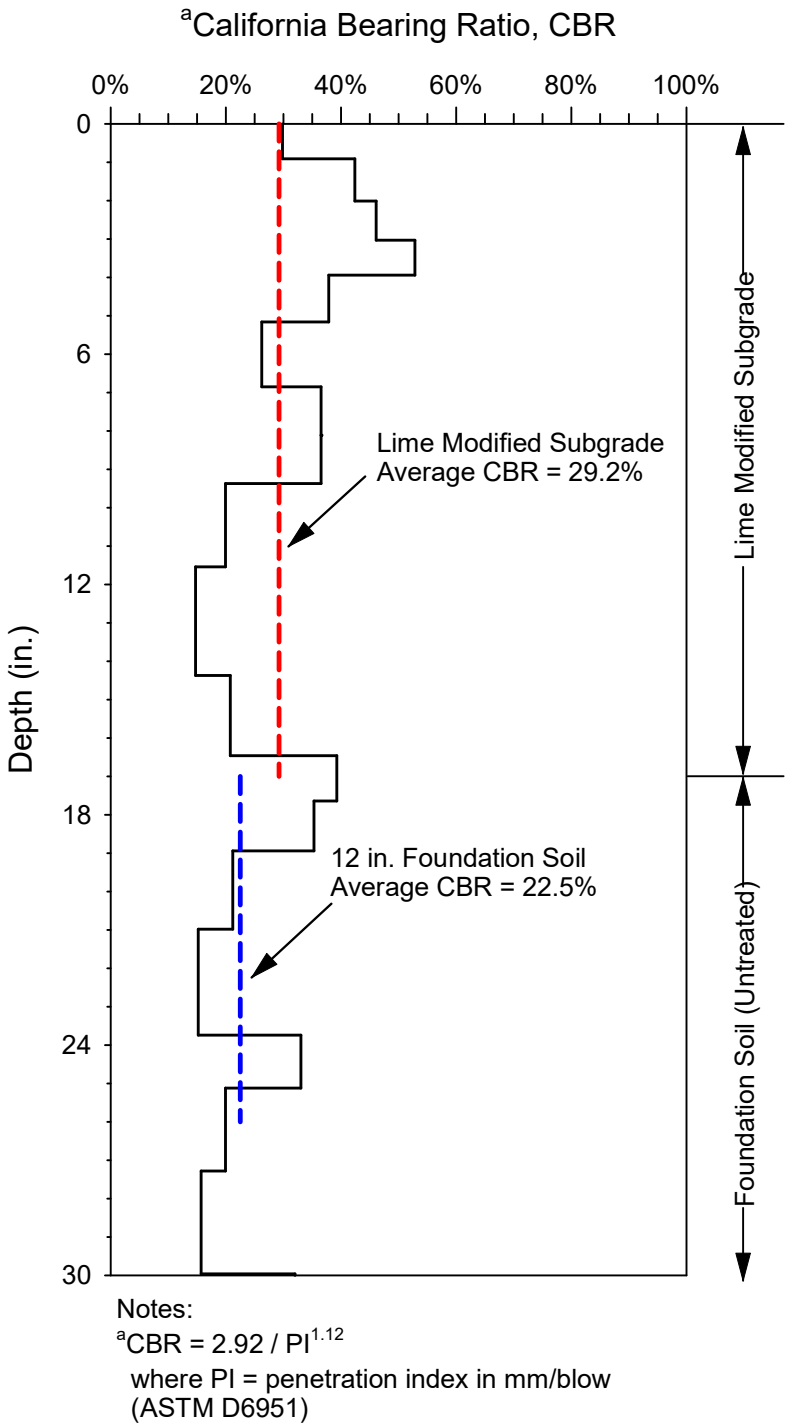

Figure A.33 California bearing ratio DCP profile for 17-inch thick lime modified subgrade sections (Lanes 3 & 4) measured 6-day after placement—Test No. 3.

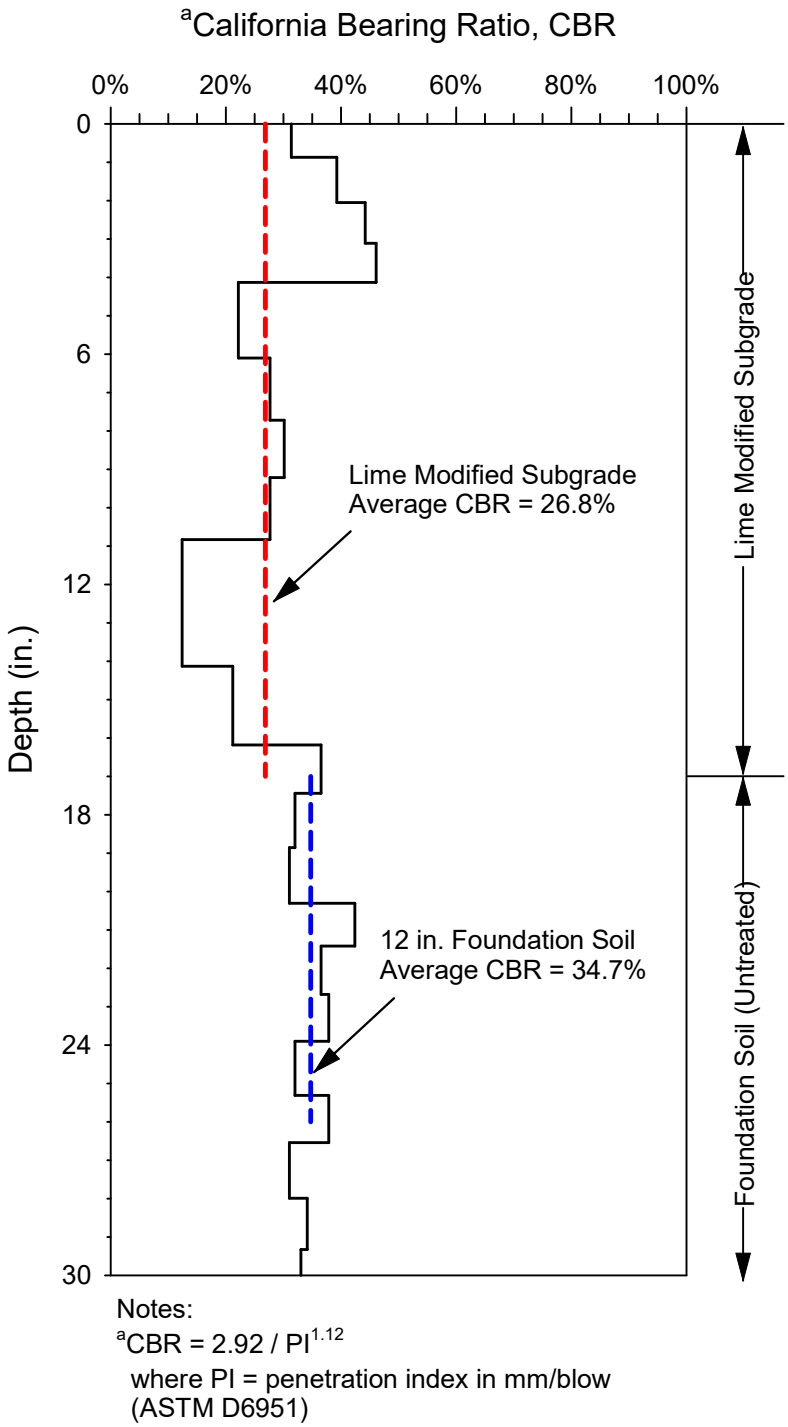

Figure A.34 California bearing ratio DCP profile for 17-inch thick lime modified subgrade sections (Lanes 3 & 4) measured 6-day after placement—Test No. 4.

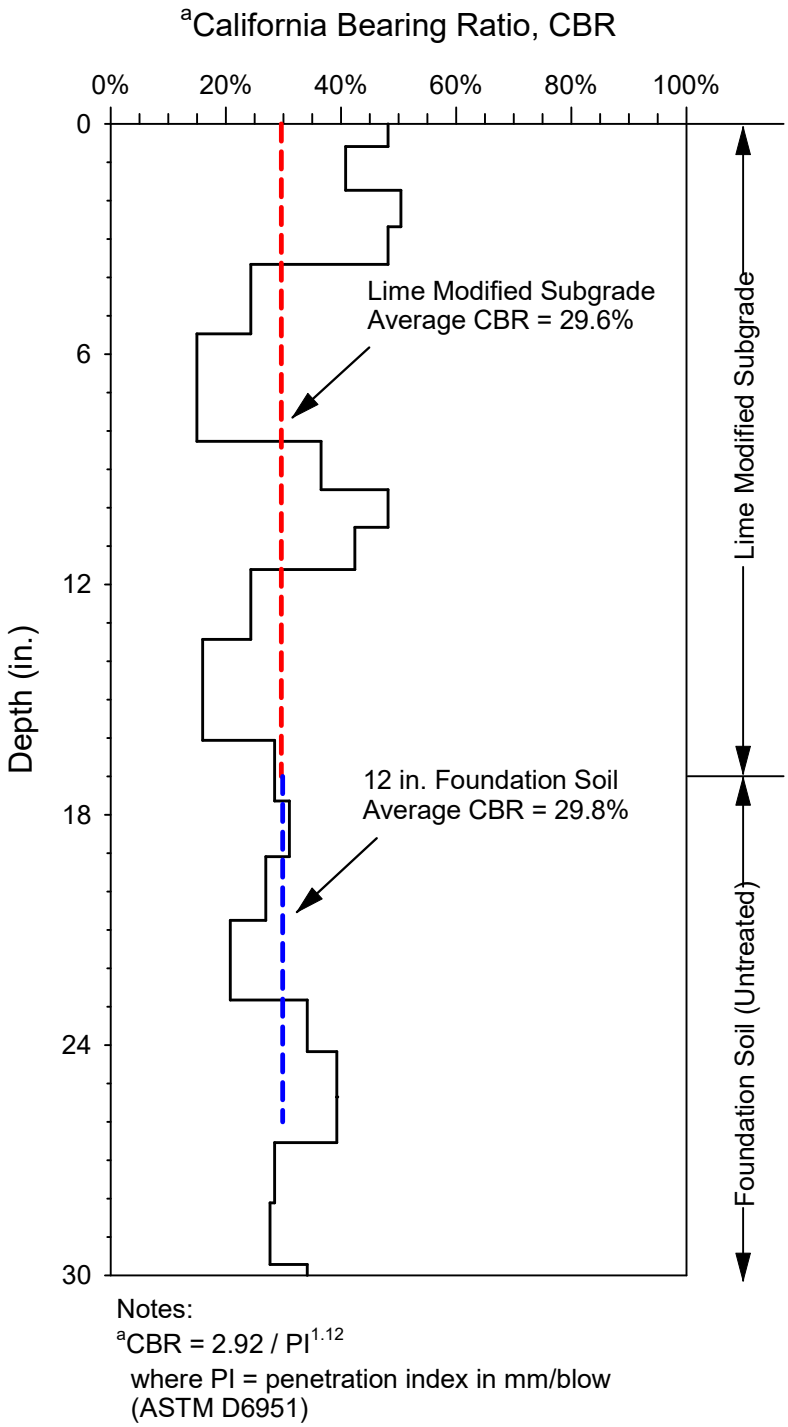

Figure A.35 California bearing ratio DCP profile for 17-inch thick lime modified subgrade sections (Lanes 3 & 4) measured 6-day after placement—Test No. 5.

APPENDIX B. RUT DEPTH EVOLUTION TRENDS

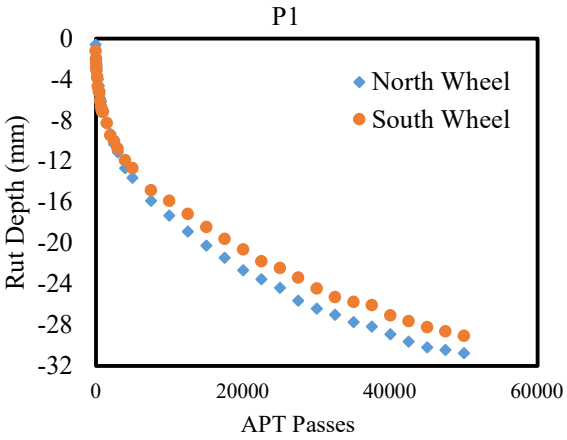

(a) Rut depth at P1

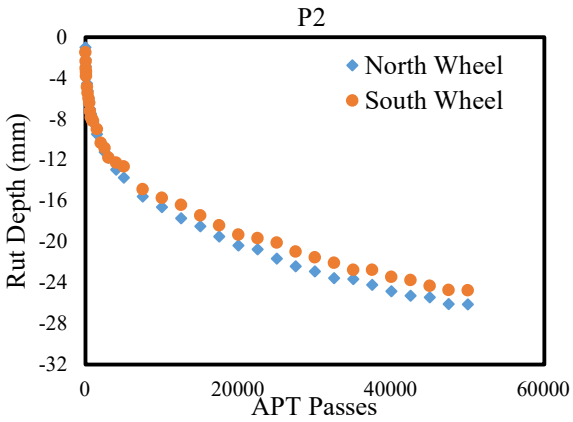

(b) Rut depth at P2

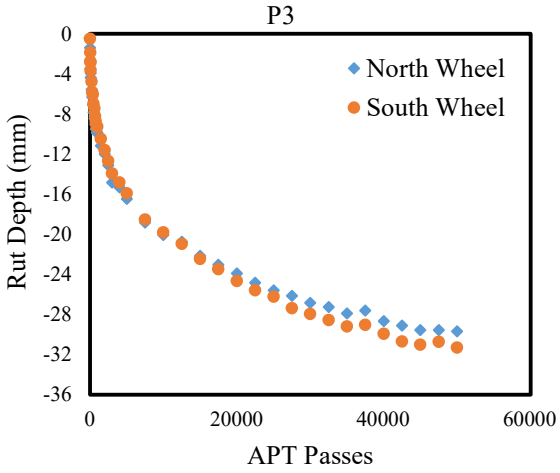

(c) Rut depth at P3

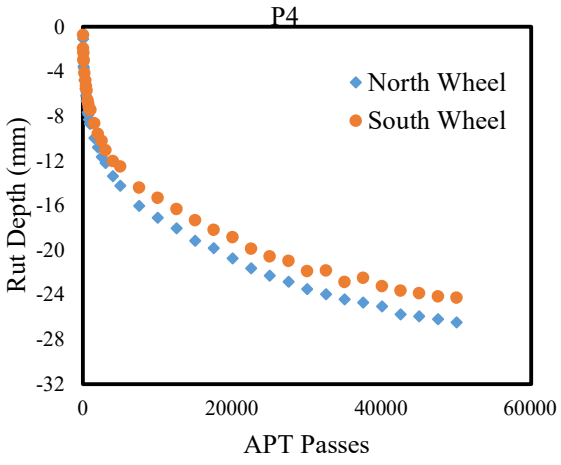

(d) Rut depth at P4

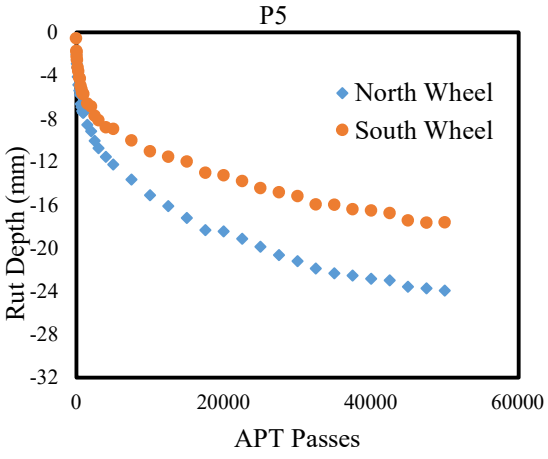

(e) Rut depth at P5

Figure B.1 Rut depth evolution for 10-inch dense-graded HMA pavement.

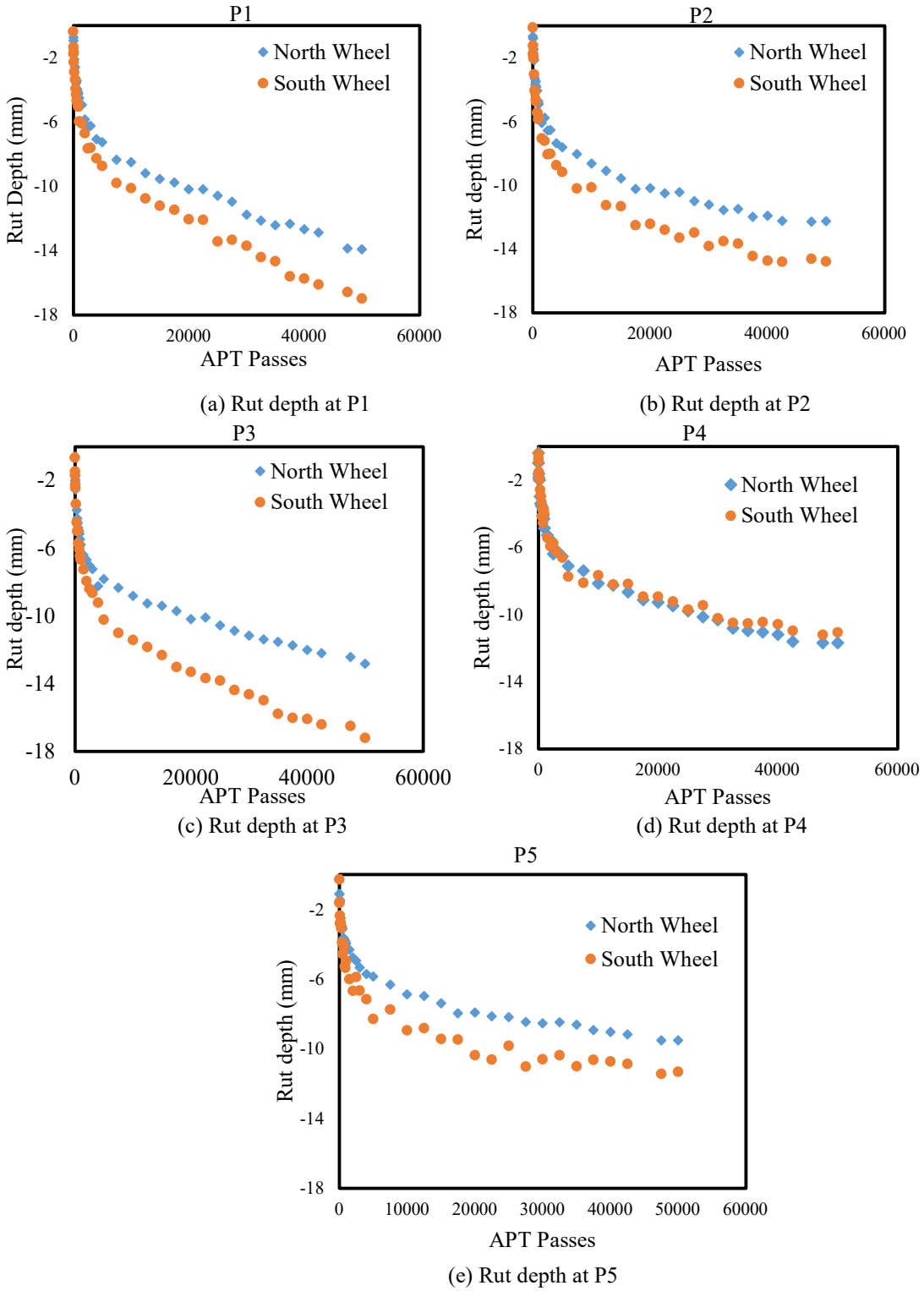

Figure B.2 Rut depth evolution for 10-inch SMA pavement.

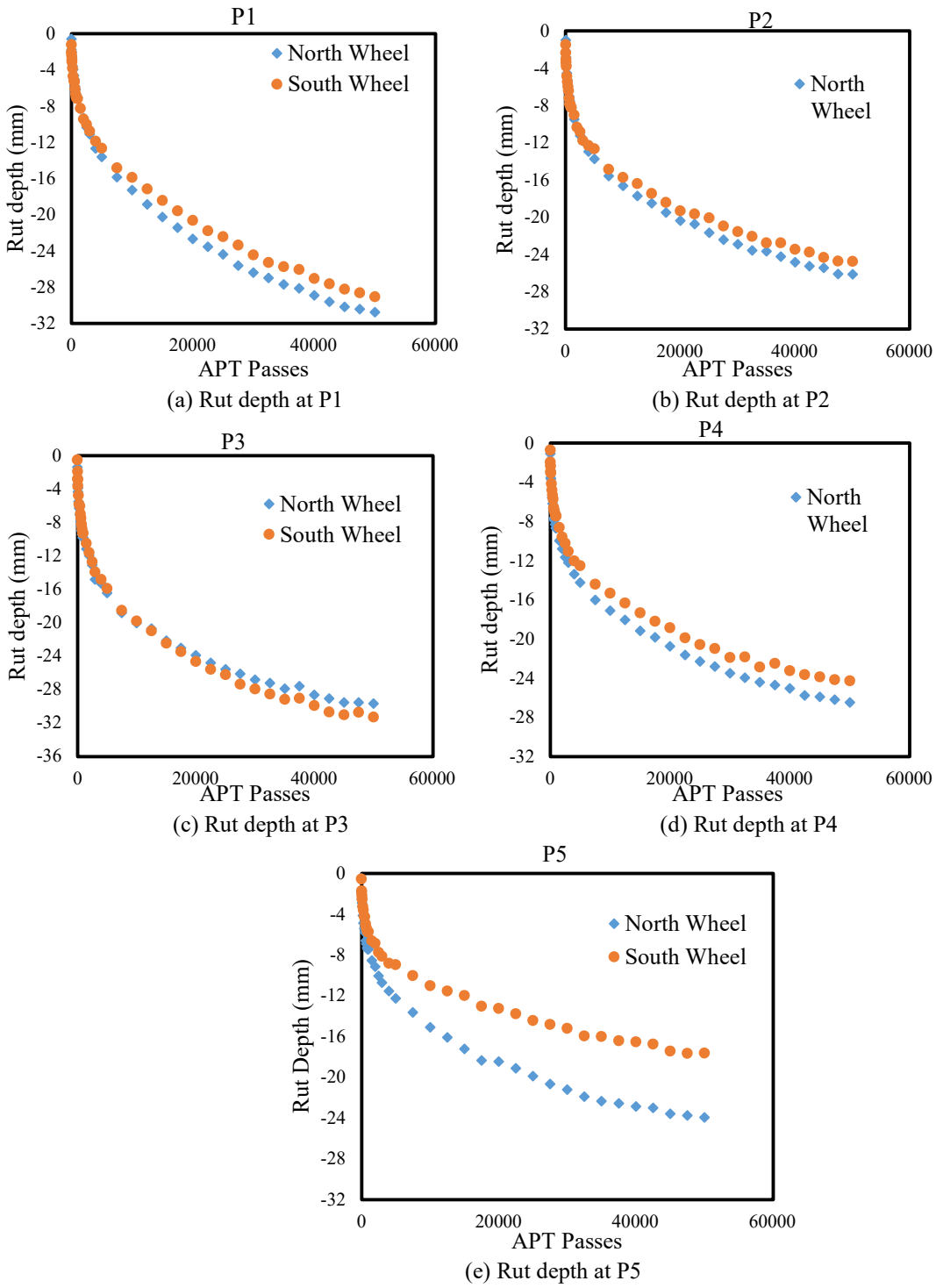

Figure B.3 Rut depth evolution for 7-inch SMA pavement.

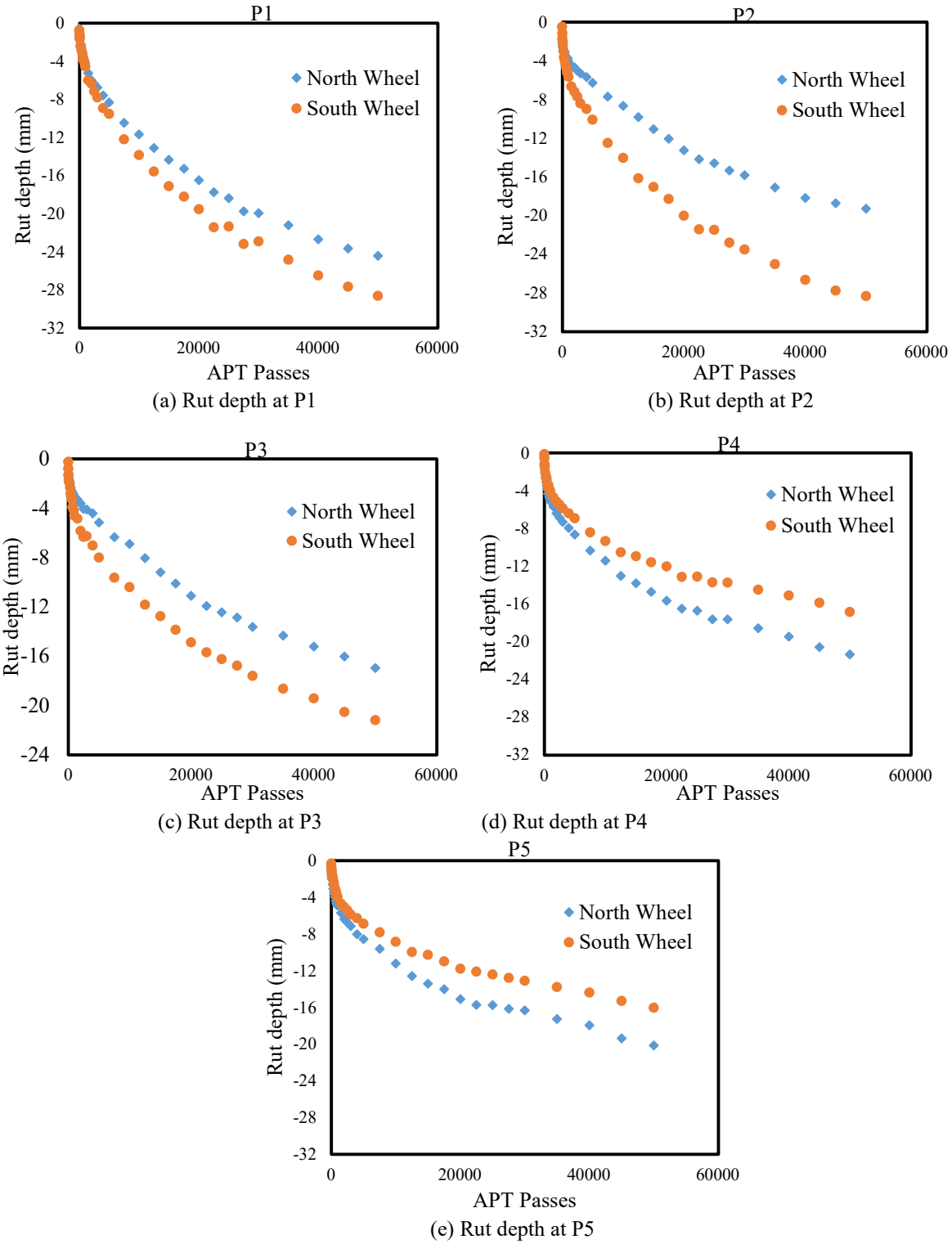

Figure B.1 Depth evolution for 7-inch dense-graded HMA pavement.

APPENDIX C. MATERIAL INPUTS

Table C.1 Material Inputs for Lane 1 and 2

	Surface	Intermediate	Base	
Layer		**HMA Mix**		**Subgrade**
G_{mm}	2.533	2.578	2.578	
Poisson's ratio	0.35	0.35	0.35	
G_{mb}	2.356	2.398	2.398	
p_b%	5.7	4.6	4.6	
G_{se}	2.787	2.787	2.787	
G_{sb}	2.716	2.719	2.719	
v_{be}%	11.2	8.9	8.9	
γ_{HMA}	147.1	149.7	149.7	
% passing ¾-inch sieve	100.0	98.6	98.6	
% passing 3/8-inch sieve	95.9	70.4	70.4	
% passing No. 4 sieve	65.7	43.2	43.2	
% passing No. 200 sieve	4.6	5.1	5.1	
PG	70-22	70-22	64-22	
		Unbound Material		
Resilient Modulus				6,956
Soil Classification				A-6
Poisson's Ratio				0.35
k_0				0.5

Table C.2 Material Inputs for Lane 3 and 4

Layer	Surface	Intermediate	Base	Subgrade
		HMA Mix		
G_{mm}	2.826	2.578	2.578	
Poisson's ratio	0.35	0.35	0.35	
G_{mb}	2.628	2.398	2.398	
p_b%	5.6	4.6	4.6	
G_{se}	3.163	2.787	2.787	
G_{sb}	3.101	2.719	2.719	
v_{be}%	13.0	8.9	8.9	
γ_{HMA}	164.1	149.7	149.7	
% passing ¾-inch sieve	100.0	98.6	98.6	
% passing 3/8-inch sieve	90.3	70.4	70.4	
% passing No. 4 sieve	38.7	43.2	43.2	
% passing No. 200 sieve	7.6	5.1	5.1	
PG	70-22	70-22	64-22	
		Unbound Material		
Resilient Modulus				9,849
Soil Classification				A-6
Poisson's Ratio				0.35
k_0				0.5

About the Joint Transportation Research Program (JTRP)

On March 11, 1937, the Indiana Legislature passed an act which authorized the Indiana State Highway Commission to cooperate with and assist Purdue University in developing the best methods of improving and maintaining the highways of the state and the respective counties thereof. That collaborative effort was called the Joint Highway Research Project (JHRP). In 1997 the collaborative venture was renamed as the Joint Transportation Research Program (JTRP) to reflect the state and national efforts to integrate the management and operation of various transportation modes.

The first studies of JHRP were concerned with Test Road No. 1—evaluation of the weathering characteristics of stabilized materials. After World War II, the JHRP program grew substantially and was regularly producing technical reports. Over 1,600 technical reports are now available, published as part of the JHRP and subsequently JTRP collaborative venture between Purdue University and what is now the Indiana Department of Transportation.

Free online access to all reports is provided through a unique collaboration between JTRP and Purdue Libraries. These are available at http://docs.lib.purdue.edu/jtrp.

Further information about JTRP and its current research program is available at http://www.purdue.edu/jtrp.

About This Report

An open access version of this publication is available online. See the URL in the citation below.

Nantung, T. E., Lee, J., Haddock, J. E., Pouranian, M. R., Alvarez, D. B., Jeon, J., Shin, B., & Becker, P. J. (2021). *Structural evaluation of full-depth flexible pavement using APT* (Joint Transportation Research Program Publication No. FHWA/IN/JTRP-2021/17). West Lafayette, IN: Purdue University. https://doi.org/10.5703/1288284317319